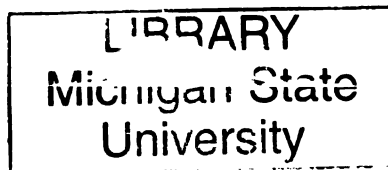


2
33



This is to certify that the
dissertation entitled

TOWARD PHOSPHORYLATED PEPTIDE ENRICHMENT
BASED ON ORGANOFUNCTIONALIZED
MESOSTRUCTURED SILICA

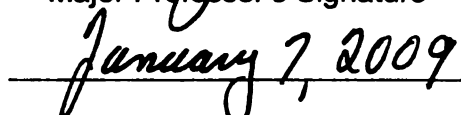
presented by

Dong-Keun Lee

has been accepted towards fulfillment
of the requirements for the

Doctoral degree in Chemistry


Major Professor's Signature


Date

PLACE IN RETURN BOX to remove this checkout from your record.
TO AVOID FINES return on or before date due.
MAY BE RECALLED with earlier due date if requested.

DATE DUE	DATE DUE	DATE DUE

**TOWARD PHOSPHORYLATED PEPTIDE ENRICHMENT BASED ON
ORGANOFUNCTIONALIZED MESOSTRUCTURED SILICA**

By

Dong-Keun Lee

A DISSERTATION

**Submitted to
Michigan State University
in partial fulfillment of the requirements
for the degree of**

DOCTOR OF PHILOSOPHY

Chemistry

2009

ABSTRACT

TOWARD PHOSPHORYLATED PEPTIDE ENRICHMENT BASED ON ORGANOFUNCTIONALIZED MESOSTRUCTURED SILICA

By

Dong-Keun Lee

Reversible protein phosphorylation is a key regulatory process in controlling many cellular events, such as cell cycle, cell growth, cell differentiation, and metabolism.^{1,2} In order to achieve detailed insight into the regulation of these reversible phosphorylation processes, it is often necessary to characterize the phosphorylation sites of specific proteins. Nevertheless, the identification of phosphopeptides including phosphorylation sites by analytical technique, such as mass spectrometric method, remains challenging. Therefore, specific isolation and enrichment of phosphorylated protein and phosphorylated peptides are often prior to analytical process. So far the most common enrichment method is IMAC.³ (immobilized metal affinity chromatography) Due to the lack of selectivity for containing carboxylate groups in IMAC enrichment, however, this method still has a limitation. Recently, to overcome this poor selectivity, a few covalent binding methods have been studied, such as covalent binding of modified phosphopeptides by β -elimination, covalent binding by α -diazo functionalized polymer resin, and covalent binding by oxidation-reduction condensation reaction

of amine functionalized polymer resin.^{4,5,6} Those methods show better selectivity, but still have limitations in the process of enrichment, such as increment of protein complexity by unwanted reactions, limitation of phosphotyrosine species enrichment, swelling problems upon solvent. Therefore, in this study I designed α -diazo functionalized mesoporous silica solid resins, which have rigid open framework structures, very high surface areas, and their wide ranges of pH and solvent stability in the application of the covalent immobilization and separation of phosphorylated peptides and proteins. In addition, for the facilitating enrichment process and minimizing sample loss, new types of separation media, for example α -diazo functionalized mesoporous thin film, were prepared.

1. Graves, J. D.; Krebs, E. G. *Pharmacol. Ther.* **1999**, *82*, 111-121
2. Hunter, T. *Cell* **2000**, *100*, 113-117
3. Posewitz, M. C.; Tempst, P. *Anal. Chem.* **1999**, *71*, 2883-2898
4. Oda, Y., Nagasu, T., Chait, B. T. *Nat. Biotechnol.* **2001**, *19*, 379-382
5. Lansdell, T. A.; Tepe, J. J. *Tet. Let.* **2003**, *45*, 91-93
6. Warthaka, M., Karwowska-Desaulniers, P., Pflum, M. *ACS Chemical Biology*, **2006**, *1*, 11, 697-701

Copyright

By

Dong-Keun Lee

2009

ACKNOWLEDGEMENTS

I want to express my appreciation to Dr. Pinnavaia for his support and guidance during my graduate studies. I greatly appreciate the intellectual and inspirational discussions we have had over the years. I also would like to convey my gratitude for the flexibility he has allowed me so that I could complete my research while taking care of my family.

I am grateful to Center for Advance Microscopy, especially Dr. Xudong Fan, Allica and Ewa for all of their support. I thank for their teaching the basic SEM and TEM, which have been very helpful to my research.

I would like to express my thanks to current and former group members for their friendship. Especially, I am thankful to Dr. Seong-Su Kim for his intellectual discussions as well as friendship.

I am grateful to my family for their support. My parents, Myung-Hun and Hye-Suk, have helped and scarified for me to achieve my goal during all their lives. Their unlimited loves have always encouraged me to endure and overcome from the time of frustration during my life. I also want to thank my sister, parents-in-law, and sister-in-law.

Most importantly, I would like to express my deepest gratitude to my son and wife, Benjamin and Eun-Sook, for all of the unconditional love and encouragement they have given over the years. Without their support and sacrifices, I would have not been able to accomplish any of this success.

TABLE OF CONTENTS

LIST OF TABLES.....	ix
LIST OF FIGURES.....	x
LIST OF SCHEME.....	xiv
ABBREVIATIONS.....	xv
1. Chapter 1	
Introduction.....	1
1.1 Research Objects and Significance.....	1
1.2 Enrichment method of phosphorylated protein.....	4
1.2.1 Immobilized Metal Affinity Chromatography (IMAC).....	4
1.2.2 Immunoprecipitation (IP).....	6
1.2.3 Metal Oxide/hydroxide Affinity Chromatography (MOAC).....	7
1.2.4 Specific chemical modification methods.....	8
1.2.5 Previous method applied in nanoscience.....	14
1.2.5.1 Dendrimer.....	14
1.2.5.2 Nanoparticle.....	17
1.2.5.3 Zeolite.....	17
1.2.5.4 Mesoporous (MCM-41).....	18
1.3 Organo-functionalized mesostructure.....	18
1.3.1 Post-synthesis pathway.....	19
1.3.2 Co-condensatioin pathway.....	22
1.4 References.....	25
2. Chapter 2	
Direct Assembly of Large Pore Organofunctionalized Silica Mesostructure from Sodium Silicate and bis(2-hydroxyethyl)-3-aminopropylsilane.....	29
2.1 Introduction.....	29
2.2 Experimental.....	32
2.2.1 Regents.....	32
2.2.2 Synthesis of a BHAPS-functionalized hexagonal MSU-H mesostructure.....	33
2.2.3 Synthesis of BHAPS-functionalized mesocellular silica foam, MSU-F..	33
2.3 Physical Characterization.....	36
2.4 Results and discussion.....	37
2.4.1 BHAPS-functionalized MSU-H hexagonal structure.....	37
2.4.2 BHAPS-functionalized MSU-F foam structure.....	46
2.5 Conclusion.....	47
2.6 References.....	51

3. Chapter 3

Diazo-functionalization of mesoporous silica for potential use in phosphopeptide enrichment.....	52
3.1 Introduction.....	52
3.2 Experimental section of NHNMPTS functionalized mesostructure.....	58
3.2.1 Reagents.....	60
3.2.2 30% NHNMPTS functionalization of SBA-15 silica by grafting reaction	60
3.2.3 10% NHNMPTS functionalization of MSU-F silica by direct assembly method.....	61
3.2.4 30% NHNMPTS functionalization of MSU-F silica by grafting method	62
3.2.5 Diazotization of NHNMPTS mesostructure.....	64
3.3 Physical Characterization.....	67
3.4 Results.....	68
3.5 Conclusion.....	76
3.6 References.....	88

4. Chapter 4

Improved Diazo-functionalization of mesoporous silica and the preparation of an IMAC-type mesoporous silica for potential use in phosphopeptide enrichment.....	89
4.1 Introduction.....	89
4.2 Experimental.....	94
4.2.1 Reagents.....	94
4.2.2 GPTS-, APTS-, and SATS-functionalized MSU-F mesocellular silica foam by direct assembly.....	95
4.2.3 30% SATS functionalized MSU-F silica by grafting method.....	98
4.2.4 Diazotization reaction of 30% GPTS-functionalized MSU-F silica...	98
4.2.5 Diazotization reaction of 30% APTS-functionalized MSU-F silica...	100
4.2.6 Absorption of organophosphate.....	100
4.2.7 Preparation of Fe ³⁺ immobilized on diacetate-functionalized MSU-F	101
4.3 Physical Characterization.....	101
4.4 Results and Discussion.....	103
4.4.1 30% GPTS functionalized MSU-F and its diazotization.....	103
4.4.2 Diazotization of Aminophenyl functionalized MSU-F silica.....	109
4.4.3 Immobilization of Fe ³⁺ on a succinate-functionalized MSU-F silica foam.....	119
4.5 Conclusion.....	125
4.6 References.....	126

5. Chapter 5

Phosphorylated protein enrichment based on diazo functionalized mesoporous silica film.....	127
--	------------

5.1 Introduction.....	127
5.2 Experimental.....	129
5.2.1 Reagents.....	129
5.2.2 Synthesis of diazo functionalized mesoporous film.....	130
5.2.3 Protein digestion.....	131
5.2.4 Methyl esterification of protein.....	131
5.2.5 Phosphorylated protein enrichment.....	132
5.3 Physical Characterization.....	132
5.4 Result and Discussion.....	133
5.4.1 X-ray diffraction analysis.....	133
5.4.2 Reflectance infrared spectroscopy.....	133
5.4.3 Transmission electron microscopy.....	134
5.4.4 Matrix assist laser desorption ionization mass spectrometry analysis	134
5.5 Conclusion.....	136
5.6 Reference.....	143

LIST OF TABLES

Table 2.1. Reaction stoichiometries used for the supramolecular assembly of BHAPS-functionalized MSU-H silica.....	35
Table 2.2. Textural properties of BHAPS-functionalized hexagonal MSU-H mesostructure.....	42
Table 2.3. ²⁹ Si solid state NMR cross-linking parameters for BHAPS-functionalized MSU-H.....	43
Table 2.4. Textural properties of BHAPS-functionalized mesocellular MSU-F foam mesostructure.....	49
Table 2.5. ²⁹ Si solid state NMR parameters for BHAPS-functionalized MSU-F...49	
Table 3.1. Reaction stoichiometries used for the supramolecular assembly of NHNMPTS-functionalized SBA-15, MSU-F, and MSU-F silica.....	63
Table 3.2. The amounts of reagents used in the diazotization of NHNMPTS-functionalized mesostructured silica.....	66
Table 3.3. UV analysis data from fmoc titration and their deprotected fmoc concentration by UV analysis.....	75
Table 3.4. Textural properties of NHNMPTS functionalized mesoporous materials determined from N ₂ adsorption isotherm.....	82
Table 3.5. Integral intensity of resonances observed in the ²⁹ Si solid state NMR of NHNMPTS-functionalized mesostructures.....	86
Table 3.6. Degrees of NHNMPTS functionalization determined by solid state NMR analysis and UV analysis of Fmoc titration.....	87
Table 4.1. Reaction stoichiometries used for the syntheses of GPTS-, APTS- and SATS-functionalized MSU-F foam silica.....	97
Table 4.2. ²⁹ Si solid state MAS NMR data for 30% GPTS functionalized MSU-F foam silica. The degree of functionalization is determined by the ratio between the integral of the T ³ resonance intensity to the total integral intensity (T ³ /(Q ⁴ +Q ³ +T ³)).....	107

LIST OF FIGURES

- Figure 1.1. Regulatory reversible mechanism by phosphorylation and dephosphorylation process in signaling pathway.....1
- Figure 1.2. Enrichment strategies using β -elimination reaction. (a) β -elimination reaction under basic condition. (b) Chemical modification based on β -elimination reaction.....12
- Figure 1.3. Enrichment strategies using chemical modification of carbodiimide condensation reaction.....13
- Figure 1.4. Schematic illustration of phosphorylated peptide isolation by using dendrimer.....16
- Figure 1.5. Schematic representation of the post-synthesis method of grafting organic groups on the mesostructure walls.....21
- Figure 1.6. Schematic representation of co-condensation pathway of incorporating organo-functional groups onto mesostructure silica.....24
- Figure 2.1. XRD spectra of BHAPS-functionalized hexagonal MSU-H samples after soxhlet extraction with ethanol. The products were formed from reaction mixture in which (A) 10%, (B) 20%, and (C) 30% of the total silicon.....40
- Figure 2.2. N_2 adsorption-desorption isotherm of BHAPS-functionalized MSU-H obtained from reaction mixture containing (A) 10%, (B) 20% and (C) 30% BHAPS. The inserts provide the BJH pore size distribution obtained from the adsorption branch of the isotherm41
- Figure 2.3. ^{29}Si solid state NMR spectra of BHAPS-functionalized MSU-H silica. The products were formed from reaction mixtures in which BHAPS represented (A) 10%, (B) 20%, and (C) 30% of the total silicon. The relative integrals of the Q^4 , Q^3 , and T^3 resonances were used to determine the amount of BHAPS incorporated into the mesostructure44
- Figure 2.4. TEM images of BHAPS-functionalized MSU-H containing 17 mole % BHAPS in the pore walls. The white circles are intended to identify the pore openings.....45
- Figure 2.5. N_2 adsorption-desorption isotherm and BJH pore size distribution for 7.5 mole % BHAPS-functionalized MSU-F formed from a reaction

mixture containing 10 mole % BHAPS. The pore size distributions were obtained from both the adsorption and desorption isotherms	48
Figure 2.6. TEM images of BHAPS-functionalized MSU-F containing 7.5% BHA-PS in the pore walls.....	50
Figure 3.1. Fluorene derivatives.....	55
Figure 3.2. Schematic illustration of phosphorylated peptide isolation by reaction with polymer-immobilized α -dialzo groups.....	56
Figure 3.3. Schematic illustration of α -dialzo groups synthesis on solid support..	57
Figure 3.4. Immobilized NHNMPTS functional group on a silica surface.....	58
Figure 3.5. Possible low angle X-ray diffractions on hexagonal mesoporous silica	69
Figure 3.6. N ₂ adsorption-desorption isotherms and BJH pore size distribution for SBA-15 silica calcined at 500 °C as determined from the adsorption isotherm.....	78
Figure 3.7. Powder X-ray diffraction pattern for calcined SBA-15 silica.....	79
Figure 3.8. IR spectra obtained after each reaction step for the dialzo functionalization of 30% NHNMPTS SBA-15 by the silane grafting method.....	80
Figure 3.9. N ₂ adsorption-desorption isotherm for 10% NMNMPTS functionalized MSU-F prepared by direct assembly and the BJH pore sizes distribution obtained from the adsorption and desorption isotherms..	81
Figure 3.10. N ₂ adsorption-desorption isotherms for 30% NMNMPTS functionalized MSU-F prepared by grafting method and the BJH pore sizes distribution obtained from the adsorption and desorption isotherms..	83
Figure 3.11. IR spectra obtained after each reaction step in the dialzo functionalization of 30% NHNMPTS MSU-F by the silane grafting method.....	84
Figure 3.12. Comparison of N ₂ adsorption and desorption isotherms for 30% NHNMPTS functionalized MSU-F, glycine-functionalized MSU-F, and dialzo functionalized MSU-F silica. The isotherms are offset by 500 cm ³ /g for clarity.....	85
Figure 4.1. N ₂ adsorption-desorption isotherm of 30% GPTS functionalized M-SU-F prepared by direct assembly method (upper panel) and the cell size	

and window size distributions (lower panel) obtained by fitting the adsorption desorption data, respectively, to the BJH model.....106

Figure 4.2. ^{29}Si solid state MAS NMR spectrum of 30% GPTS functionalized MSU-F foam silica.....107

Figure 4.3. IR spectra for the step-wise conversion of 30% GPTS functionalized MSU-F foam (made by direct synthesis) to diazo functionalized MSU-F.....108

Figure 4.4. N_2 adsorption-desorption isotherms for 30% aminophenyl functionalized MSU-F silica prepared by direct assembly (upper panel) and the cell and window size distributions obtained from the adsorption and desorption branches of the isotherms, respectively (lower panel)...111

Figure 4.5. Infrared spectra for aminophenyl functionalized MSU-F silica and the corresponding diazotized derivative made by reaction with sodium nitrite.....114

Figure 4.6. ^{31}P Solid state NMR spectrum of methyl phosphate covalent bonded to MSU-F foam silica wall by Sandmeyer-Gattermann aromatic substitution reaction after hydrochloric acid washing. The two peaks separated by 4 kHz from the line at -7 ppm are spinning side bands115

Figure 4.7. ^{31}P Solid state NMR spectrum of methyl phosphate on 30% aminophenyl functionalized MSU-F. The organophosphate anion was introduced into aminophenyl-functionalized MSU-F silica with the cyclohexyl ammonium salt of $[\text{PO}_3(\text{OCH}_3)]^{2-}$ in methanol solution116

Figure 4.8. ^{31}P Solid state NMR spectrum of methyl phosphate electrostatically bonded to cyclohexyl ammonium on pure MSU-F. The organophosphate anion was introduced into MSU-F silica with the cyclohexyl ammonium salt of $[\text{PO}_3(\text{OCH}_3)]^{2-}$ in methanol solution117

Figure 4.9. ^{31}P Solid state NMR spectrum of methyl phosphate covalent bonded to MSU-F foam silica wall by Sandmeyer-Gattermann aromatic substitution reaction. The four peaks separated by 4kHz as shown above is the spinning side bands of covalently bonded methyl phosphate species at -7 ppm.....118

Figure 4.10. N_2 adsorption-desorption isotherms for 10% succinic anhydride (SATS) functionalized MSU-F silica prepared by direct assembly method

	(upper panel) and the cell and window size distributions obtained from the adsorption and desorption isotherm, respectively.....	120
Figure 4.11.	N ₂ adsorption-desorption isotherms for pure MSU-F silica (upper panel) and the cell and window size distributions obtained from the adsorption and desorption isotherms, respectively. This silica was used to prepare a 30% succinic anhydride functionalized derivative by the grafting method.....	121
Figure 4.12.	IR spectra for succinate-functionalized MSU-F silica prepared by grafting reaction of SATS and for the corresponding derivative containing complexed Fe(III) cation.....	123
Figure 4.13.	TEM image (upper panel) and EDX spectrum (lower panel) for Fe(III) succinate functionalized MSU-F silica prepared by grafting method	124
Figure 5.1.	Powder X-ray diffraction pattern for HMS film on silicon wafer. (Structure direct agent was removed by soxhlet ethanol extraction.)....	137
Figure 5.2.	IR spectra obtained in each reaction step for the diazo functionalized mesoporous silica film synthesis. a) nitrile functionalized mesoporous silica film, b) carboxylic acid functionalized mesoporous silica film, c) diazo functionalized mesoporous silica film. Circles indicate the characteristic vibration of functional group. Each spectrum is offset by 15.....	138
Figure 5.3.	TEM image for organo-functionalized (COOH) mesoporous silica film.....	139
Figure 5.4.	MALDI mass spectra of 10 pmole of tryptic digested ovalbumin. a) conventional MALDI spectra of ovalbumin (no enrichment), b) ovalbumin enrichment on diazo mesoporous silica film. (The asterisks indicate the phosphorylated peptide fragments.).....	140
Figure 5.5.	MALDI mass spectra of 10 pmole of tryptic digested methyl-esterified ovalbumin. a) conventional MALDI spectra of methyl esterified ovalbumin (no enrichment), b) methyl esterified ovalbumin enrichment on diazo mesoporous silica film. (The asterisks indicate the phosphorylated peptide fragments.).....	141
Figure 5.6.	MALDI mass spectra of 10 pmole of tryptic digested methyl esterified β -casein. a) conventional MALDI spectra of β -casein (no enrichment), b) methyl esterified β -casein enrichment on diazo mesoporous silica film. (The asterisks indicate the phosphorylated peptide fragments.)	142

LIST OF SCHEMES

Scheme 3.1. Organosilane Grafting pathway.....	54
Scheme 3.2. Direct assembly pathway (co-condensation pathway).....	54
Scheme 3.3. The immobilization of Fmoc-glycine on mesostructure.....	59
Scheme 3.4. Fmoc deprotecting process and analyte for UV analysis.....	74
Scheme 4.1. Elimination of Glycidyl group by cyclization reaction.....	91
Scheme 4.2. Possible elimination mechanism of glycidyl group by nucleophilic cycliczation.....	92
Scheme 4.3. Nucleophiles which possibly react with terminal epoxide group....	94

ABBREVIATIONS

APTS	p-aminophenyltrimethoxysilane
BET	Brunauer-Emmett-Teller
BHAPS	Bis(2-hydroxyethyl)-3-aminopropyltriethoxysilane
BJH	Barrett-Joyner-Halenda
Boc	t-butyl carbamate
DCM	Dichloromethane
DHB	Dihydroxybenzoic acid
DMF	N, N-Dimethylformamide
DMSO	Dimethyl sulfoxide
EDC	Ethyl carbodiimide
EDX	Energy-dispersive X-ray spectroscopy
Fmoc	9H-fluoren-9-ylmethoxycarbonyl
FT-IR	Fourier transform Infrared
GPTS	(3-Glycidoxypropyl)trimethoxysilane
HMS	Wormhole mesostructured silica synthesized with amine surfactant using hydrogen bonding interaction
HONO	Nitrous acid
IDA	Iminodiacetic acid
IMAC	Immobilized metal affinity chromatography
IP	Immunoprecipitation
IUPAC	International Union of Pure and Applied Chemistry

LC	Liquid chromatography
MALDI	Matrix assisted laser desorption ionization
MAS NMR	Magic angle spinning nuclear magnetic resonance
MCF	Mesostructured cellular foam
MCM-41	Mobil composition of matter 41
Mmole	Millimoles
MOAC	Metal affinity chromatography
MRI	Magnetic resonance imaging
MSU-F	Mesostructured cellular foam synthesized with triblock copolymer surfactant, trimethylbenzene and water soluble silicate at near neutral assembly conditions
MSU-H	Hexagonal mesostructured silica synthesized with triblock copolymer surfactant and water soluble silicate at near neutral assembly conditions
MSU-X	Wormhole mesostructured silica synthesized with triblock copolymer surfactants and TEOS under neutral (N^oI^o) assembly conditions
NHNMPTS	N-hydroxyethyl-N-methylpropyltriethoxysilane
NTA	Nitrilotriacetic acid
PEO	polyethylene oxide
P123	Pluonic 123 ((EO)₂₀(PO)₇₀(EO)₂₀)
PTMs	Post-translational modifications
Q²	Incompletely condensed silica sites Si(OSi)₂(OH)₂

Q³	Incompletely condensed silica sites Si(OSi)₃(OH)
Q⁴	Completely condensed silica sites Si(OSi)₄
SATS	3-(Triethoxysilyl)propylsuccinic anhydride
SBA-15	Large pore hexagonal mesostructured silica assembled under high acid low pH conditions with TEOS as the inorganic precursor and triblock copolymer surfactant
T²	Functionalized Q² site RSi(OSi)₂(OH)
T³	Functionalized Q³ site RSi(OSi)₃
TED	Tris-(carboxymethyl)-ethylendiamine
TEM	transmission electron microscopy
TEOS	tetraethylorthosilicate
TFA	Trifluoroacetic acid
THF	Tetrahydrofuran
TMB	Trimethylbenzene
UV-Vis	Ultraviolet-Visible
XRD	X-ray diffraction
MALDI	Matrix assisted laser desorption ionization

Chapter 1

Introduction

1.1 Research Objects and Significance

Reversible protein phosphorylation is a key regulatory mechanism involved in major cellular events, like proliferation, differentiation, and apoptosis through complex signaling processes. As shown below, this regulatory reversible mechanism is mainly controlled by combining two reactions of different classes of enzymes: protein kinases, which catalyze the transfer of a phosphate group to an aminoacid side-chain of proteins and phosphatases which catalyze a hydrolysis of phosphoester bonds.^{1,2,3} Therefore, the defects or alterations of two types of enzymes, protein kinase and phosphatase, might result in serious diseases such as cancer and neurodegeneration diseases.

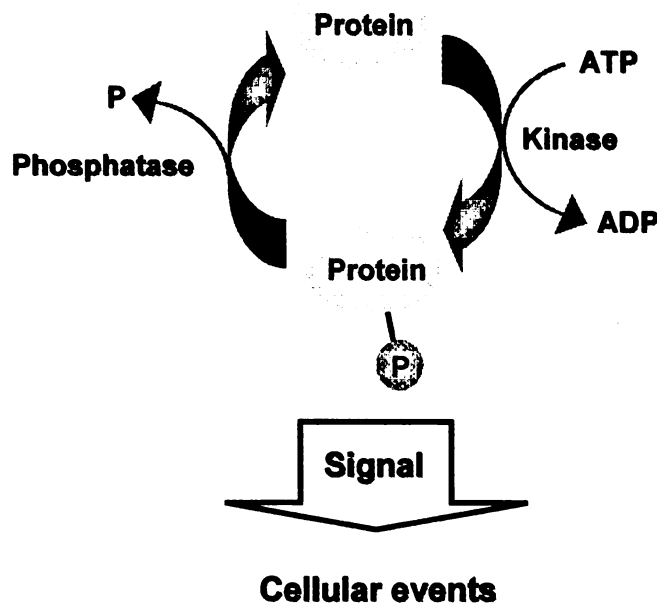


Figure 1.1. Regulatory reversible mechanism by phosphorylation and dephosphorylation process in signaling pathway

To understand these detailed biological processes and signaling pathways in a system requires information regarding the phosphorylated proteins involved in these processes, and how, where and when these phosphorylation processes take place. These reversible protein modifications by phosphorylation on serine, threonine and tyrosine residue occur in at least one-third of all proteins at any one time in a life cycle. It also is estimated that there are more than 100,000 potential phosphorylation sites in the human proteome.^{4,5} Unfortunately, however, only a few thousand phosphorylation sites are currently known, and even fewer are well characterized because of several limitations in detection. First of all, phosphorylated protein abundances are much lower than the amount of proteins, because only a small fraction of the proteins within cells is phosphorylated at a given time during a signaling pathway. Only 1~2% of all proteins exist in phosphorylated form.⁶ Moreover, as mentioned, variation in phosphorylation sites enhances the complexity of phosphorylation patterns. Secondly, the phosphorylation process is a labile and highly dynamic event regulated by kinases and phosphatases on a very short timescale.⁵ Thus, one of the huge tasks in proteomics studies of signal transduction is the development and optimization of strategies suitable for the investigation of low-abundant phosphorylated proteins and sensitive detection of post-translational modifications (PTMs). Recently, to overcome these limitations, a faster, and highly sensitive phosphorylated protein analysis method, mass spectrometry analysis, has been developed in proteomics.^{7,8} However, the phosphorylated protein peaks are often suppressed by unphosphorylated proteins in a mass

spectrometry analysis of complex protein mixtures. Therefore, despite mass spectrometry's huge improvement in proteomics, there is no routinely available method that allows the simple and straightforward analysis of phosphorylated protein in complex protein mixtures.⁹ Recently, the exceptional physical and chemical properties of mesostructured metal oxides, such as rigid open framework structures, very high surface areas, pH and solvent stability ranges exceeding the stability ranges of proteins, and narrow pore size distributions, have received attention for applications in biomolecule separations. My research is aimed at developing such novel mesostructured materials to have high loading capabilities and high selectivities toward phosphorylated proteins. The specific objectives of this research are as follows:

1. To develop the methodology for the supramolecular assembly of organofunctional mesostructured molecular sieves having suitably large pores via the co-condensation of organosilicon and inorganic silicate precursors.
2. To extend the known synthesis strategies for organofunctionalized meso-structures and the chemically modify the surface organic groups for use in phosphorylated protein enrichment.
3. To investigate new types of organofunctional mesostructures having a high percentage of surface organic groups for phosphorylated protein enrichment.

1.2 Enrichment method of phosphorylated protein

Phosphoproteins have been analyzed through the use of total protein lysates. However, due to the small fractions of the total proteins in cellular lysates, the identification of phosphoproteins relevant to signaling processes from complex protein mixtures still can be challenging. Therefore, enrichment strategies are essential to identify the very low abundance of phosphoproteins.⁵ Here, I introduce some enrichment methods which have been developed to purify phosphoproteins as well as phosphopeptides from complex protein mixtures, namely, i) Immobilized Metal Affinity Chromatography (IMAC); ii) Immunoprecipitation (IP); iii) Metal Oxide Affinity Chromatography (MOAC); iv) Specific chemical modification method. Furthermore, the state-of-the-art enrichment techniques, in combination with nano-science will be also discussed.

1.2.1 Immobilized Metal Affinity Chromatography(IMAC)¹⁰⁻¹⁹

Immobilized metal affinity chromatography is presently the most popular and frequently utilized enrichment technique, originally introduced by Porath in 1986.^{10,11} This IMAC technique is based on the high binding constant of phosphoserine for Fe^{3+} ($>10^3$).¹² The binding involves the electrostatic interaction of two components, such as a negatively charged phosphate group and a positively charged metal ion species immobilized onto iminodiacetic acid (IDA), nitrilotriacetic acid (NTA), or tris-(carboxymethyl)-ethylendiamine(TED) chelating ligand.¹³ Various metal ions other than Fe^{3+} have been investigated for better selectivity and phosphoprotein recovery. Generally, the metal ions

can be categorized into three kinds of acids, hard, intermediate, and soft. These characteristics are related to the specific anion bindings governed by the hard-soft-acid-base rule. Hard metal ions, such as Fe^{3+} , and Al^{3+} , show better binding affinity with oxygen. Soft metal ions, such as Cu^+ , and Hg^+ , show their preferences for sulfur. Intermediate metal ions, such as Zn^{2+} , Ni^{2+} , and Co^{2+} , can be favorably bound to nitrogen, oxygen, and even sulfur. Therefore, the oxygen atoms on phosphate groups attaching to serine, threonine, and tyrosine show a high affinity to a hard metal ion such as Fe^{3+} , which has been the most common binding between metal ion and phosphate group in IMAC phosphoprotein separation.

Another method using Zirconium for enrichment can be described as a direct method without the need for an elution process. Originally this method¹⁴ used a porous silica wafer as a substrate. The porous silica wafers were modified by a phosphonate group followed by binding of Zr^{4+} . The zirconium phosphonate (ZrP) modified surface had a strong interaction with phosphopeptides and specifically captured the phosphopeptides from complex peptide mixtures. In addition, the captured phosphopeptides on the zirconium phosphonate-modified wafer were directly placed on a MALDI target for further analysis by MALDI MS.

Ga(III) has been also studied in IMAC phosphoprotein separation. In 1999, Tempst¹⁵ and a colleague claimed Ga(III) showed even better selectivity and elution-off properties than Fe(III) for phosphoprotein separation. In their studies, they compared a Fe(III) , Zr(IV) , and Ga(III) IMAC columns, all of which

captured phosphorylated proteins very well. However, in the elution process, Fe(III) and Zr(IV) IMAC columns still retained the acidic residues of various peptides after an extensive washing process. Also, the columns did not efficiently elude phosphorylated proteins at dilute basic condition. At present, although this method is most powerful in phosphorylated protein binding, it has been problematic in its specificity. Due to its electrostatic binding characteristic, this IMAC method sometimes binds to non-phosphorylated proteins or peptides having high number of acidic residues, such as aspartate and glutamate, which is the significant limitation of this method. For this reason, another IMAC approach has been discussed.^{16,17} In 2002, Ficarro *et. al.*¹⁶ suggested that methyl esterification of the C-terminus and of acid residue such as glutamate and aspartate in protein mixture before the enrichment process can reduce the non-specific binding in an IMAC application. This specific chemical modification on carboxylic acid is able to increase the selectivity in phosphorylated protein enrichment. In this study, more than 200 peptide sequences, and 380 phosphorylation sites are determined by mass spectrometry analysis after the enrichment of tryptic phosphopeptides by IMAC. However, due to the relatively strong and restricted reaction conditions, such as the use of concentrate HCl and dried methanol in an anhydrous reaction environment, esterification reactions might lead to sample complexity depending on an experimental conditions.

1.2.2 Immunoprecipitation (IP)

Immunoprecipitation (IP) is the enrichment method for precipitation of an

antigen by an antibody specific to that antigen. In a phospho-specific antibody, anti-phosphotyrosine antibodies are commonly used for enriching a tyrosine-phosphorylated protein from a protein mixture. Although these antibodies have been relatively effective at enriching low-abundance tyrosine phosphorylated proteins, there are still no immunopurification protocols having high selectivity for the phosphotyrosine of peptides.^{20,21,22} Moreover, anti-phosphoserine and anti-phosphothreonine antibodies are not currently available for the enrichment of proteins containing phosphorylated serine and threonine residue. Therefore, the immunoprecipitation method is not generally suitable for enriching phosphoproteins from a complex protein mixture

1.2.3 Metal Oxide/hydroxide Affinity Chromatography (MOAC)

Recently, a new alternative method to IMAC has been reported. This approach is based on the specific affinity of phosphate group to a metal oxide surface. Basically, three metal oxide or hydroxide particles have been widely studied, titania (TiO_2),²³⁻²⁸ zirconia (ZrO_2),²⁸ and aluminum hydroxide ($\text{Al}(\text{OH})_3$).²⁹ Larsen and colleagues²⁷ recently reported the use of titania for phosphorylated peptides enrichment. In their study, dihydroxybenzoic acid (DHB) was used for the selective enhancement of phosphorylated peptides in competition with non-phosphorylated peptides on TiO_2 . Due to the thermodynamically stable bond between dihydroxybenzoic acid and TiO_2 , named chelating bidentate bond, dihydroxybenzoic acid effectively inhibits the single weak binding of nonphosphorylated peptides. Dihydroxybenzoic acid doesn't affect or less

affects the binding of the phosphorylated peptides, but it retards binding of non-phosphorylated peptides. In the comparison with IMAC, this novel methodology showed superior results in terms of the selectivity and sensitivity of phosphorylated peptide binding. In addition, the simplicity of this procedure and ease of materials handling can expedite the analysis process, which typically required less than 5 min per sample. Zirconia has been also applied to phosphopeptides enrichment. Kweon et al.²⁸ first demonstrated the phosphopeptides enrichment by using the ZrO₂ microtip syringe. In her study, she compared the selectivity and sensitivity of the ZrO₂ microtip with those of the TiO₂ microtip, which showed similar result to each other in overall performance. In selectivity, however, singly phosphorylated peptides were better enriched with ZrO₂ microtips. On the other hand, TiO₂ microtips favorably enriched multiply phosphorylated peptides.

In another MOAC study of proteomics, a novel Al(OH)₃ based enrichment method also has been shown to have a good phosphorylated peptide selectivity from a complex peptide mixture by ligand exchanges of OH groups with phosphate groups. Wolshin et al.²⁹ reported this method is even more selective and cost effective than the commercially available IMAC and other phosphoprotein-enrichment kits.

1.2.4 Specific chemical modification methods

To achieve phosphoprotein enrichment, a site-specific modification of the phosphate moiety in a protein has been applied. To date, two methods have

been reported. The first method uses the chemical modification of the phosphorylation sites of serine and threonine by β -elimination^{30,31} under strong alkaline conditions, which results in a dehydroalanine and dehydroaminobutyric acid residue. This unsaturated residue readily reacts with a nucleophile (in this case ethanedithiol) and subsequently a thiol terminal group can be linked to a biotin affinity tag or other immobilizing agent, which is illustrated in Figure 1.2. These biotinylated peptides can be bound to avidin or streptavidin bead and separated. Through this process, the labile phosphate groups can be also substituted by various stable marker molecules which give better ionization efficiency in mass spectrometry analysis. However, there are some drawbacks to this application. First of all, unprotected cysteine and methionine residues can become involved in unwanted side reactions with the unsaturated dehydroalanine and dehydroaminobutyric acid residue. In a Michael-type addition reaction, the non bonding electrons on sulfur groups of cysteine and methionine residue act as a nucleophile and can produce side products. To overcome this problem, the cysteine residue of the sample should be oxidized by performic acid, thereby inactivating it. Secondly, O-linked sugar moieties can generate an additional complication in this enrichment process. This O-linked sugar moiety might also undergo a β -elimination reaction and change to a dehydroalanyl residue, which is the same result as the phosphate residue. Removing this glycosylated peptide prior to the modification reaction can be a solution for this problem.

The second method is a multi-step derivatization method reported by

Zhou *et al.* in 2001.³² As shown in Figure 1.3, ethyl carbodiimide (EDC) catalyzes the addition of cystamine to a phosphate group on the protein via phosphoroamidate-bonds, which can thereby be covalently bound to a solid glass bead containing an immobilized iodoacetyl group. Elution of phosphorylated peptides is accomplished by cleavage of phosphoroamidate bonds by trifluoroacetic acid (TFA). One major advantage of this method is it can be applied all types of phosphorylated proteins, unlike the first method. However, the second method has a drawback in that all amino- and carboxy-groups must be blocked prior to enrichment to prevent intramolecular and intermolecular condensation. At present, these two methods are quite novel and promising techniques for isolating and enriching phosphorylated peptides from a mixture. However, these methods still have some problems, in that they need a significant amount of phosphorylated protein or peptide for successful subsequent mass spectrometry analysis. Also, the selectivities of these methods are still questionable. Instead of the chemical derivatization of a protein mixture in solution, solid support has been chemically modified for isolating phosphorylated peptides.

Tepe *et al.*³³ established a new type of solid support that contains an α -diazot functional group on the surface. In his approach, the α -diazot functional group can be easily substituted by a nucleophile such as the phosphate group of a phosphorylated peptide. This leads to a covalent bond between the solid support and the phosphate group. Tepe also claimed this method enhances selectivity, compared with electrostatic IMAC binding. Moreover, elution of the

protein can be conducted by simple filtration. However, this method also has difficulties. In order to confirm the selective binding of phosphorylated peptides onto α -diazo functional group, the carboxylic acid moiety must be blocked through esterification reaction. The unprotected carboxylic acid can be a nucleophile and then attack the α -diazo functional group, which can reduce the selectivity of this this approach.

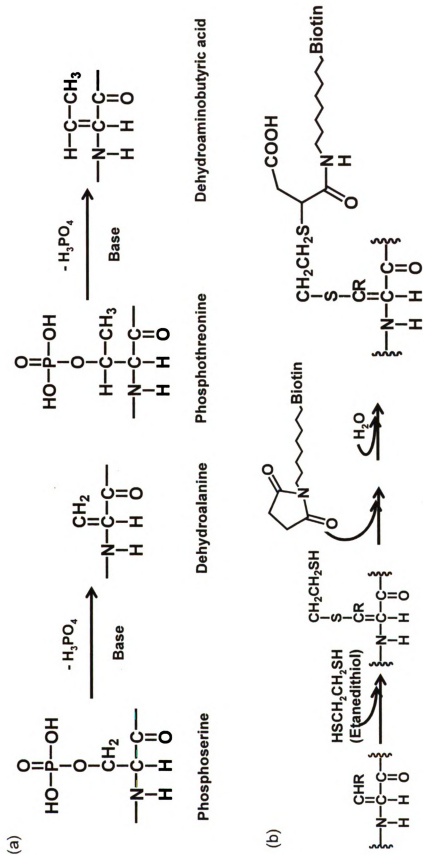


Figure 1.2 Enrichment strategies using β -elimination reaction. (a) β -elimination reaction under basic condition. (b) Chemical modification based on β -elimination reaction. ^{8,29,30}

1.2.5 Previous method applied in nanoscience

During last few decades, nanoscience has been one of the most active fields in science and technology. Especially, due to their various practical applications, such as absorbents,³⁴ catalysts,³⁵ heavy metal ion traps,³⁶⁻³⁹ optics,⁴⁰ sensors⁴¹ and etc., nanomaterials have stimulated studies of their synthesis and properties. Recently, these nanomaterials have been also applied in biological science, as drug delivery carriers,⁴² proteolysis reactors,^{43,44} and MRI contrasting agents.⁴⁵ In addition, because their important physical properties (eg. high surface area) are not owned by bulk materials, these nanomaterials have been studied as a affinity probe toward a specific target in the field of bioanalytical chemistry, especially as a selective enrichment medium of low-abundance phosphopeptides from enzymatic digest products. Here I introduce some nanomaterials which have been applied to the enrichment process in phosphoproteomics, namely i) dendrimer, ii) nanoparticle, iii) zeolite, iv) mesostructure.

1.2.5.1 Dendrimer

Aebersold *et al.*⁴⁶ have established a new phosphopeptide enrichment method by using dendrimer support, which is shown in Figure 1.4. One of the notable aspects of this approach is that he covalently coupled phosphorylated peptides to a synthetic polyamine (dendrimer) in a single step by adding ethyl carbodiimide (EDC) and imidazole. The covalently immobilized phosphopeptides on dendrimer were separated from nonphosphorylated

peptides by simple filtration, recovered via acid hydrolysis, and subsequently characterized by LC/MS/MS. With this method, Aebersold could identify phosphorylation sites. He also produced an esterification reaction prior to binding phosphopeptides to dendrimer, which enhanced the selectivity of this method. Finally, Aebersold and colleagues applied this method to the study of tyrosine phosphoproteins in human T cells, which showed the isolation of a total of 97 tyrosine phosphoproteins and interacting partners and also the identification and quantification of 75 tyrosine phosphorylation sites as well as 80 serine and threonine sites.

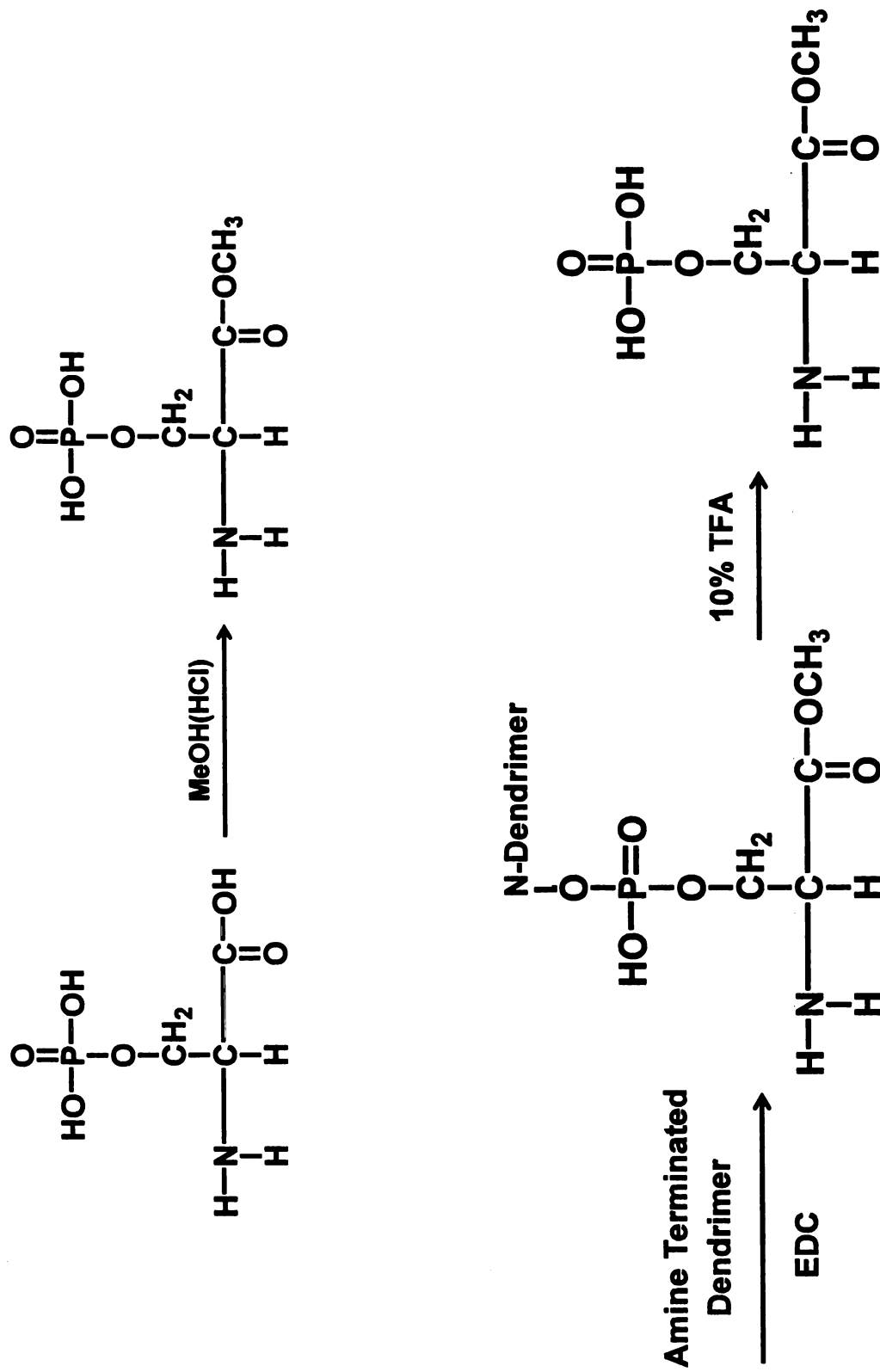


Figure 1.4 Schematic illustration of phosphorylated peptide isolation by using dendrimer⁴⁵

1.2.5.2 Nanoparticle

To date, microsized metal oxide particles have been used for enrichment of phosphorylated peptides from a complex mixture. However, in the enrichment process of low abundant phosphopeptides, relatively low binding capacities will have low sensitivity toward target species. Therefore, high surface area materials such as nanoparticles will surely have an advantage for a potentially higher trapping sensitivity in enrichment process. Here, a new type of core/shell nanoparticles has been reported. Chen *et al.* in 2005⁴⁷ introduced TiO₂-coated Fe₃O₄ magnetic nanoparticles (ca.50nm) to isolate and identify the phosphorylated peptides from the peptides mixture. As mentioned above in MOAC, selectivity of TiO₂ toward phosphorylated peptides is quite satisfying. Moreover, Fe₃O₄ magnetic nanoparticles in a core allow phosphopeptide-bound nanoparticles to isolate readily from the mixture solution by applying a magnetic field. In this paper, Chen *et al.* claimed the lowest detectable concentration of phosphopeptides by using this approach is 500pM for 100μL, which is a much lower detection limit than any other current method.

1.2.5.3 Zeolite

Recently, a porous nanoparticle also has been applied to phosphorylated peptide enrichment. Zhang *et al.* in 2004⁴⁸ reported Fe³⁺-immobilized zeolite-beta nanoparticles (ca.100nm) have been used, for the first time to enrich and identify phosphopeptides from a tryptic β-casein digested peptide mixture. In this study, he claimed the zeolites' large external surface areas make a large

quantity of Fe^{3+} groups on the surface and also produce a sufficient number of effective bindings with the target species. Moreover, high dispersibility can easily facilitate the chelation process of phosphorylated peptides. Although this method still needs further development, it opens up a new possibility for the enrichment of phosphopeptides.

1.2.5.4 Mesostructure (MCM-41)

The first synthesized Fe^{3+} - immobilized mesostructure has been reported for the phosphorylated peptides enrichment application by Pan *et al.* in 2006.⁴⁹ In this study, he prepared *ca.* 600nm particle size and 3nm pore size mesostructure with a Fe^{3+} modified surface and then it was used as the adsorbent to phosphorylated peptides in tryptic α -casein and β -casein digests. After the separation by Fe^{3+} - immobilized MCM-41, the peaks of phosphopeptides were enhanced by the reduction of non-phosphorylated peptides' peaks, which illustrated Fe^{3+} - immobilized MCM-41 was successfully applied in proteomics research. However, it still has the certain amount of nonspecific bindings with peptides mixture as IMAC has. Moreover, given the small size of pore, I assume the high degree of functionality originated from its high surface is not totally used for this application, and thus it still needs further development.

1.3 Organo-functionalized mesostructure

Since mesostructures received attention with their prominent features,

such as their high surface area, narrow pore size distribution, and large pore volume etc., mesostructures have been widely studied in various applications. They are used extensively as adsorbents,³⁴ ion exchangers,⁵⁰ heterogeneous catalysts for petroleum refining,⁵¹ and sensory materials.⁴¹ Moreover, due to their pH and solvent stability and easily accessible void spaces, they have been researched as chromatographic separation media.⁵² Recently, to expand utilization of mesostructures, like trapping heavy metal ions,³⁶⁻³⁹ and delivering drugs,⁴² they have been functionalized with various organic groups. The specific affinity and reactivity of these mesostructures can be tuned by appropriate organic moiety on their surfaces. Thiol functionalization is best for mercury adsorption,^{36,38} and amine moiety on the surface prefers arsenate adsorption.^{37,39} Lin *et al.*⁴² also reported new type of spherical MCM-41 having amine functional groups as a drug delivery carrier. In his research, due to holding drug molecules inside the pores, the amine functional groups are covalently bound to capping materials by amidation reaction. To prepare these materials, generally two chemical approaches are used, which are the post-synthesis pathway (grafting pathway) and co-condensation pathway (direct-assembly pathway)

1.3.1 Post-synthesis pathway

Post-synthesis pathway is the functionalization method accomplished by the condensation reaction between an organosilane and the silanol group on the silica mesostructure. The first grafting functionalization was reported by Beck *et*

al. by anchoring chlorotrimethylsilane on the mesostructure MCM-41.⁵³ In 1997, for heavy metal ion binding, hexagonal MCM-41 and wormhole-like HMS silica were also functionalized by the grafting of 3-mercaptopropyltrimethoxysilane, which shows unprecedented high loading capacities for mercury (2.5mmole/g and 1.5mmole/g respectively).^{36,38} However there are some drawbacks to the post-synthesis pathway. First of all, due to the differences in geometrical conformations between the silanol group on the mesostructured surface and the hydrolysable alkoxide group in organosilane, the functional groups are not linked completely to the surface. Therefore, some amount of organosilane groups on the mesostructure materials can be easily removed through hydrolysis during uses. In addition, the inability to control the anchoring liquid organic moiety on the solid mesostructure make inhomogeneous dispersion of organosilane, which leads to the limitation of functionality by pore blockages. Figure 1.5 shows the schematic representation of the post-synthesis pathway.

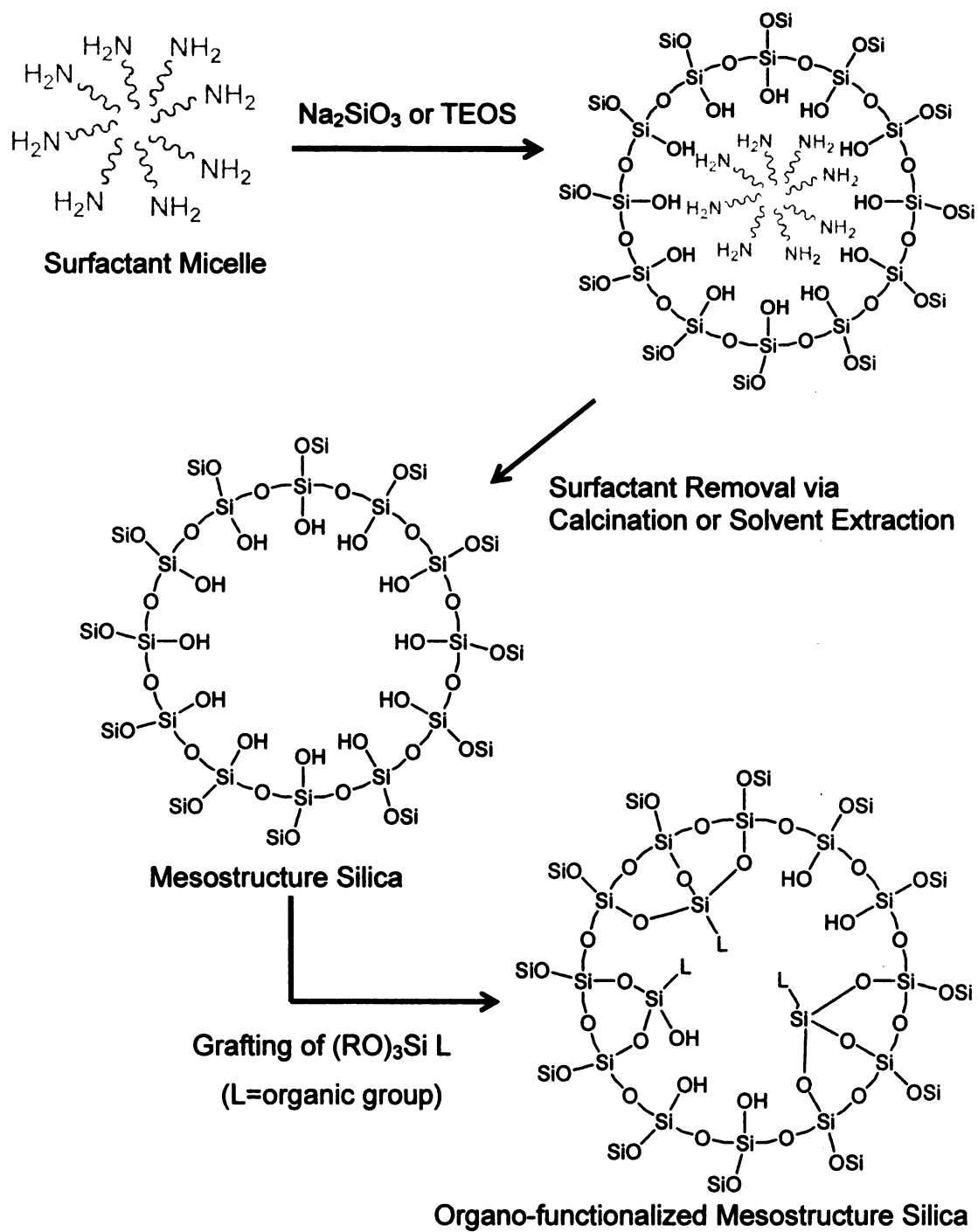


Figure 1.5 Schematic representation of the post-synthesis method of grafting organic groups on the mesostructure walls

1.3.2 Co-condensation pathway

The co-condensation pathway is a one-pot synthesis based on the co-condensation of siloxane and organosilane precursors during the assembly of the mesostructures, which is illustrated in Figure 1.6. Due to this co-condensation reaction, organosilane group should be more uniformly distributed on the mesostructure surface. Moreover, in comparison to the grafting pathway, direct assembly pathway leads to a more complete crosslinking of the organosilane to the mesostructure framework. Therefore, it might be a much more promising pathway to the preparation of stable organo-functionalized mesostructured molecular sieves. However, one of the problems associate with the co-condensation pathway is the loss of structural order at high loading percentages, like 15 mol% or more. Moreover, if the organic moiety is hydrophilic, such as hydroxyl group, functional group might be buried inside the framework, which results in low degree of valid functionalization. The first co-condensation synthesis has been done on MCM-41, reported by Burkett *et al.*⁵⁴ In his few papers, he reported functionalized MCM-41 with various functional groups including aminophenyl, mercaptopropyl, phenyl and octyl. However, due to the strong interaction between templating surfactant and framework, in some cases the functionalized MCM-41 decomposed upon removing the templating surfactant from the pores by acid. The functionalized mesostructures are also prepared by hydrogen bonding assembly, namely functionalized HMS and MSU-X. In this non-electrostatic technique, functionalized mesostructures are stable to the removal of surfactant by extraction techniques. In 2001, Pinnavaia and

colleagues reported up to 50mol% thiol functionalized HMS.⁵⁵ In his research, the materials retained well expressed mesostructures after removing surfactants with about 3.0 nm of pore sizes, 0.7 cm³/g of pore volumes, and 1230 m²/g of surface areas. Recently, in order to incorporate bio-molecules into ordered mesostructure silica materials, large pore materials like SBA-15 and MCF are very attractive because a suitable pore size required for internal adsorption of large molecules.^{56,57} Moreover, the surface modification on silica by direct assembly also plays an important role in binding protein as this will influence the strength of the interaction between the biomolecules and the internal surface of the mesostructure silica. Zhao *et al.*⁵⁶ reported functionalized SBA-15 with various functional groups by co-condensation pathway. In this paper, he prepared 5 different functional groups on the mesostructures, such as amine, nitrile, vinyl, phenyl and thiol. He also claimed the level of disorder of the mesostructures depended on the type and amount of the organosilanes in the synthesis.

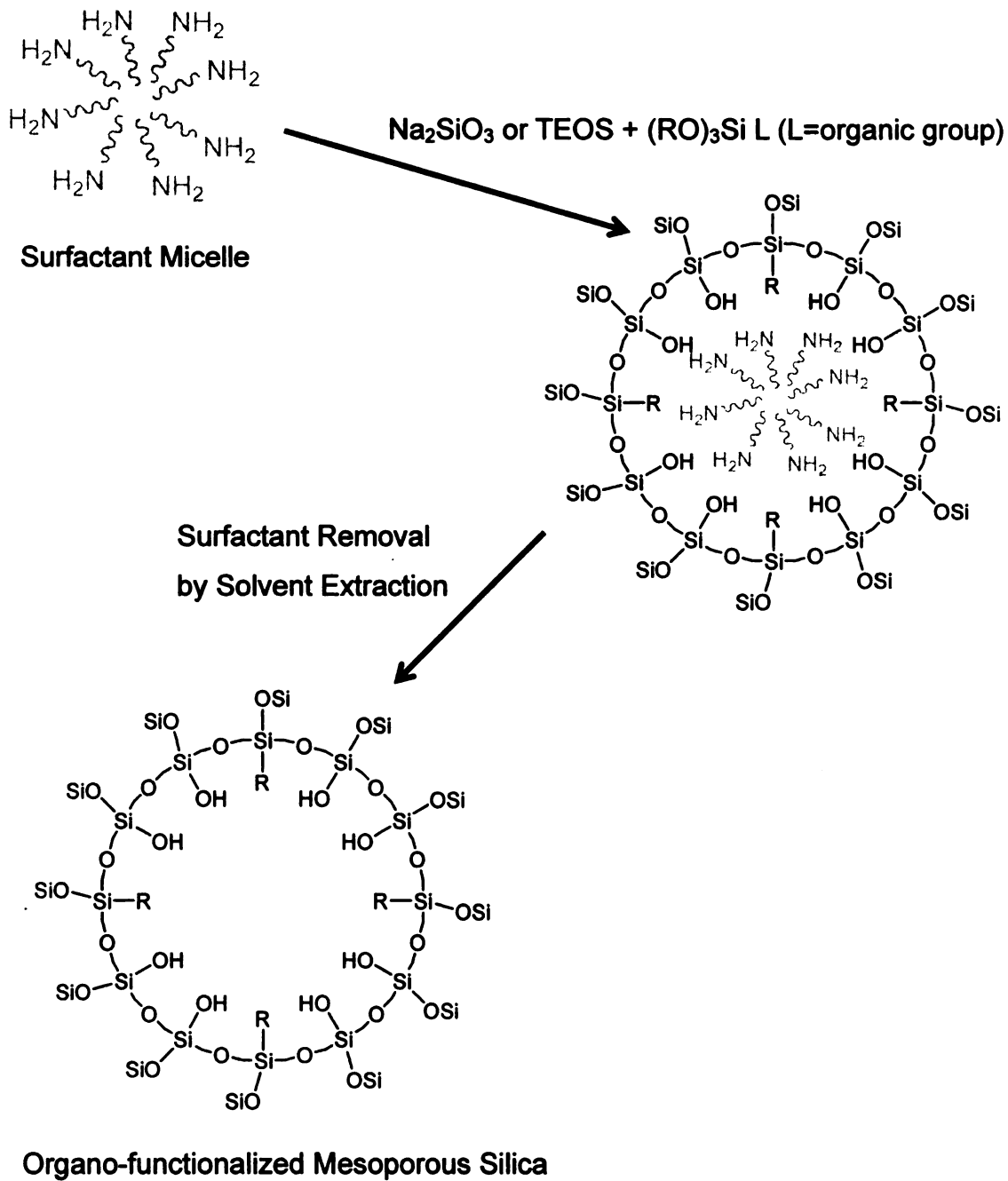


Figure 1.6 Schematic representation of co-condensation pathway of incorporating organo-functional groups onto mesostructure silica

1.5 References

- (1) Venter, J. C., Adams, M. D., Myer, E. W., Li, P. W., Mural, R. J., Sutton, G. G., Smith, H. O., Yandell, M., Evans, C. A., Holt, R. A., *et al.* *Science* **2001**, 291, 1304-1351
- (2) Manning, G., Whyte, D. B., Martinez, R., Hunter, T., Sudarsanam, S. *Science* **2002**, 298, 1912-1934
- (3) Alonso, A., Susan, J., Bottini, N., Friedberg, I., Osterman, A., Godzik, A., Hunter, T., Dixon, J., Mustelin, T. *Cell* **2004**, 117, 699-711
- (4) Zhang, H., Zha, X., Tan, Y., Hornbeck, P. V. *et al.* *J. Biol. Chem.* **2002**, 277, 39379-39387
- (5) Kalume, D. E., Molina, H., Pandey, A. *Curr. Opin. Chem. Biol.* **2003**, 7, 64-69
- (6) Schlessinger, J., *Harvey Lect.* **1993**, 89, 105-123
- (7) Sickmann, A., Meyer, H. E. *Proteomics* **2001**, 1, 200-206
- (8) Mann, M., Ong, S. E., Gronborg, M., Steen, H., Jensen, O. N., and Pandey, A. *Trends Biotechnol.* **20**, 261-268
- (9) Arnott, D., Gawinowicz, M. A., Grant, R. A., Neubert, T. A., Packman, L. C., Speicher, K. D., Stone, K., Turck, C. W., *J. Biomol. Tech.* **2003**, 14, 205-215
- (10) Andersson, L., Porath, J. *Anal Biochem* **1986**, 154 250-254
- (11) Stensballe, A., Andersen, S., Jensen, O. N. *Proteomics* **2001**, 1, 207-222
- (12) Porath, J., Carlsson, J., Olsson, I., and Belfrage, G. *Nature*, **1975**, 258, 598-599
- (13) Gaberc-Porekar, V., Menart, V. *J. Biochem. Biophys. Methods* **2001**, 49, 335-360
- (14) Zhou, H., Xu, S., Mingliang, Y, Feng, S., Pan, C., jiang, X., Li, X., Han, G., Fu, Y., Zou, H. *J. Proteome. Res.* **2006**, 5, 2431-2437
- (15) Posewitz, M. C., Tempst, P. *Anal Chem.* **1999**, 71, 2883-2892
- (16) Ficarro, S. B., McClelland, M. L., Stukenberg, P. T., Burke, D. J. *et al.* *Nat. Biotechnol.* **2002**, 20, 301

- (17) Brill, L. M., Salomon, A. R., Ficarro, S. B., Mukherji, M. et al. *Anal. Chem.* **2004**, *76*, 2763-2772
- (18) Blacken, G. R., Gelb, M. H., Turecek, F. *Anal. Chem.* **2006**, *78*, 6065-6073
- (19) Kokubu, M., Ishihama, Y., Sato, T., Nagasu, T., Oda, Y. *Anal. Chem.* **2005**, *77*, 5144-5154
- (20) Pandey, A., Podtelejnikov, A. V., Blagoev, B., Bustelo, X. R., Mann, M., Lodish, H. F. *Proc. Natl. Acad. Sci* **2000**, *97*, 179-184
- (21) Kratchmarova, I., Blagoev, B., Haack-Sorensen, M., Mann, M., *Science* **2005**, *308*, 1472-1477
- (22) Zhang, G., Neubert, T. A. *Proteomics* **2006**, *6*, 571
- (23) Sano, A., Nakamura, H. *Anal. Sci.* **2004**, *20*, 565-566
- (24) Kimura, Y., Shibasaki, S., Morisato, K., Ishizuka, N., Minakuchi H., Nakanishi, K., Matsuo, M. et al. *Anal. Biochem.* **2004**, *326*, 262-266
- (25) Pinkse, M. W., Uitto, P. M., Hilhorst, M. J., Ooms, B., Heck, A. J. R. *Anal. Chem.* **2004**, *76*, 3935-3943
- (26) Miyazaki, S., Morisato, K., Ishizuka, N., Minakuchi, H., Shintani, Y., Furuno, M., Nakanishi, K., *J. Chromatogr. A* **2004**, *1043*, 19-25
- (27) Larsen, M. R., Thingholm, T. E., Jensen, O. N., Roepstorff, P., Jorgensen, T. *J. D. Mol Cell Proteomics* **2005**, *4*, 873-886
- (28) Kweon, H. K., Hakansson, K. *Anal. Chem.* **2006**, *78*, 1743-1749
- (29) Wolshin, F., Wienkoop, S., Weckwerth, W. *Proteomics* **2005**, *5*, 4389-4397
- (30) Oda, Y., Nagasu, T., Chait, B. T. *Nat. Biotechnol.* **2001**, *19*, 379-382
- (31) Meyer, H. E., Eisermann, B., Heber, M., Hoffmann-Posorske, E., Korte, H., Weigt, C., Wegner, A., Hutton, T., Donella-Deana, A., Perich, J. W. *Faseb. J.* **1993**, *7*, 776-782
- (32) Zhou, H., Watts, J. D., Aebersold, R. *Nat. Biotechnol* **2001**, *19*, 375-378
- (33) Lansdell, T. A., Tepe, J. J. *Tetrahedron Lett.* **2004**, *45*, 91-93
- (34) Davies, M. E. *Chemistry & Industry* **1992**, 137
- (35) Clark, J. H., Macquarrie, D. J. *Chem. Commun.* **1998**, 853-860

- (36) Mericier, L., Pinnavaia, T. J. *Adv. Mater.* **1997**, *9*, 500-&
- (37) Fryxell, G. E., Liu, J., Hauser, T. A., Nie, Z. M., Ferris, K. F., Mattigod, S., Gong, M. L., Hallen, R. T. *Chem. Mater.* **1999**, *11*, 2148-2154
- (38) Feng, X., Fryxell, G. E., Wang, L. Q., Kim, A. Y., Liu, J., Kemner, K. M. *Science* **1997**, *276*, 923-926
- (39) Yoshitake, H., Yokoi, T., Tatsumi T. *Chem. Mater.* **2002**, *14*, 4603-4610
- (40) Trindade, T., O'Brien, P., Pickett, N. L. *Chem. Mater.* **2001**, *13*, 3843-3858
- (41) Xu, X., Tian, B., Zhang, S., Kong, J., Zhao, D., Liu, B. *Analytica Chimica Acta* **2004**, *519*, 31-38
- (42) Giri, S., Trewyn, B. G., Stellmaker, M. P., Lin, V. S.-Y. *Angew. Chem. Int. Ed.* **2005**, 5038-5044
- (43) Shui, W., Fan, J., Yang, P., Liu, C., Zhai, J., Lei, J., Yan, Y., Zhao, D., Chen, X. *Anal Chem.* **2006**, *78*, 4811-4819
- (44) Zuo, C., Yu, W., Zhou, X., Zhao, D., Yang, P. *Rapid Commun. Mass. Spectrom.* **2006**, *20*, 3139-3144
- (45) Lee, J., Huh, Y., Jun, Y., Seo, J., Jang, J., Song, H., Kim, S., Cho, E., Yoon, H., Suh, J., Cheon, J. *Nat. Medicine* **2006**, *13*, 95-99
- (46) Tao, W. A., Wollscheid, B., O'Brien, R., Eng, J. K., Li, X., Bodenmiller, B., Watts, J. D., Hood, L., Aebersold, R. *Nat. Methods* **2005**, *2*, 591
- (47) Chen, C., Chen, Y. *Anal. Chem.* **2005**, *77*, 5912-5919
- (48) Zhang, Y., Yu, X., Wang, X., Shan, W., Yang, P., Tang, Y. *Chem. Comm.* **2004**, 2882-2883
- (49) Pan, C., Ye, M., Liu, Y., Feng, S., Jiang, X., Han, G., Zhu, J., Zou, H. *J. Proteome. Res.* **2006**, *5*, 3114-3124
- (50) Lim, M., Blanford, C. F., Stein, A. *Chem. Mater.* **1998**, *10*, 467-470
- (51) Corma, A., Martinez, A., Martinez-Soria, V., Monton, J. B. *J. Catal.* **1995**, *153*, 25-31
- (52) Boissiere, C., Kümmel, M., Persin, M., Larbot, A., Prouzet, E. *Adv. Funct. Mater.* **2001**, *11*, 129-135

- (53) Beck, J. S., Vartuli, J. C., Roth, W. J., Leonowicz, M. E., Kresge, C. T., Schmitt, K. D., Chu, C. T. W., Olson, D. H., Sheppard, E. W., McCullen, S. B., Higgins, J. B., Schlenker, J. L. *J. Am. Chem. Soc.* **1992**, 114, 10834-10843
- (54) Burkett, S. L., Sims, S. D., Mann, S. *Chem. Commun.* **1996**, 11, 1367-1368
- (55) Mori, Y., Pinnavaia, T. J. *Chem. Mater.* **2001**, 13, 2173-2178
- (56) Chong, A. S. M., Zhao, X. S., Kustedjo, A. T., Qiao, S. Z. *Micropor. Mesopor. Mater.* **2004**, 72, 33-42
- (57) Han, Y., Stucky, G. D., Butler, A. J. *J. Am. Chem. Soc.* **1999**, 121, 9897-9898

Chapter 2

Direct Assembly of Large Pore Organofunctionalized Silica Mesopore Structure from Sodium Silicate and bis(2-hydroxyethyl)-3-aminopropylsilane

2.1 Introduction

In order to extend the materials applications of mesopore structures, organofunctionalized mesopore structures containing various organic groups have been studied. These materials can be tuned for specific use through the incorporation of appropriate organic moieties, such as thiol, amine, carboxylic acid, and vinyl. Consequently, organofunctionalized mesopore structure has been an important topic for research in areas, such as catalysts, and heavy metal ion trapings. Moreover, if we combined the chemical specificity of an organic group and the large porosity of a mesopore structure, it might suggest further applications, such as large biomolecule separations.

In general, two methods have been used for the synthesis of organofunctionalized mesopore structures, namely, i) grafting of organosilanes onto the surface silanol groups of a pre-assembled mesopore structure; and ii) direct assembly involving a one-step co-condensation reaction of TEOS (tetraethylorthosilicate) or sodium silicate with an organosilane.

However, the grafting method has some drawbacks. First, due to the limited number of surface silanol groups on the walls of the mesopores, the loading level of organosilanes can be restrained. Second, in a grafting

synthesis, controlling the uniformity of organofunctional group distribution within the mesostructure is very difficult. Third, because of the heterogeneous distribution of surface silanols, organosilanes cannot be fully cross-linked into the mesostructure, and thus might lead to the weak linking of the organic groups to the mesostructure. Finally, the grafting method requires more processing steps than the direct assembled pathway for organofunctionalized mesostructure synthesis.

The first direct assembly of a large pore organofunctionalized mesostructure was accomplished by Stucky *et al.* in 2000. The hexagonal structural order was maintained up to 15 mole percent incorporation of organosilane group. However, because of the strongly acidic synthesis conditions, the direct assembly pathway of SBA-15 has some drawbacks. For example, for an amine functionalized SBA-15 synthesis, the structural order was preserved up to only 5 mole percent functionalization. It was suggested that the protonated silyl amine under acidic condition could hydrogen bond with surface silanol groups of silica and this could lead to the destruction of the ordered mesostructure. In addition, the functionalization of SBA-15 with an unstable organic group in acid media, such as t-butyl carbamate (Boc), might be a problem for the direct assembly pathway. The Boc group has been known as a good protecting group under basic conditions. However, the Boc group can be hydrolyzed to an amine group under acid conditions, which can be a limitation in preparing organofunctionalized SBA-15 by the co-condensation route.

Therefore, we need another pathway to synthesize large-pore

organofunctionalized mesostructures, particularly one that can be carried out under pH-neutral condition pathway. Also, instead of costly TEOS as a silica source, a cheaper silicon source, like sodium silicate, is desirable for economic reasons. (Sodium silicate is almost 300 times cheaper than TEOS) Although sodium silicate is an economically favorable silicon source, only a few studies have been focused on the synthesis of large pore organofunctionalized mesostructures by using sodium silicate. The objective of the work described in this chapter is to the development synthetic techniques for the assembly of large pore organo-functionalized MSU-H and F silica and to overcome the limitation for the synthesis of these materials from water-soluble silicate sources.

In 2000, Pinnavaia and co-workers synthesized large pore silica mesostructures using cost-effective sodium silicate under pH-neutral conditions, designated MSU-H and MSU-F. The objective of the present work is to use this procedure to prepare, novel large pore organofunctionalized mesostructures. For the synthesis of organofunctionalized hexagonal MSU-H structures, the approach is focused on preventing condensation reaction of the organosilane itself in the presence of the water as a reaction medium. The presence of a water medium causes the organosilane to precipitate before it anchors to the mesostructured framework during direct assembly synthesis. To circumvent this problem, a non-aqueous solvent was used for the synthesis of organofunctionalized MSU-H.

In previously reported MSU-F mesostructured foam synthesis, an “oil in water” microemulsion was used as the structure-directing agent. The

microemulsion was prepared by mixing of water as a solvent, (EO)₂₀(PO)₇₀(EO)₂₀(Pluronic P123) as a surfactant, and 1,3,5-trimethylbenzene (TMB) as a co-surfactant. However, this aqueous emulsion template causes precipitation of the organosilanes itself, which results in little or no functionalization of the mesostructure. To succeed in the preparation of non-aqueous microemulsion droplets, polar organic solvent formamide has been used. This solvent has previously been used to form titania foam structures. On the basis of this approach, bis(2-hydroxyethyl)-3-aminopropyltriethoxysilane (BHAPS) functionalized derivatives of hexagonal MSU-H and mesocellular MSU-F were successfully prepared.

2.2 Experimental

2.2.1 Reagents

The non-ionic surfactant, Pluronic 123 ((EO)₂₀(PO)₇₀(EO)₂₀), was obtained from BASF for the synthesis of large pore functionalized MSU-H and MSU-F derivatives. As silicate sources, bis(2-hydroxyethyl)-3-aminopropyltriethoxysilane (BHAPS) was purchased from Gelest Inc., and sodium silicate solutions (NaOH 14%, SiO₂ 27%) was obtained from Aldrich. Glacial acetic acid and formamide were purchased from Spectrum. Absolute ethanol was purchased in-house. All the above reagents were used without further purification. Water used for the hydrolysis reaction was purified by a double-exchanged Millipore filter apparatus to remove cations and anions.

2.2.2. Synthesis of a BHAPS-functionalized hexagonal MSU-H meso-structure

The functionalized MSU-H structure was prepared by a direct assembly pathway from bis(2-hydroxyethyl)-3-aminopropyltriethoxysilane, along with cost effective sodium silicate. In order to prevent self-condensation reaction of the organosilane in the following step, ethanol was used as a solvent instead of water. Pluronic 123 (0.80g, 0.013mmole) was dissolved in glacial acetic acid (0.6g, 10mmole) and ethanol (1.3~3.5 g, 28~76 mmole). Then, BHAPS (0.605~1.85 g, 1.21~3.64 mmole) was added to the mixture at an ambient temperature. After the addition of aqueous sodium silicate (2.43 g (11.1 mmole) ~ 1.89 g (8.63 mmole) sodium silicate and 30 g H₂O (1.7mole)), the mixture was stirred at 60 °C for 1 day. The surfactant was then removed from the air-dried product by soxhlet extraction with ethanol. The overall reaction stoichiometry for obtaining the desired derivatives was in Table 2.1.

(1-x) SiO₂ : X BHAPS : 0.011 P123 : 0.81 Glacial acetic acid : 2.3~6.2 Ethanol : 138 H₂O, where x=0.1 to 0.3

2.2.3 Synthesis of BHAPS-functionalized mesocellular silica foam, MSU-F

The synthetic procedure used to prepare organofunctionalized MSU-F foam structures was similar to the one used to prepare MSU-H. In order to prepare the microemulsion template without hydrolysis while allowing for condensation reaction of the organosilane, formamide was used as a solvent.

For the preparation of MSU-F, 0.6 g (5.0 mmole) of TMB (1, 3, 5 – trimethylbenzene) was added to the surfactant solution which is prepared by mixing Pluronic 123 (0.8 g, 0.013 mmole), glacial acetic acid (0.6g, 10mmole), and formamide (11.34 g, 252 mmole). Then a microemulsion template forming, BHAPS (0.605 g, 1.21 mmole) was added to the previous solution mixture, followed by the addition of sodium silicate solution (2.43 g (11.1 mmole) sodium silicate and 30 g (1.7 mole) H₂O). The reaction mixture was allow to age at 25°C for 1 day followed by one day at 100 °C. The procedure for removing the surfactant was the same as MSU-H. The molar compositions of the reaction mixtures used to prepare the MSU-F derivatives were as follows

(1-x) SiO₂ : X BHAPS : 0.011 P123 : 0.405 TMB : 0.81 Glacial acetic acid : 10~20
Formamide : 138 H₂O, where x=0.1

Table 2.1. Reaction stoichiometries used for the supramolecular assembly of BHAPS-functionalized MSU-H silica

Mole % of BHAPS in Reaction Mixture	TEOS (mmole)	BHAPS (mmole)	P123 (mmole)	HOAc (mmole)	Ethanol (mmole)	Water (mole)	Fraction of BHAPS in final product^a
10 %	11.1	1.21	0.13	10	28	1.67	0.05
20 %	9.70	2.43	0.13	10	28	1.67	0.1
30 %	8.63	3.64	0.13	10	75	1.67	0.17

^a Determined by ²⁹Si solid state MAS NMR

2.3 Physical Characterization

The mesostructured BHAPS-functionalized hexagonal MSU-H and foam-like MSU-F were characterized by powder x-ray diffraction (XRD) analysis, nitrogen adsorption-desorption measurement, ^{29}Si solid state magic angle spinning nuclear magnetic resonance (MAS NMR) spectroscopy, and transmission electron microscopy (TEM).

Low angle X-ray diffraction patterns were obtained by a Rigaku Rotaflex Diffractometer using $\text{CuK}\alpha$ radiation ($\lambda=1.542 \text{ \AA}$). Nitrogen adsorption-desorption isotherms were taken at $-196 \text{ }^\circ\text{C}$ on a Micromeritics Tristar 3000 sorptometer. The samples were outgassed at 100°C under 10^{-6} torr for about 12 hours prior to analysis. Surface area was calculated from the BET plot according to IUPAC recommendations. The Barret-Joyner-Halenda (BJH) model was used to derive pore size distribution from adsorption branch of the isotherms. TEM images were obtained on a JOEL 2200FS instrument with an accelerating voltage of 200 kV. TEM samples were prepared by sonicating mesostructured products in ethanol for 30 minutes, which is followed by dropping of the suspension onto carbon coated copper grid. ^{29}Si solid state MAS NMR spectra were taken on a Varian 400 solid state NMR spectrometer at a 4 kHz spinning frequency with 400 seconds pulse delay.

2.4 Results and discussion

2.4.1 BHAPS - functionalized MSU-H

Powder X-ray diffraction analysis

Figure 2.1 illustrates the low angle XRD reflections for three different mole BHAPS-functionalized MSU-H mesostructures formed from reaction mixture in which 10, 20, 30% of the total silicon in the reaction mixture was in the form of BHAPS. The products were assembled from sodium silicate in the presence of a nonionic structure directing agent (P123) under near-neutral pH conditions (pH~6 or 6.5) and at different levels of BHAPS concentration. The three functionalized products exhibit (100), (110), (200) reflections consistent with hexagonal framework order. The XRD patterns are consistent with previously reported results for hexagonal MSU-H or SBA-15 structure types. Long-range hexagonal order is retained up to 30 mole percent BHAPS in the reaction mixture, as indicated by the presence of higher order d_{110} and d_{200} reflections, in addition to the d_{100} peak in the XRD patterns.

N₂ adsorption desorption isotherm

N₂ adsorption-desorption isotherms for the organofunctionalized MSU-H products formed from reaction mixture containing 10%, 20% and 30% BHAPS are shown in Figure 2.2. All three products show the well-expressed adsorption steps at a partial pressure of about 0.8, which confirms the presence of large uniform framework pores for each of these mesostructures. In addition, the shapes of adsorption and desorption hysteresis loops between partial pressure of

0.6 to 0.8 indicate the presence of well-ordered pores. Table 2.2 summarizes the physical properties obtained from the N₂ isotherms. The surface areas range from 650 ~ 720 m²/g. Pore volumes are in the range of 0.8 ~1.4 cm³/g, and pore size varied from 7.1 ~ 8.7 nm, respectively.

²⁹Si solid state MAS NMR spectroscopy

Figure 2.3 shows representative ²⁹Si MAS NMR spectra for the presence of BHAPS functionalized MSU-H silica. Resonances around -110 ppm and -102 ppm correspond to fully cross-linked Q⁴ silicon sites and to Q³ sites containing one OH terminal site group. The third peak around -70 ppm is assigned to T³ LSiO₃ centers where L is BHAPS. Also, ²⁹Si MAS NMR allows us to quantify the level of organosilane functionalization for each reaction product. The increase in the T³ band intensity in Figure 3 is correlated with the amount of the organosilane incorporated into the mesostructure. Table 2.3 provides the degree of functionalization obtained by ²⁹Si solid state MAS NMR analysis. The degree of functionalization achieved was less the level theoretically expected on the basis of the initial reaction mixture. It is assumed that some of hydroxyl group of the BHAPS organosilanes are hydrogen-bonded to PEO groups of the structure directing agents and are extracted when the structure directing agents are removed by soxhlet extraction. ²⁹Si MAS NMR analysis shows that approximately half of the initial amounts of organosilane in the reaction mixture is incorporated directly into the assembled mesostructures.

Transmission Electron microscopy (TEM)

Figure 2.4 provides the TEM micrograph for the 17% BHAPS-functionalized MSU-H product obtained from the reaction mixture containing 30% BHAPS. Even though there is a high degree of functionalization, the product exhibits a well ordered hexagonal structure. In addition, the pore size estimated from the image corresponds to the value obtained from the N₂ isotherm analysis. In the image of Figure 2.4 the dark and light contrast regions represent the pore and walls of the mesostructure, respectively.

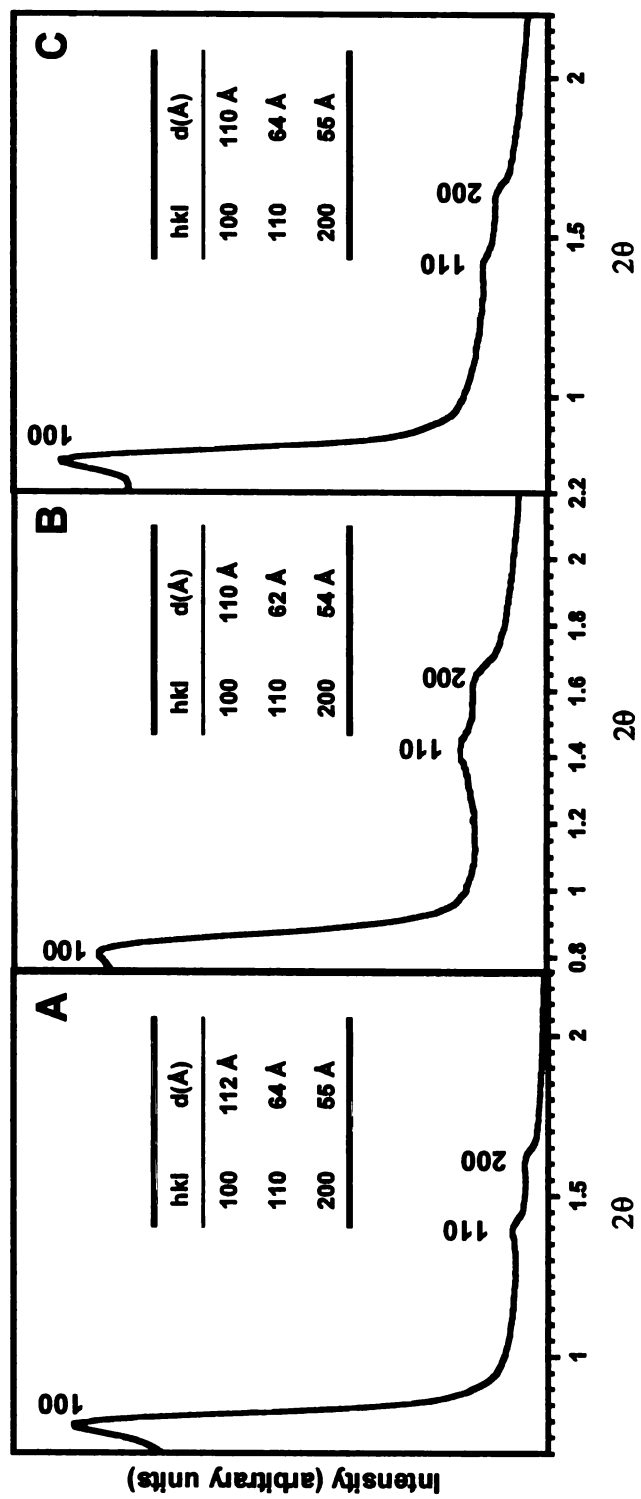


Figure 2.1. XRD spectra of BHAPS-functionalized hexagonal MSU-H samples after soxhlet extraction with ethanol. The product were formed from reaction mixture in which (A) 10%, (B) 20%, and (C) 30% of the total silicon.

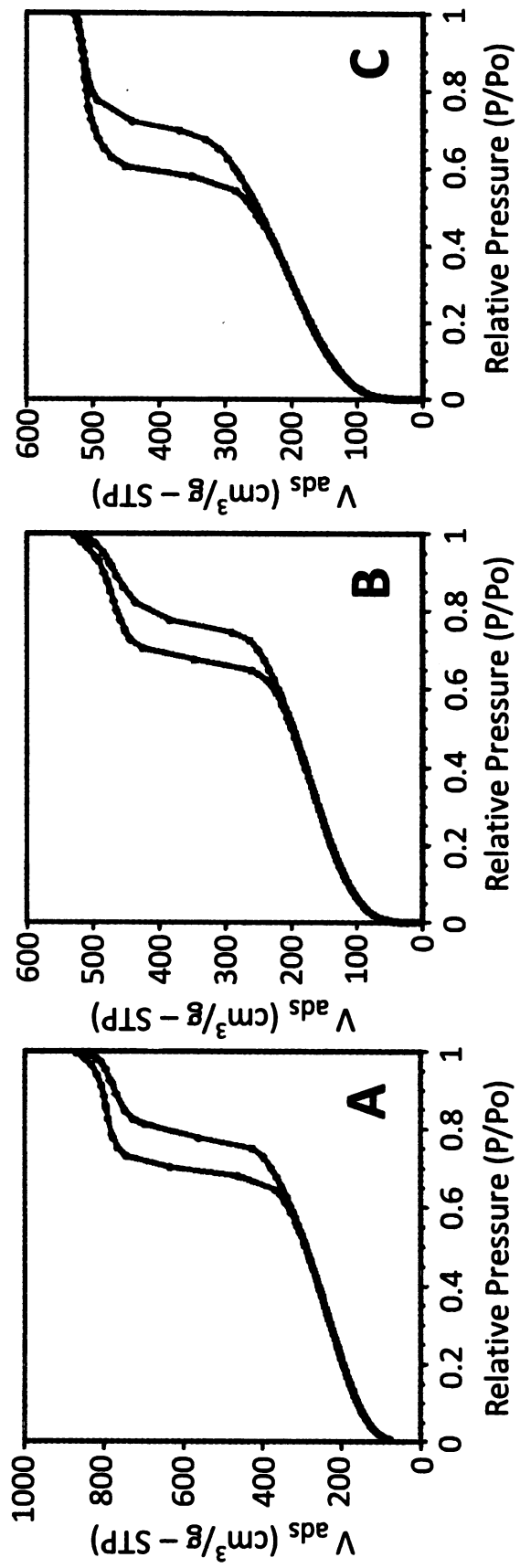


Figure 2.2. N₂ adsorption-desorption isotherm of BHAPS-functionalized MSU-H obtained from reaction mixture containing (A) 10%, (B) 20% and (C) 30% BHAPS.

Table 2.2. Textural properties of BHAPS-functionalized hexagonal MSU-H mesostructure.

Mole % BHAPS in Reaction Mixture	d spacing (nm)	Pore diameter (nm) ^a	Wall thickness (nm) ^b	Surface Area (m ² /g) ^c	Pore volume (cm ³ /g) ^d
10 %	11.2	8.7	2.5	717	1.35
20 %	11.0	8.7	2.3	520	0.82
30 %	11.0	7.1	3.9	648	0.82

^a Determined from the adsorption branch BJH model; ^b Obtained from the difference between d_{100} spacing and the pore diameter;

^c Calculated by the Brunauer-Emmett-Teller (BET) method; ^d Pore volume determined at $P/P_0=0.99$.

Table 2.3. ²⁹Si solid state NMR cross-linking parameters for BHAPS-functionalized MSU-H.

Mole % BHAPS in Reaction Mixture	Q ⁴	Q ³	T ³	Degree of functionalization ^a	Q ⁴ +T ³ /Q ³
10 %	112.2	67.5	9.6	5%	1.8
20 %	83.7	41.6	14.1	10%	2.4
30 %	747.3	298.8	211.5	17%	3.2

^a Calculated from relative intensities T₃/(Q₄+Q₃+T₃).

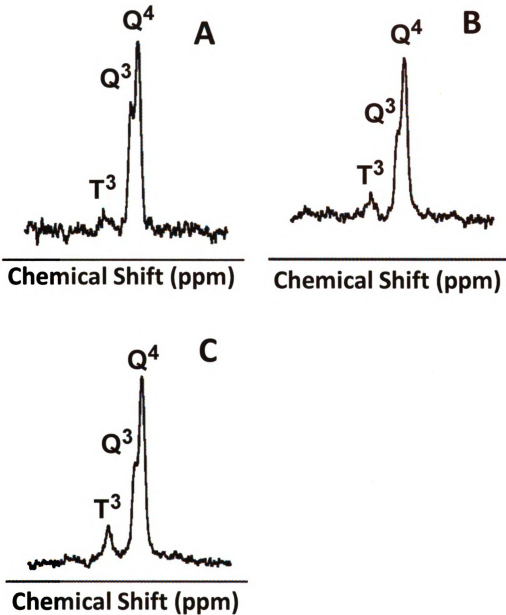


Figure 2.3. ^{29}Si solid state NMR spectra of BHAPS-functionalized MSU-H silica. The products were formed from reaction mixtures in which BHAPS represented (A) 10%, (B) 20%, and (C) 30% of the total silicon. The relative integrals of the Q^4 , Q^3 , and T^3 resonances were used to determine the amount of BHAPS incorporated into the mesostructure.

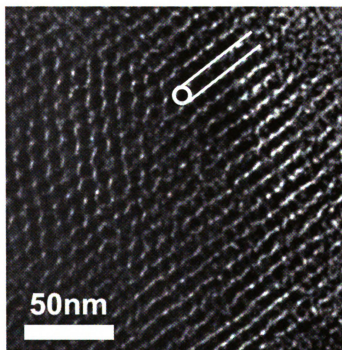
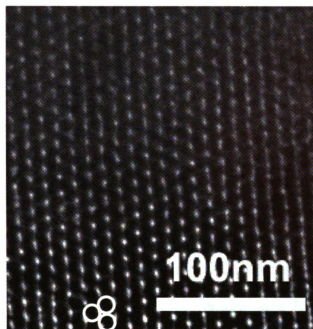


Figure 2.4. TEM images of BHAPS-functionalized MSU-H containing 17 mole % BHAPS in the pore walls. The white circles are intended to identify the pore openings.

2.4.2 BHAPS- functionalized MSU-F foam structures

N₂ isotherms

Figure 2.5 shows the N₂ adsorption-desorption isotherms for the mesocellular foam structure formed from a reaction mixture in which 10% of the silicon is in the form of BHAPS. The well-expressed adsorption step at relative pressure above 0.9 reflects the very large cell size of this material, which is about 49 nm. In addition, the derivative contains a secondary pore size centered near 14 nm. From the desorption loop, we could also calculate the window size, which is about 11 nm. The ratio of cell to window size for the primary pore structure is 4.45, corresponding to a “closed cell” foam structure. The secondary pore structure has a cell to window size of 1.3 correspond to an open cell structure. The summary of physical properties obtained from the N₂ isotherms for the mesocellular BHAPS functionalized MSU-F foam structure is in Table 2.4. The surface area is 385 m²/g and pore volume is 2.20 cm³/g, respectively.

²⁹Si solid state MAS NMR

Table 2.5 provides the ²⁹Si solid state MAS NMR for a BHAPS-functionalized mesocellular MSU-F foam formed from a reaction mixture in which 10% of the silicon was in the form of BHAPS. From this ²⁹Si solid state MAS NMR analysis, we can quantify the amount of organic moieties on mesostructures. Based on these data, we find that 7.5% BHAPS is incorporated onto the mesocellular foam walls. Thus, about 75% of the

BHAPS available in the reaction mixture is incorporated into the final reaction product.

TEM (Transmission electron microscope)

Figure 2.6 shows the TEM micrograph of 7.5% of a BHAPS functionalized MSU-F foam. The image is typical of a mesocellular foam structure. The imaged pores have a diameter of about 50 nm, which agrees with the large pore size found by nitrogen adsorption.

2.5 Conclusion

By using a non-aqueous reaction medium for direct supramolecular assembly, we successfully synthesized large pore (7 to 50 nm) and well ordered BHAPS-functionalized hexagonal and cellular foam mesostructures, denoted MSU-H and MSU-F, respectively. In the case of BHAPS-functionalized hexagonal MSU-H the use of ethanol in place of water prevents self-condensation reaction of the organosilane. Up to 17 mole percent BHAPS could be incorporated into the pore walls of the mesostructure with approximately 50% efficiency. In the organo-functionalized mesocellular MSU-F synthesis, a non-aqueous microemulsion template was formed using formamide as a solvent, (EO)₂₀(PO)₇₀(EO)₂₀ (Pluronic P123) as a surfactant, and 1,3,5-trimethylbenzene (TMB) as a co-surfactant. The resulting microemulsion was highly effective in producing a mesocellular foam containing 7.5 mole percent BHAPS in the pore walls with 75% efficiency.

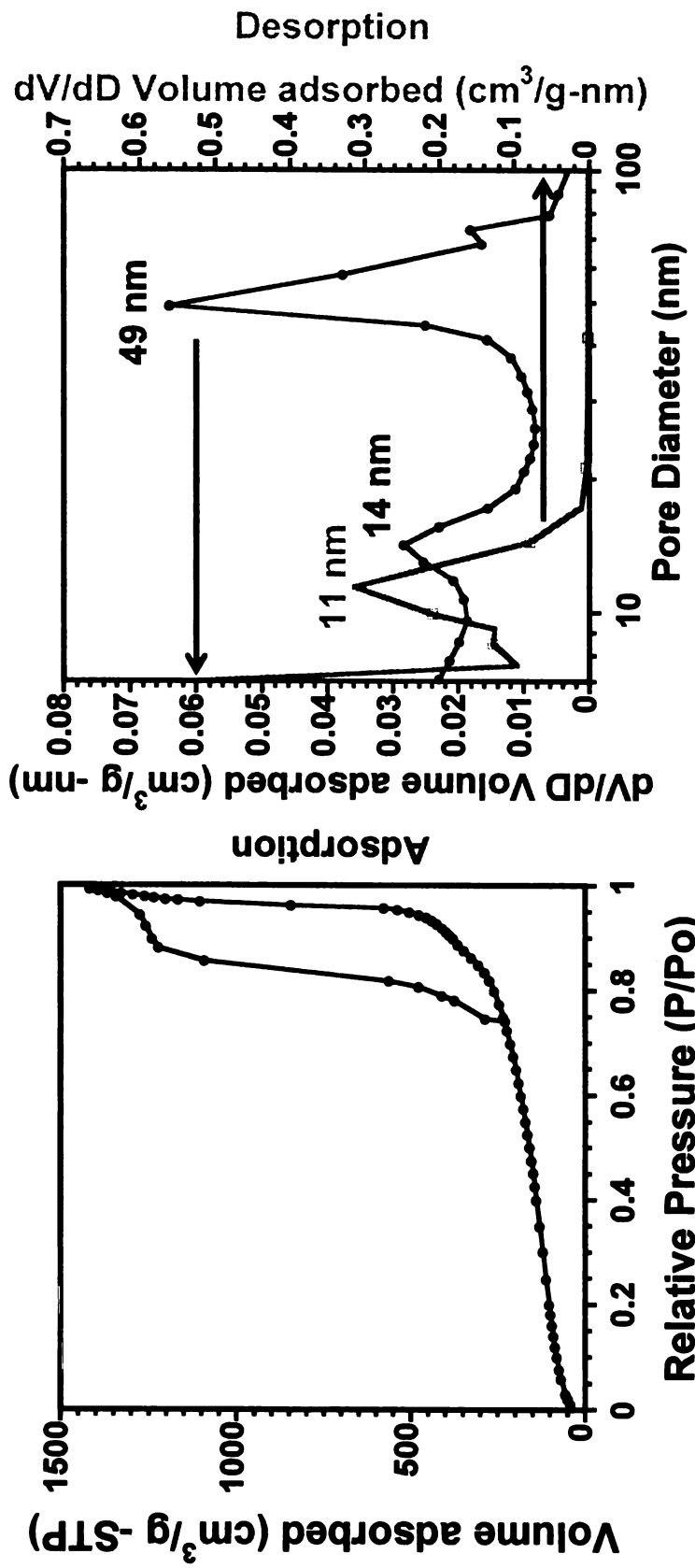


Figure 2.5. N₂ adsorption-desorption isotherm and BJH pore size distribution for 7.5 mole % BHAPS-functionalized MSU-F formed from a reaction mixture containing 10 mole % BHAPS. The pore size distributions were obtained from both the adsorption and desorption isotherms.

Table 2.4. Textural properties of BHAPS-functionalized mesocellular MSU-F foam mesostructure.

Mole % BHAPS in reaction mixture	Pore diameter (nm) ^a	Window size (nm) ^b	Surface area (m ² /g) ^c	Pore volume (cm ³ /g) ^d
10%	49, 14	11	385	2.20

a,b Determined from the adsorption branch BJH model; ^c Calculated by the Brunauer-Emmett-Teller (BET) method; ^d Pore volume determined at P/P₀=0.99.

Table 2.5. ²⁹Si solid state NMR parameters for BHAPS-functionalized MSU-F.

Mole % BHAPS in reaction mixture	Q ⁴	Q ³	T ³	Degree of functionalization ^a	Q ⁴ × Q ³ / Q ³
10%	217	53.2	21.8	7.5%	4.5

^a Calculated by $T^3 / (Q^4 + Q^3 + T^3)$; ^b Calculated by $(Q^4 + T^3) / Q^3$.

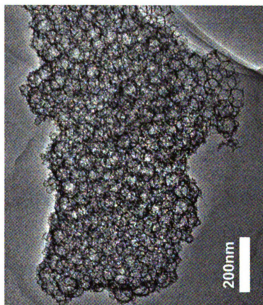
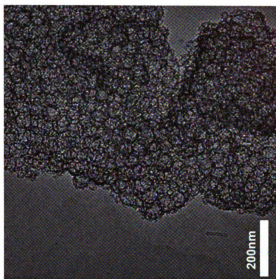


Figure 2.6. TEM images of BHAPS-functionalized MSU-F containing 7.5% BHAPS in the pore walls.

2.6 Reference

- (1) Chong, A. S. M., Zhao, X. S., Kustedjo Angeline T., Qia, S. Z. *Microporous Mesoporous Mater.* **2004**, *72*, 33-42
- (2) Fowler, C. E., Burkett, S. L., Mann, S. *Chem. Commun.* **1997**, 1769-1770
- (3) Huh, S., Wiench, J. W., Yoo, J.-C., Pruski, M., Lin, V. S. Y. *Chem. Mater.* **2003**, *15*, 4247-4256
- (4) Carvalho, W. A., Wallau, M., Schuchardt, U. *J. Mol. Catal. A* **1999**, *144*, 91-99
- (5) Corma, A., Martinez, A., Martinez-Soria, V., Monton, J. B. *J. Catal.* **1995**, *153*, 25-31
- (6) Beck, J. S., Vartuli, J. C., Roth, W. J., Leonowicz, M. E., Kresge, C. T., Schmitt, K. D., Chu, C. T. W., Olson, D. H., Sheppard, E. W., McCullen, S. B., Higgins, J. B., Schlenker, J. L. *J. Am. Chem. Soc.* **1992**, *114*, 10834- 10843
- (7) Burkett, S. L., Sims, S. D., Mann, S. *Chem. Commun.* **1996**, *11*, 1367-1368
- (8) Margolese, D., Melero, J. A., Christiansen, S. C., Chmelka, B. F., Stucky, G. D. *Chem. Matter.* **2000**, *12*, 2448-2459
- (9) Chong, A. S. M., Zhao, X. S., *J. Phys. Chem. B* **2003**, *107*, 12650-12657
- (10) Kim, S. S., Pauly, T. R., Pinnavaia, T. J. *Chem. Commun.* **2000**, *17*, 1661-1662
- (11) Kim, S. S., Karkamkar, A., Pinnavaia, T. J. *Phys. Chem. B* **2001**, *105*, 32, 7663-7670

Chapter 3

Diazo-functionalization of mesoporous silica for potential use in phosphopeptide enrichment

3.1. Introduction

As described in chapter 1, many enrichment methods, particularly immobilized metal affinity chromatography (IMAC)¹, selective adsorption on metal oxide column (TiO₂, Al₂O₃, and ZrO₂)^{2,3,4}, and immunoprecipitation of phosphoprotein by specific antibodies⁵, have been used to enhance the separation and identification of phosphorylated peptides. Among these strategies, IMAC is the most widely used technique as an enrichment method. However, nonspecific binding between the acidic carboxylate moieties in nonphosphorylated peptides and the metal cations on the IMAC column often results in low specificity and sensitivity for target phosphorylated peptides.

Recently, Tepe *et al.*⁶ invented a new type of polymer supported reagent containing α -diazo groups for phosphoprotein enrichment. This method is based on the reaction of surface immobilized α -diazo groups with the phosphate group of peptides. The resulting covalent binding between the polymer immobilized α -diazo group and the phosphorylated peptide results in improved selectivity compared with the electrostatic binding mechanism of IMAC. This general reaction scheme between immobilized α -diazo groups and phosphorylated peptides is illustrated in Figure 3.2. However, this method has a drawback.

Polymer resins are generally densely entwined and lacking in porosity and surface area. In order to improve reactions with immobilized organic groups of the polymer, the polymer should be swellable. However, in order to achieve the swollen state of the polymer during reaction, only certain solvents can be used. This limits the usefulness of polymer matrices. In order to better implement the Tepe's method for phosphoprotein enrichment, there is a need for organofunctionalized rigid framework solids having a high surface area and porosity.

During the past 15 years, mesostructured forms of silica have drawn attention in the catalyst area because of their large surface areas and uniform pore sizes.⁷ Furthermore, their surface silanol groups can be used to link metal oxides or organic groups on the pore surfaces for catalytic purposes. These same attractive physical and chemical properties of mesoporous silica are also a great attraction to overcome the weakness of polymer resins for improving phosphorylated peptide enrichment. In order to apply Tepe's method to mesostructured silicas, surface modifications by organo silanes is needed. As described previously in chapter 1 and 2, there are two approaches to the surface modification of mesostructured silica, namely the grafting method and the direct assembly method. In the grafting method⁸, specific organic groups are introduced by condensation reaction of an organosilane with the silanol groups of pre-assembled mesoporous silica. Surface modification by the direct assembly pathway⁹ is achieved by condensation reaction of an organosilane with silica precursors during supramolecular assembly process. The grafting and direct

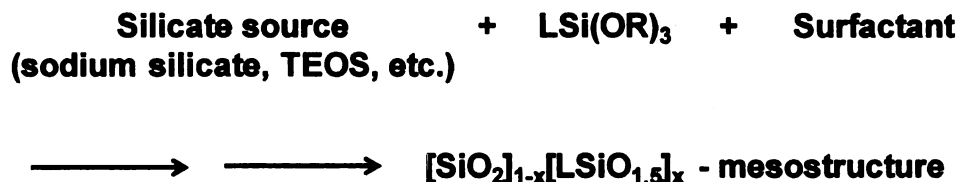
assembly pathways are represented in the following schemes (Scheme 3.1 and 3.2):

Scheme 3.1. Organosilane Grafting pathway



where L is a hydroxyl-functional organo group.

Scheme 3.2. Direct assembly pathway (co-condensation pathway)



where L is a hydroxyl-functional organo group, and x is the degree of functionalization

After modification of the mesostructured silica surfaces by organosilanes, further reactions are needed to achieve phosphorylated protein enrichment by the Tepe's method.⁶ As the first step toward diazo functionalization, fmoc-glycin is coupled to hydroxide-functionalized mesostructure through the use of 2,6-dichloro benzoyl chloride. 2,6-Dichloro benzoyl chloride is a good coupling

reagent to produce the anhydride form with fmoc-glycine, which facilitates ester bond formation between hydroxyl group on mesostructures and the fmoc-glycine. After formation of the fmoc-glycine ester on the mesostructure surfaces, a deprotection reaction of fmoc group is carried out on the fmoc group. As shown below, fluorene is a polycyclic hydrocarbon having an ionizable proton at the 9 position with a pKa of 22.6 in DMSO. Proton dissociation is facilitated by the delocalization of electron over the aromatic rings. Therefore, under base conditions, as in the presence of piperidine in DMF solvent, fmoc-glycine modified mesostructures dissociate to form 9-methylene-9H-fluorene, CO₂, and amine groups on mesostructure as shown in Figure 3.3. In addition, the 9-methylene-9H-fluorene generated in the reaction can be quantified by UV analysis, which allows determination of the amount of glycine ester immobilized on the silica surface.¹⁰

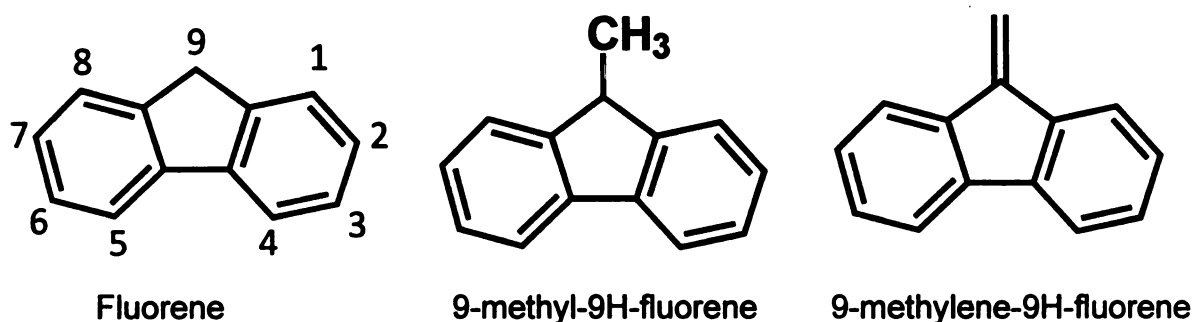


Figure 3.1. Fluorene derivatives

In the last step, HONO (nitrous acid) gas is used as the nitrosating agents for diazotization. When sodium nitrite solutions are acidified by sulfuric acid, nitrous acid is generated, which reacts with amine residues grafted to the

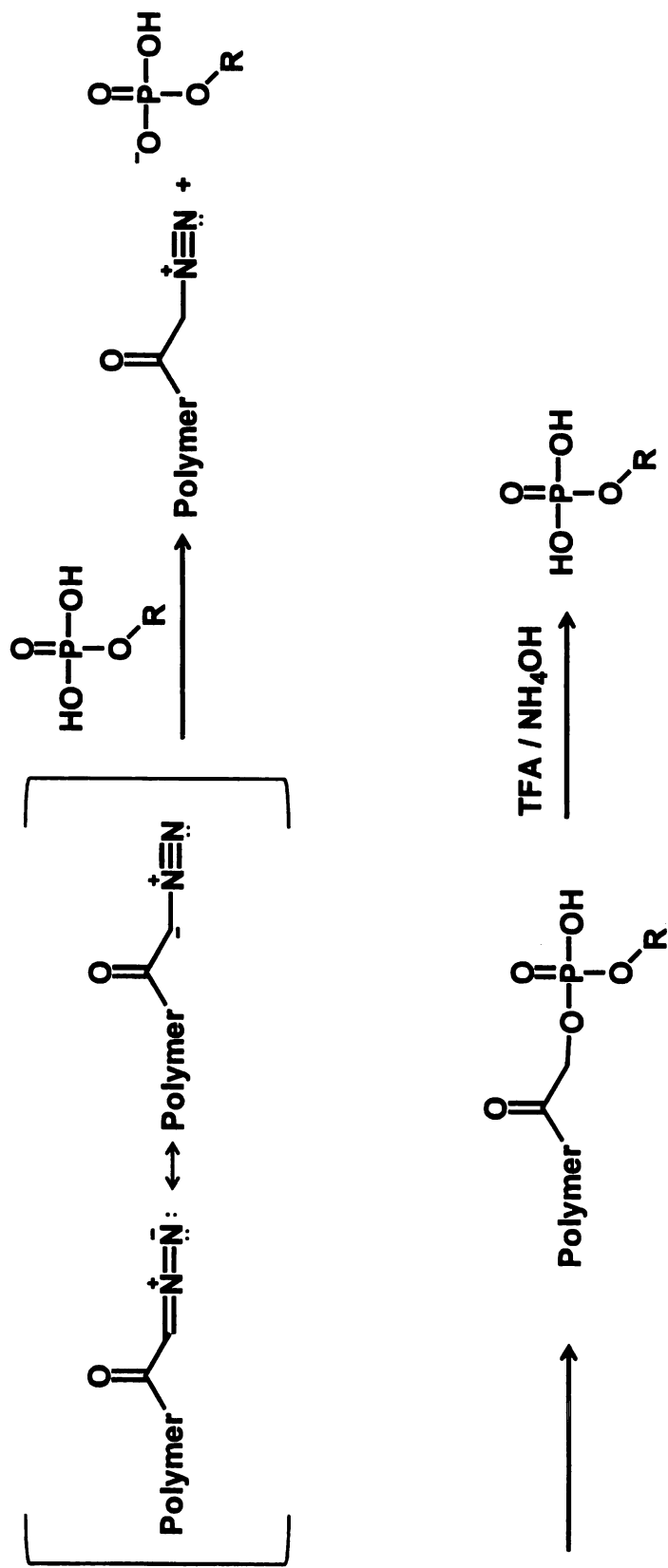


Figure 3.2. Schematic illustration of phosphorylated peptide isolation by reaction with polymer-immobilized α -diazo groups.

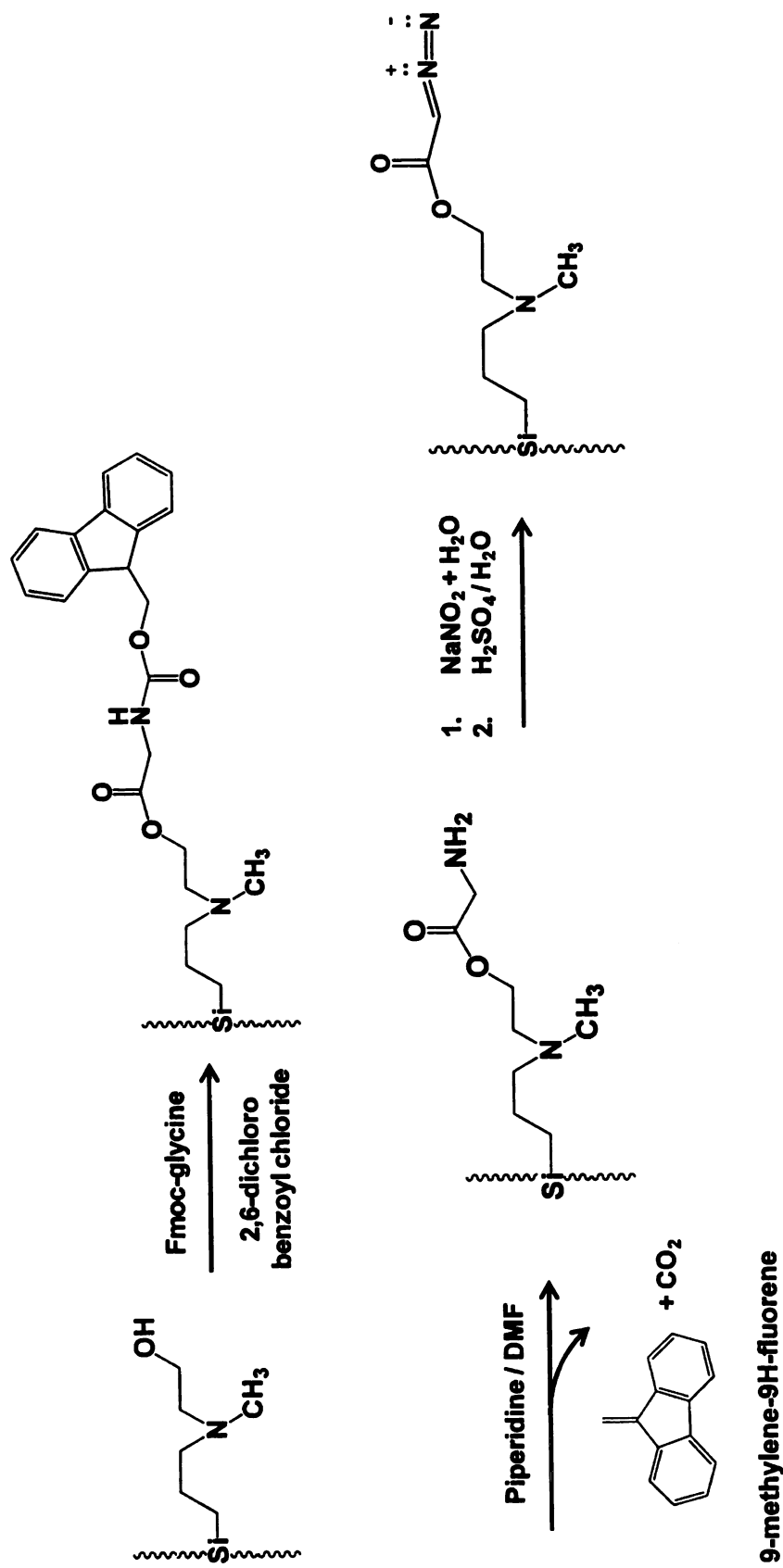


Figure 3.3. Schematic illustration of α -diazo groups synthesis on solid support.

mesostructure and generates α -diazo groups which are needed as functional groups for phosphorylated peptide enrichment applications.

In this chapter, I will describe the synthesis of large pore silica mesostructures having N-hydroxyethyl-N methyl amino groups as the precursors to α -diazo group functionalized mesostructures. I also will propose a new diazotization synthesis for large pore silica mesostructures for improved specificity and efficiency in the enrichment of phosphopeptides.

3.2 Experimental section of NHNMPTS functionalized mesostructure

The diazotization reactions on the silica surfaces were carried out on three different samples prepared either by the direct synthesis method or by the silane grafting method. The initial immobilized functional mesostructures contained 30% N-hydroxyethyl-N-methylamino-propylsilyl groups (NHNMPS) immobilized on hexagonal SBA-15 silica by grafting reaction, a 10% NHNMPTS functionalized foam-like MSU-F silica made by direct assembly, and a 30% NHNMPTS functionalized foam-like MSU-F silica made by silane grafting reaction. The surface immobilized NHNMPTS group is illustrated in Figure 3.4.

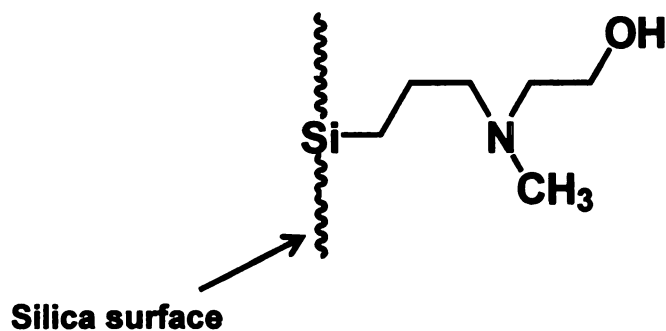
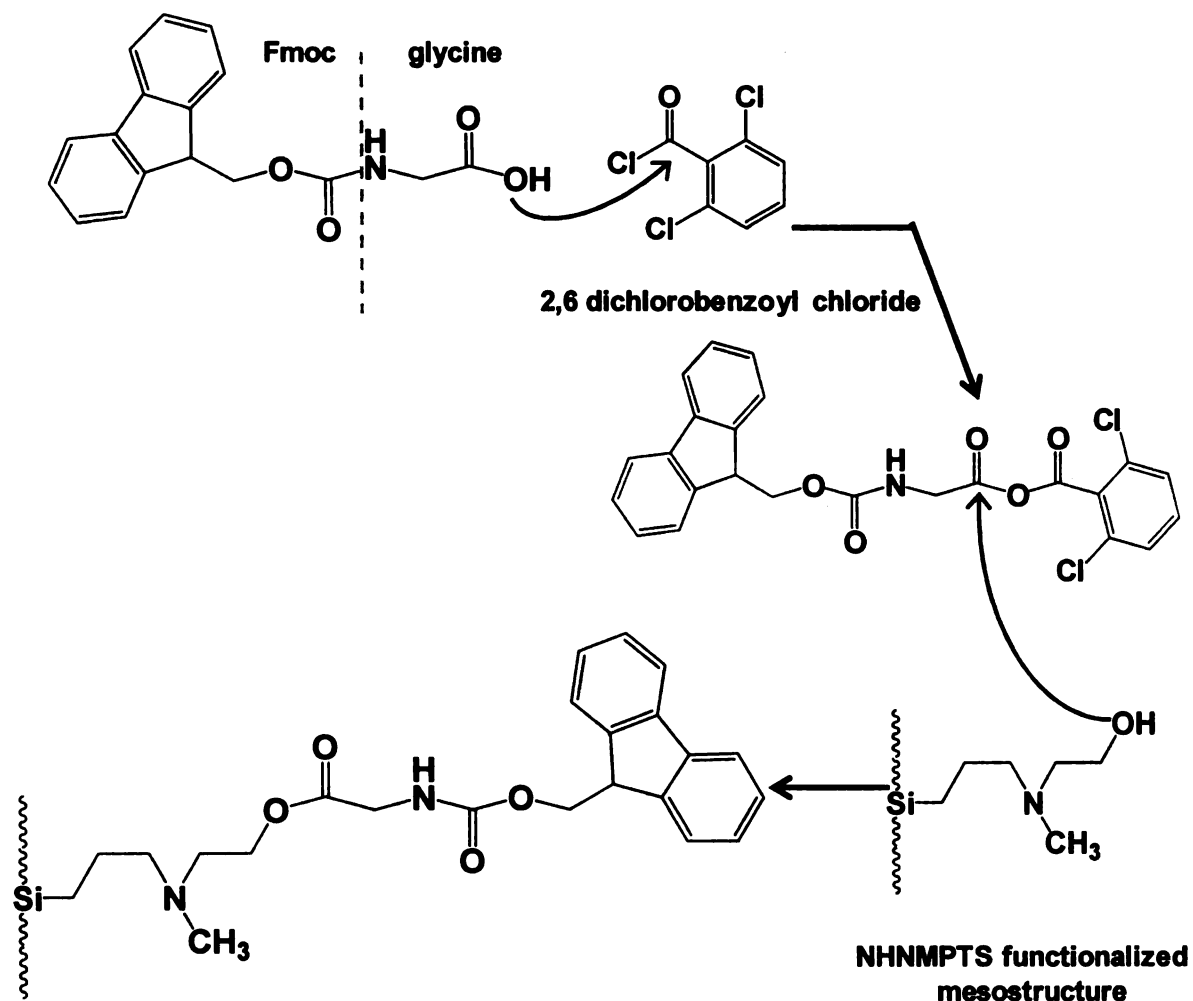


Figure 3.4. Immobilized NHNMPTS functional group on a silica surface

This functional group has a hydroxyl group at its terminal position. The hydroxyl group is a good nucleophile, which can react with the anhydride form of fmoc-glycine derivative to form the immobilized fmoc-glycine ester. The anhydride form of fmoc-glycine was prepared by in situ reaction of fmoc-glycine with 2,6-dichlorobenzoyl chloride as illustrated in the following scheme.

Scheme 3.3. The immobilization of Fmoc-glycine on mesostructure



3.2.1. Reagents

The non-ionic surfactant, Pluonic 123 ((EO)₂₀(PO)₇₀(EO)₂₀), was obtained from BASF for the preparation of large pore SBA-15 and MSU-F mesoporous silica. As an organosilicate source, N-hydroxyethyl-N-methylpropyl triethoxysilane (NHNMPTS) was purchased from Gelest Inc. The silicate sources, tetraethyl orthosilicate (TEOS, reagent grade 98%) and sodium silicate solution (NaOH 14%, SiO₂ 27%), were purchased from Aldrich. Glacial acetic acid, hydrochloric acid and formamide were obtained from Spectrum. Absolute ethanol was obtained in-house. Water used in the synthesis was obtained from a double-exchanged Millipore filter apparatus. For the diazotization synthesis, Fmoc-glycine was purchased from Fluka. 2,6-dichlorobenzoyl chloride, piperidine, and dried N,N-dimethyl formamide (DMF) were purchased from Alrich. Pyridine was purchased from Jade scientific. Dichloromethane was also purchased from Jade scientific, and was dried for the reaction. Sodium nitrite was obtained from Spectrum. All the above chemicals except dichloromethane were used without further purification.

3.2.2. 30% NHNMPTS functionalization of SBA-15 silica by grafting reaction.

The NHNMPTS functionalized SBA-15 mesoporous silica was prepared by a grafting pathway from N-hydroxyethyl-N-methylpropyltriethoxysilane. Pluronic 123 (4 g, 0.7 mmole) was dissolved in 2 M hydrochloric acid solution (120 g, 0.24 mole) and water (30 g, 1.7 mole). Then, tetraethyl orthosilicate

(8.50 g, 0.04 mole) was added to the mixture with stirring at ambient temperature. After the addition of TEOS, the mixture was stirred at 40°C for 20 hours followed by aging in an oven at 100 °C for 2 days. The surfactant was then removed by calcination at 500 °C for 4 hours. During calcination the temperature was heated to 500 °C at a rate of 2 °C/min. After the calcinations, it was cooled to room temperature in 4 °C/min decrements. The overall reaction stoichiometries used for the preparation of the SBA-15 mesoporous silica is given in Table 3.1. After pure SBA-15 silica was prepared, 0.5 g of pure SBA-15 mesoporous silica (7.7 mmol) was mixed in 15 mL toluene solvent with NHNMPTS (1.05 g, 3.3 mmol) for 3 hours at 25 °C and 4 hours at 110 °C for reflux. The 30% NHNMPTS functionalized SBA-15 material was then filtrated, washed with ethanol and dried at 25 °C.

3.2.3. 10% NHNMPTS functionalization of MSU-F silica by direct assembly method.

The direct assembly synthesis of NHNMPTS functionalized MSU-F silica was prepared by same procedure as described on chapter 2. First of all, the surfactant solution was prepared by mixing Pluronic 123 (0.8 g, 0.13 mmol), glacial acetic acid (0.6 g, 10 mmol), and formamide (11.34 g, 252 mmol). Then, 0.6 g (5.0 mmol) of TMB (1, 3, 5 – trimethyl-benzene) was added to the surfactant solution to form a micro-emulsion template. NHNMPTS (0.384 g, 1.21 mmol) was added to the micro-emulsion template solution, followed by the

addition of sodium silicate solution (2.7 g (11.1 mmol) sodium silicate and 30 g (1.7 mol) H₂O). The reaction mixture was allowed to age at 25 °C for 1 day followed by one day at 100 °C. The removal of surfactant was carried out by soxhlet extraction method using ethanol as the solvent. Table 3.1 provides the reaction stoichiometries for the preparations of NNMPTS functionalized MSU-F silica by direct assembly method.

3.2.4. 30% NNMPTS functionalization of MSU-F silica by the silane grafting method.

30% NNMPTS functionalized MSU-F silica was prepared by anchoring the NNMPTS organosilane on pre-assembled MSU-F foam silica. In the synthesis of pure MSU-F foam silica, Pluronic 123 (1.2 g, 0.206 mmol) was stirred with 1.0 M of acetic acid (10 ml, 10 mmol) and water (10 ml) until it was dissolved. To make the micro-emulsion template, TMB (1, 3, 5 – trimethylbenzene) (1.0 g, 8.3 mmol) was mixed with surfactant solution for 30 min. Then, sodium silicate solution (2.43 g (12.1 mmol) of sodium silicate and 30 g (1.7 mole) of H₂O) was added to the micro-emulsion template for making MSU-F mesostructure. The final reaction mixture was stirred for 1 day at 25 °C and kept in an oven for 1 day at 100 °C. After the reaction, this sample was filtered, dried and calcined at 500 °C for 4 hours. The surface of this calcined MSU-F silica was then functionalized by NNMPTS organosilane. This procedure of the functionalization was the same as that described for SBA-15, which was provided in section 3.2.2.

Table 3. 1. Reaction stoichiometries used for the synthesis of NHNMPTS-functionalized SBA-15, MSU-F, and MSU-F

Materials ^a	Silica source (mmole)	NHNMPTS (mmole)	P123 (mmole)	TMB (mmole)	HOAc (mmole)	HCl (mmole)	formamide (mole)	Water (mole)	Fraction of NHNMPTS in final product ^c
30 % SBA-15 (G) ^b	40	17	0.7	-	-	240	-	6.7	0.18
10 % MSU-F (D) ^b	11.1	1.21	0.13	5	10	-	0.25	2.3	0.07
30 % MSU-F (G) ^b	12.1	3.64	0.21	8.3	10	-	-	2.8	0.20

^a The percentage given in the materials designation indicated the targeted level of organofunctionalization

^b The designation "G" and "D" refer to the silane grafting and the direct assembly methods, respectively. In the case of the grafting method, organosilane amount is recalculated based on the amount of silicon source on table. (Grafting reaction is actually done by 0.5g of SBA-15 and MSU-F. The silicon source of SBA-15 is tetraethyl orthosilicate. For the functionalized MSU-F, the silica source was sodium silicate (Na₂SiO₃).

^c The observed fraction of organofunctional silicon centers in the final product was determined by ²⁹Si solid state MAS NMR spectroscopy. For example, $(T^3 + T^2)^4 / (Q^4 + Q^3 + T^3 + T^2)$

3.2.5. Diazotization of NHNMPTS mesostructures

The diazo functionalized mesostructures were obtained by a three-step route. First, esterification of the alcohol groups on the mesostructured NHNMPTS-silica surface was accomplished by reaction with the with anhydride formed from fmoc-glycine and 2,6-dichlorobenzoylchloride. In this esterification reaction, the vacuum-dried mesostructure having NHNMPTS functional groups was dispersed in DMF solvent. (100 mL DMF per mmol NHNMPTS) In a separate flask under a nitrogen atmosphere, fmoc-glycine (10 eq. per 1 eq. of NHNMPTS) was dissolved in an equal volume of dried DMF, followed by the addition of 2,6-dichlorobenzoyl chloride (10 eq). After 30 minutes, pyridine (15 eq) was added to the stirred reaction mixture and the mixture was aged for an additional 15 minutes. The resulting was transferred to the NHNMPTS functionalized MSU-F dispersed in DMF solvent, and mixture was stirred for overnight under nitrogen condition. After formation of the fmoc-glycine ester bond in the mesostructure, the fmoc protecting group was detached by the addition of 20% piperidine/DMF solution (2:8 by volume). The volume of piperidine/DMF solution was 50ml per mmonl NHNMPTS. As a last step, the amine group, on the immobilized glycine residue was diazotized by the addition of a nitrosolating agent, acidified NaNO_2 . First, sodium nitrite (4.5 g, 55 mmol) was dissolve in H_2O (10 mL). Through the use of a canula, the flask containing sodium nitrite solution was connected to a second flask containing the glycine-functionalized mesostructures (100 mg) suspended in dichloromethane (10 mL). Then, the sodium nitrite solution was purged with nitrogen gas overnight. After

being purged with nitrogen gas, 10% sulfuric acid (0.5 mL in 4.5 mL H₂O) was added to the sodium nitrite solution resulting in the generation of nitrous acid gas. The gas was transferred by canula for reaction with the amine group of the glycine-functionalized mesostructure for a period of 20-30 minutes. The actual amounts of reagents used for synthesizing α -diazo group of three different mesostructure materials are listed in Table 3.2.

Table 3.2. The amounts of reagents used in the diazotization of NHHMPTS-functionalized mesostructured silica.

Materials	Fmoc-glycine	2, 6-dichlorobenzoyl chloride	Pyridine	DMF	Piperidine/DMF	Sodium nitrite	Water	Dichloromethane (DCM)
30% NHHMPTS SBA-15 (G) – 5 g	4.82 g	3.40 g	1.93 g	76.6 g	14.0 g / 61.3 g	4.5 g	10 g	10 ml
10% NHHMPTS MSU-F (D) – 5 g	2.09 g	1.48 g	0.84 g	33.3 g	4.90 g / 26.6 g	4.5 g	10 g	10 ml
30% NHHMPTS MSU-F (G) – 5 g	4.82 g	3.40 g	1.93 g	76.6 g	14.0 g / 61.3 g	4.5 g	10 g	10 ml

3.3. Physical characterization

The physical properties of NHNMPTS-functionalized mesostructures and their derivatives were determined by reflectance-Infrared spectroscopy, UV-Vis spectroscopy analysis, ^{29}Si solid state magic angle spinning nuclear magnetic resonance (MAS NMR) spectroscopy, powder x-ray diffraction (XRD) analysis, and nitrogen adsorption-desorption analysis.

For the chemical transformation of NHNMPTS groups to diazo groups, each step was confirmed by observing the characteristic vibration of the functional groups on the mesostructure surfaces using Nicolet Protégé 400 Magna reflectance infrared spectrophotometer equipped with a Barnes analytical/spectra-tech diffuse reflectance accessory. Each spectrum was collected in the $700 - 4000 \text{ cm}^{-1}$ spectral region. The number of scan was 32 and data spacing was 1.928 cm^{-1} .

For the determination of the degree of functionalization, UV-Vis spectra in the range 200-500nm were obtained on a Hitachi U-4001 spectrophotometer. The scan speed was 300 nm/min, and the data collection interval was 0.5 nm. For the quantification of functionalization, the absorbance at 301 nm for the piperidine-dibenzylfulvene adduct formed in the reaction allowed quantification of the degree of functionalization. Samples for the UV-Vis studies were prepared by stirring 5 mg of fmoc-glycine functionalized sample in 0.4 ml dichloromethane (DCM) and 0.4 ml piperidine for 30 minutes, followed by the addition of 1.6 mL of MeOH and 7.6 mL of DCM. For the baseline correction, the reference sample was also prepared by mixing 0.4 mL piperidine, 1.6 mL MeOH, and 8 mL DCM.

In order to further verify the degree of the functionalization, ^{29}Si MAS solid state NMR was used. ^{29}Si MAS solid state NMR spectra were obtained at 79 MHz on a Varian VXR-400S solid state NMR spectrometer operating at 4 kHz spinning frequency. The pulse delay was 400 seconds, which was enough time to fully relax the magnetization of the ^{29}Si nuclei before another pulse was applied. Samples were contained in 6mm zirconia rotors. Talc was used as a chemical shift reference with a value of -98.1 ppm.

Powder XRD data were collected on a Regaku Rotaflex Diffractometer using $\text{CuK}\alpha$ radiation ($\lambda=1.542 \text{ \AA}$) generated at 45 kV and 100 mA. Data were collected from 0.7 degree to 5 degree in 0.02 degree increments.

N_2 adsorption-desorption isotherms were obtained at $-196 \text{ }^\circ\text{C}$ on a Micromeritics Tristar 3000 sorptometer. Prior to analysis the samples were degassed at $90 \text{ }^\circ\text{C}$ and 10^{-6} torr for about 12 hours. Surface area were calculated from a BET plot of the adsorption data between 0 and 0.30 P/Po. From the adsorption branch of the isotherm pore size distributions were derived by using the Barret-Joyner-Halenda (BJH) model.

3.4 Results

The N_2 adsorption-desorption isotherm and framework pore size distribution of SBA-15 silica are shown in Figure 3.6. The characteristic type IV isotherm and hysteresis loop indicates capillary condensation takes place. At a partial pressure of about 0.8, the isotherm exhibits a sharp adsorption step which is indicative of the presence of uniform cylindrical pores of 9 nm. (Figure 3.6)

Another characteristic of hexagonal SBA-15 silica is the presence of low angle reflections in the X-ray powder diffraction pattern. As shown below, a well ordered hexagonal array of pores is expected to show three major reflections, namely the (100), (110), and (200) reflections. The powder XRD pattern in Figure 3.7 contains these reflections.

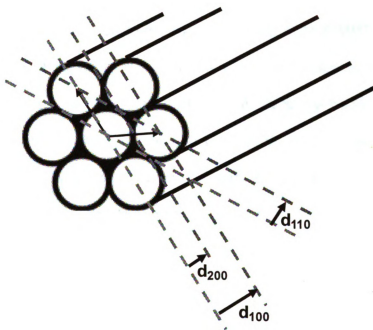


Figure 3.5. Possible low angle X-ray diffractions on hexagonal mesostructure

Figure 3.8 compares IR spectra obtained after each reaction step for the diazo functionalization of 30% NHNMPTS SBA-15 by the silane grafting method. First of all, the bottom spectrum shows the typical IR spectrum of mesoporous silica. The peak around $1000 \sim 1200 \text{ cm}^{-1}$ represents the stretching vibration of the silicon-oxygen-silicon bonds. The stretching vibration of isolated surface

silanol group occur at 3750 cm^{-1} , while the broad band centered at 3400 cm^{-1} represent the hydrogen bonding interaction between silanol groups in the mesostructure. After the NHNMPTS group has been grafted to the mesoporous silica surface, carbon-hydrogen stretching and bending vibrations appear in the spectrum. The three adsorption bands near $2800 \sim 2900\text{ cm}^{-1}$ are assigned to the stretching vibrations of the C-H centers on the NHNMPTS group. The carbon-hydrogen bending vibrations are at $1450 \sim 1550\text{ cm}^{-1}$. In next reaction step, fmoc-glycine is attached to the hydroxyl group of NHNMPTS to form fmoc-glycine ester. The reaction was confirmed by the presence of two major IR adsorption vibrations, namely, the vibration of the carbonyl bond (1730 cm^{-1}) and the bending vibration of the aromatic C-H bond (800 cm^{-1}). After the fmoc group was removed, the band below 800 cm^{-1} clearly disappeared. However, due to unexpected side reactions (like mustard gas type reactions or cyclic amide reactions which will be discussed in Chapter 4), the stretching frequency of the carbonyl group is weaker than expected. Also, because of the overlapping of the stretching bands of the hydrogen bonded O-H bonds of the silanol groups and the N-H bonds of the amine, the primary amine band at was not observed at $3300 \sim 3500\text{ cm}^{-1}$. However, the band at 1640 cm^{-1} can be assigned as the bending vibration of the N-H bond, verifying its presence. Following the diazo functionalization step a weak but clearly expressed band for the diazo group is found at 2112 cm^{-1} .

Diazo function nalization also was applied to 10% NHNMPTS functionalized MSU-F silica foam prepared by direct assembly synthesis. Due to

its large pore feature, the mesocellular foam structure can be characterized by X-ray analysis only at very low angle which makes normal Powder XRD analysis impossible. Therefore, mesocellular foam silica generally is characterized by the nitrogen adsorption-desorption isotherms and framework pore size distributions derived from the adsorption and desorption branches. As shown in Figure 3.9, the sharp adsorption step above $P/P_0 = 0.9$ is representative of the extremely large cell size of the structure. The large cell size might be caused by the formamide solvent acting as a co-surfactant. From the adsorption branch, the cell sizes of the MSU-F mesocellular foam are found to be bimodal with the dominant size at 74nm and the lesser at 15.4 nm. The window size as determined from the desorption branch is 15.4 nm. Detailed isotherm data are given in Table 3.4.

For comparison of efficiency between grafting method and direct assembly synthesis, 30% NHNMPTS functionalized MSU-F foam silica was prepared by the grafting method. The 30% NHNMPTS functionalized MSU-F foam silica also was characterized by nitrogen adsorption-desorption isotherm analysis. Figure 3.10 shows typical N_2 isotherms of a mesocellular foam structure with a 17 nm cell size calculated from the adsorption branch and 15 nm and 6 nm window sizes calculated from desorption branch. Two different window sizes can be explained by the inhomogeneity in functionalization by the grafting method. The texture properties are given in Table 3.4.

Figure 3.11 compares the IR spectra obtained after each reaction step in diazo functionalization of 30% NHNMPTS MSU-F foam silica prepared by the

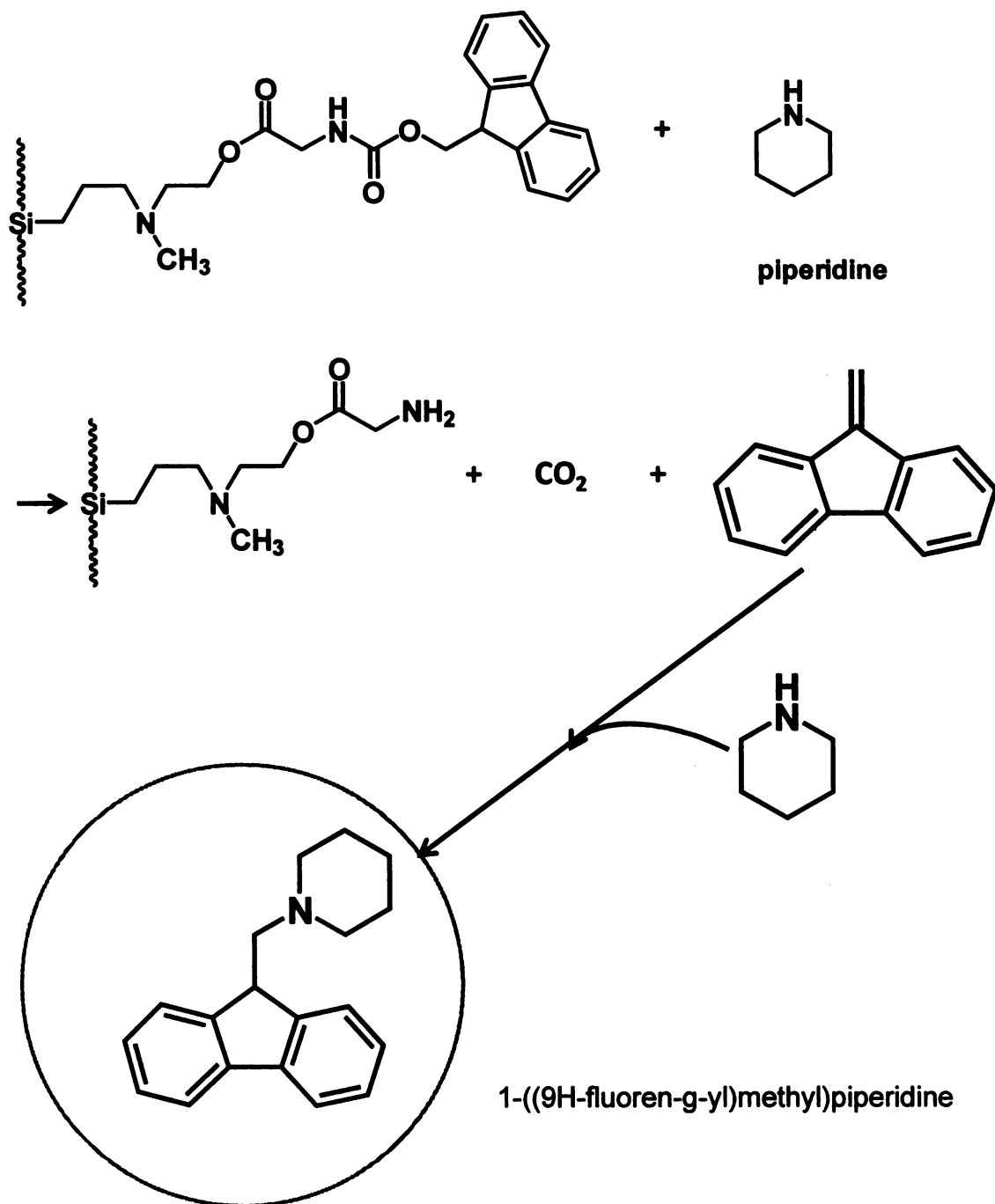
grafting method. The assignments of major IR absorption peaks for each step in the functionalization process are given in Figure 3.11. The 30% NNMPTS MSU-F silica foam shows much better IR spectral resolution than 30% NNMPTS SBA-15 prepared by the same pathway. In the spectrum for the mesostructure having attached fmoc groups, the intensity of the carbonyl vibration is much stronger than that of functionalized SBA-15. Also, this spectrum shows the aromatic C-H vibration at 3050 cm^{-1} which was not found for the SBA-15 derivative. After deprotection of fmoc group, the IR spectrum still shows the sharp carbonyl stretching vibration at 1740 cm^{-1} , while the corresponding 30% NNMPTS SBA-15 did not. Presumably, the larger pore mesocellular foam silica derivative has a high degree of organo-functionalization than hexagonal SBA-15. A more detailed discussion of the degree of functionalization will be provided later along with ^{29}Si solid state MAS NMR data. In Figure 3.11, the diazo vibration at 2110 cm^{-1} and the carbonyl vibration at 1740 cm^{-1} are clearly evident. These bands verify the successful diazo functionalization of the structure.

In order to use the high surface area and large pore volumes of diazo functionalized SBA-15 and MSU-F materials for the future proteomic applications, the accessibility of the framework pore structure after diazo functionalization is very important. In order to determine mesoporosity, the nitrogen adsorption-desorption isotherms for the following three samples were collected, namely 30% NNMPTS MSU-F made by grafting method, the 30% glycine functional derivative, and the 30% diazo derivative. As shown in Figure

3.12, diazo functionalized MSU-F retains an isotherm typical of mesocellular foam silica structures with a high surface area and a large framework pore structure. However, in comparison with the 30% NHNMPTS, there was some loss of pore volume, which may be caused by two possible reasons. Some amount of degradation may occur for the pore structures during synthesis, particularly through the use of the base, piperidine. The pore volume is inversely related to the weight of the sample. Therefore, increased weight caused by organofunctionalization contributes to a lowering of the specific pore volume.

As shown in table 3.5, the degree of functionalization was determined by ^{29}Si solid state MAS NMR and UV analysis after fmoc titration. From ^{29}Si solid state MAS NMR analysis, we can quantify the fraction of organo-functional silicon centers in the silica mesostructure. The ratio of organic groups to the total amount of silicon species provides the degree of functionalization, upon NHNMPTS functionalization at the initial reaction stage. However, fmoc titration method, as followed by UV-Vis analysis, shows the degree of functionalization at a different reaction step. In this reaction step fmoc groups are removed from the mesostructure using 20% piperidine/DMF, resulting in glycine-functionalized MSU-F. The piperidine also generates 9-methylene-9H-fluorene and carbon dioxide as a side product. In this process, this 9-methylene-9H-fluorene reacts with extra piperidine in the DMF solution and forms 1-((9H-fluoren-9-yl)methyl)piperidine (piperidine-dibenzylfulvene adduct) which is UV-active at 301 nm. The fmoc deprotecting process and the analyte for UV analysis are illustrated in the following reaction schemes. (Scheme 3.4)

Scheme 3.4. Fmoc deprotecting process and analyte for UV analysis



For the determination of the degree of functionalization by fmoc titration, the concentration of fmoc was calculated using Beer's law:

$$\text{Absorbance} = \text{molar absorbance (7800 mol}^{-1} \text{ cm}^{-2}) \times \text{concentration of absorbing material} \times \text{cell length(1 cm)}$$

Table 3.3. UV analysis data from fmoc titration and their deprotected fmoc concentration by UV analysis

Sample	Absorbance	Concentration (mmole/g)
30% NHNMPTS SBA-15 (G)	1.000	0.26
10% NHNMPTS MSU-F (D)	0.072 (16 times diluted)	0.30
30% NHNMPTS MSU-F (G)	0.131 (16 times diluted)	0.53

A plot of absorbance versus molar concentration will be straight line because molar absorbance and cell length are constant values. In reality, the plot is not linear over the entire concentration range, particularly beyond an absorbance of 1.0. Therefore, for the better accuracy, the concentrations of fmoc from the 10% NHNMPTS MSU-F (D) and 30% NHNMPTS MSU-F (G) samples were calculated using a 16 fold dilution of the deprotection solution.

3.5 Conclusion

In this experiment, I reported diazo-functionalized mesostructured silica for potential use in proteomic analysis have been successfully synthesized. However, as revealed by IR spectral analyses, the degree of diazo functionalization is still low compared to the initial degree of NHNMPTS functionalization obtained by grafting or direct assembly synthesis (see Table 3.6). In order to increase the level of diazo functionalization, here is some aspect to consider for the preparation of functional mesostructure materials.

Grafting and direct methods

On the basis of the NMR and UV-VIS analytical data for the 10% NHNMPS MSU-F sample made by the direct assembly method and for the 30% NHNMPS MSU-F made by silane grafting synthesis (c.f., Table 3.6), we conclude that the methods result in formation of products in which 8 % and 20 % of the silicon centers are actually functionalized. Thus, the grafting method is less efficient than direct assembly in providing functionalized derivatives. It is likely that the organosilane used in grafting synthesis are not evenly distributed on the surface and are clustered in domain rich in NHNMPTS group. Under these condition steric constraints will lead to low level of fmoc glycine coupling. Direct assembly pathway is the best synthesis method to prepare a functionalized mesostructure for better efficiency. But efforts to increase the level of NHNMPTS functionalization to values greater than 10% did not provided foam mesostructures.

30%

by

ha

fr

tw

nr

hi

di

30% NHNMPS SBA-15 (grafting) and 30% NHNMPS MSU-F (grafting)

The NMR data in Table 3.5 shows that 30% NHNMPS SBA-15 prepared by the grafting method and 30% NHNMPS MSU-F prepared by grafting method have similar degrees of functionalization. However, the UV-VIS data for the fmoc-glycine derivatives show the large pore MSU-F (74 nm pore size) to have twice the functionalization than the relatively small pore SBA-15 derivative (10 nm pore size). Therefore, large pore mesostructures are the best candidates for higher degree of functionalization, probably because they allow more uniform distribution of functional groups on the silica surface.

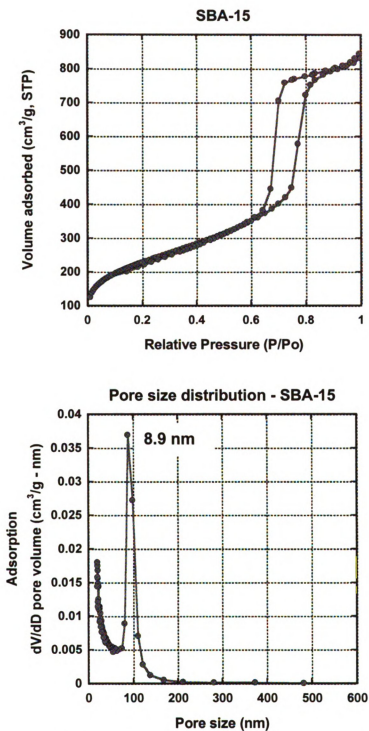


Figure 3.6. N_2 adsorption-desorption isotherms and BJH pore size distribution for SBA-15 silica calcined at 500 °C as determined from the adsorption isotherm.

XRD of SBA-15

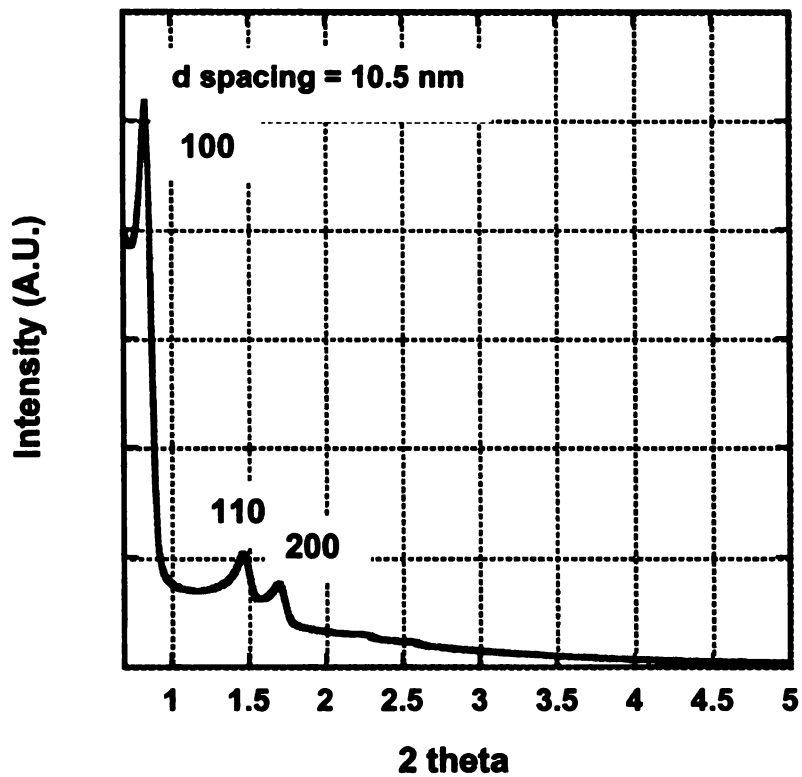


Figure 3.7. Powder X-ray diffraction pattern for calcined SBA-15 silica.

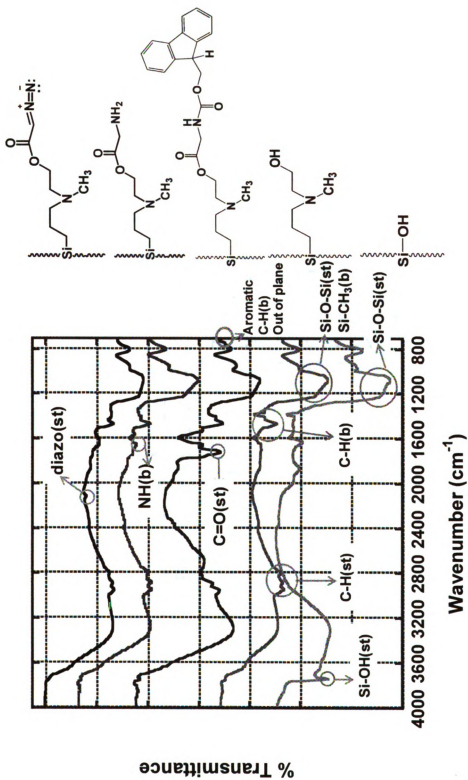


Figure 3.8. IR spectra obtained after each reaction step for the diazo functionalization of 30% NHMPTS SBA-15 by the silane grafting method.

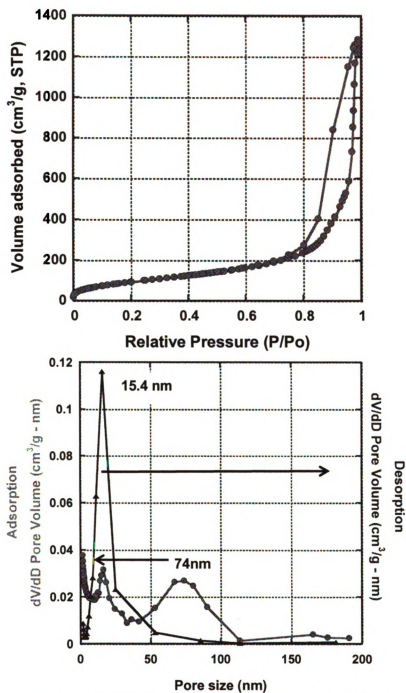


Figure 3.9. N₂ adsorption-desorption isotherm for 10% NMNMPMS functionalized MSU-F prepared by direct assembly and the BJH pore sizes distribution obtained from the adsorption and desorption isotherms.

Table 3.4. Textural properties of NHNMPPTS functionalized mesoporous materials determined from N₂ adsorption isotherm.

Sample	Pore diameter (nm)	Surface area (m ² /g)	Pore volume (cm ³ /g)
30% NHNMPPTS SBA-15 (G)	8.9	825	1.31
10% NHNMPPTS MSU-F (D)	74, 15.7 (15.4)	338	1.99
30% NHNMPPTS MSU-F (G)	17 (6.0, 15)	415	1.62

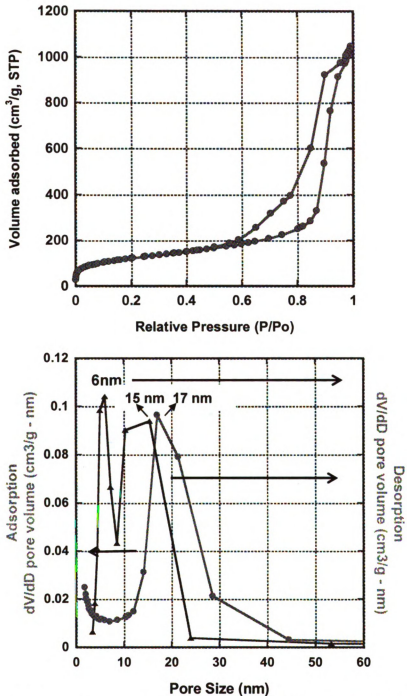


Figure 3.10. N₂ adsorption-desorption isotherms for 30% MNMPTS functionalized MSU-F prepared by grafting method and the BJH pore sizes distribution obtained from the adsorption and desorption isotherms.

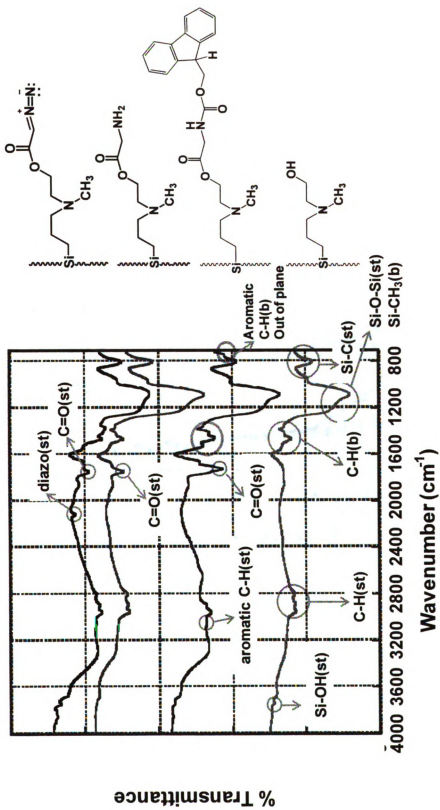


Figure 3.11. IR spectra obtained after each reaction step in the diazo functionalization of 30% NHHMPTS MSU-F by the silane grafting method.

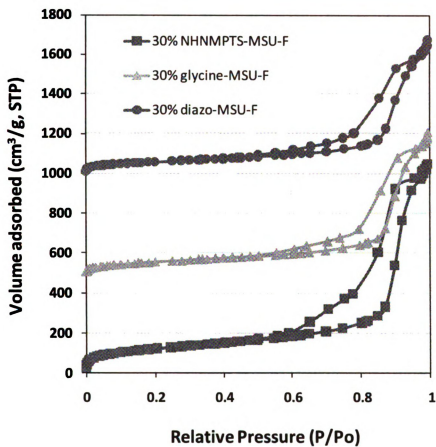


Figure 3.12. Comparison of N₂ adsorption and desorption isotherms for 30% NHHMPTS functionalized MSU-F, glycine-functionalized MSU-F, and diazo functionalized MSU-F silica. The isotherms are offset by 500 cm³/g for clarity.

Table 3.5. Integral intensity of resonances observed in the ^{29}Si solid state NMR of NHNMPPTS-functionalized mesostructures.

Sample	Q^4	Q^3	T^3	T^2	Degree of organo functionalization ^a
30% NHNMPPTS SBA-15 (G)	380	115	87	18	18 %
10% NHNMPPTS MSU-F (D)	400	217	57	-	8 %
30% NHNMPPTS MSU-F (G)	561	309	192	20	20 %

^a Give the formula used to obtain these data. For example, $(T^3 + T^2) / (Q^4 + Q^3 + T^3 + T^2)$.

Table 3.6. Degrees of NHNMPPTS functionalization determined by solid state NMR and UV analysis of Fmoc titration.

Sample	% functionalization determined by Solid state NMR analysis before fmoc attachment	Organo concentration determined by fmoc titration (mmole/g)	Verification of diazo functionalization by Infrared spectroscopy
30% NHNMPPTS SBA-15 (G)	18% (2.2 mmole/g) ^a	0.26	Yes
10% NHNMPPTS MSU-F (D)	8% (1.2 mmole/g) ^a	0.30	Yes
30% NHNMPPTS MSU-F (G)	20% (2.4 mmole/g) ^a	0.53	Yes

^aThe values in parentheses are the concentrations of immobilized organic moieties per gram of samples, which are based on the degrees of functionalization obtained by ²⁹Si solid state NMR data. First, the formula weight was calculated for (SiO₂)_{1-x}(LSiO_{1.5})_x, (where x is the degree of functionalization, and the moles of immobilized organic group per mole of sample was determined.) Then, this mole of immobilized organic group was divided by the formula weight of the sample to obtain the concentration of immobilized organic moiety.

3.6 Reference

- (1) Andersson, L., Porath, J. *Anal Biochem* **1986**, *154* 250-254
- (2) Sano, A., Nakamura, H. *Anal. Sci.* **2004**, *20*, 565-566
- (3) Kweon, H. K., Hakansson, K. *Anal. Chem.* **2006**, *78*, 1743-1749
- (4) Wolshin, F., Wienkoop, S., Weckwerth, W. *Proteomics* **2005**, *5*, 4389-4397
- (5) Pandey, A., Podtelejnikov, A. V., Blagoev, B., Bustelo, X. R., Mann, M., Lodish, H. F. *Proc. Natl. Acad. Sci* **2000**, *97*, 179-184
- (6) Lansdell, T. A., Tepe, J. J. *Tetrahedron Lett.* **2004**, *45*, 91-93
- (7) Corma, A., Martinez, A., Martinez-Soria, V., Monton, J. B. *J. Catal.* **1995**, *153*, 25-31
- (8) Beck, J. S., Vartuli, J. C., Roth, W. J., Leonowicz, M. E., Kresge, C. T., Schmitt, K. D., Chu, C. T. W., Olson, D. H., Sheppard, E. W., McCullen, S. B., Higgins, J. B., Schlenker, J. L. *J. Am. Chem. Soc.* **1992**, *114*, 10834- 10843
- (9) Burkett, S. L., Sims, S. D., Mann, S. *Chem. Commun.* **1996**, *11*, 1367-1368
- (10) Chan, W.C., White, P.D. *In Fmoc Solid Phase Peptide Synthesis – A Practical Approach*, Oxford University Press, New York. **2000**, 62-63

Chapter 4

Improved Diazo-functionalization of mesoporous silica and the preparation of an IMAC-type mesoporous silica for potential use in phosphopeptide enrichment

4.1. Introduction

In the last chapter, three NHNMPTS functionalized mesoporous silicas and their diazotization reactions have been discussed. However, a few questions have been arisen from the research presented in the last chapter. First of all, there was a big difference between the degree of functionalization based on the initial reaction rate and the amount of surface functional group detected by UV analysis. Also, as mentioned in Chapter 3, an unexpected loss in carbonyl band intensity in the IR spectrum was observed after the deprotection of the fmoc group. The purpose of this chapter is to investigate possible reasons for these observations and to examine other approaches to diazotized mesoporous materials with an improved degree of functionalization. Also, a new IMAC type of mesoporous silica for potential use in phosphopeptide enrichment is described.

In Chapter 3, we determined the degree of organo-functionalization by two instrumental analyses techniques, namely, ^{29}Si solid state NMR and UV analysis. However, there was a big difference in the results provided by these two techniques. For example, the actual degree of functionalization for formally 10%

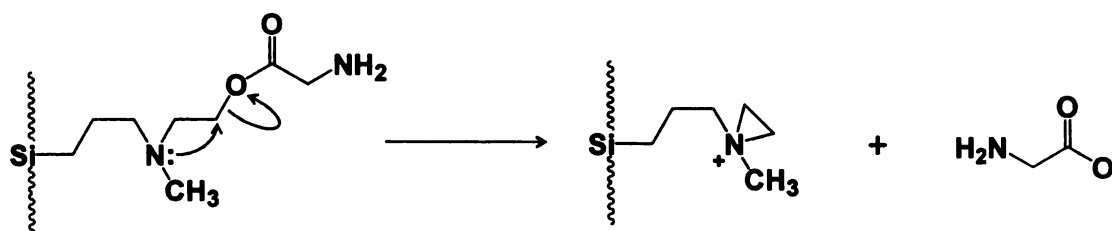
NHNMPTS MSU-F silica foam by direct assembly synthesis was 8%, as determined by solid state NMR. This level of functionalization corresponds to 1.2 mmole/g. However, the concentration of functional group on the mesostructure surface was found to be only 0.3 mmole/g by UV-VIS analysis of the fmoc groups liberated from the mesostructure surface. Generally ^{29}Si solid state NMR analysis distinguishes and quantifies the types of silicon centers. The resonances of immobilized organosilane centers having Si-C bonds can be distinguished from SiO_4 silicon centers and the fraction of each type of center can be quantitatively determined by integration of the resonance lines, provided that the delay time between pulses allows for the complete relaxation of the nuclei. This measurement shows how much organic moiety is incorporated onto the mesostructure surface.

For fmoc titration by UV analysis^{1,2}, the fmoc groups initially react with the OH functional groups on mesostructure surface, as shown in the scheme on page 57 in Chapter 3. Upon complete reaction, as shown on page 74 in Chapter 3, the reaction residues, 9-methylene-9H-fluorene and carbon dioxide, are generated through deprotect of the fmoc group. During this process, the 9-methylene-9H-fluorene residue reacts with excess piperidine, and produces 1-((9H-fluoren-9-yl) methyl) piperidine (piperidine-dibenzylfulvene adduct), which can be quantified by UV-Vis spectroscopy. This measurement determines how much organic moiety is actively participating in the diazotization reaction. Therefore, through comparison of the solid state NMR data and UV-VIS fmoc titration data, we can determine all the hydroxyl ethyl functional groups on the

silica surface that do not participate in the organo-functionalization reaction. This allows us to conclude that some of the terminal hydroxyl functional groups of NHNMPTS interact with the silica framework or is embedded into the framework, which leads low accessibility toward other organic reagents.

We also anticipated a potential problem in losing an undesirable amount of carbonyl species during deprotection of the fmoc group. As shown in Figure 3.8, the intensity of the 1730 cm^{-1} carbonyl stretching band for the fmoc group attached to the surface of MSU-F silica (third spectrum, two carbonyl group) is much stronger than that of the fmoc deprotected MSU-F silica product (fourth spectrum, one carbonyl group). There are a few possible explanations for this observation. First of all, the nonbonding electrons on the nitrogen atom may participate in a cyclization reaction leading to the elimination of the glycidyl groups, as shown on below:

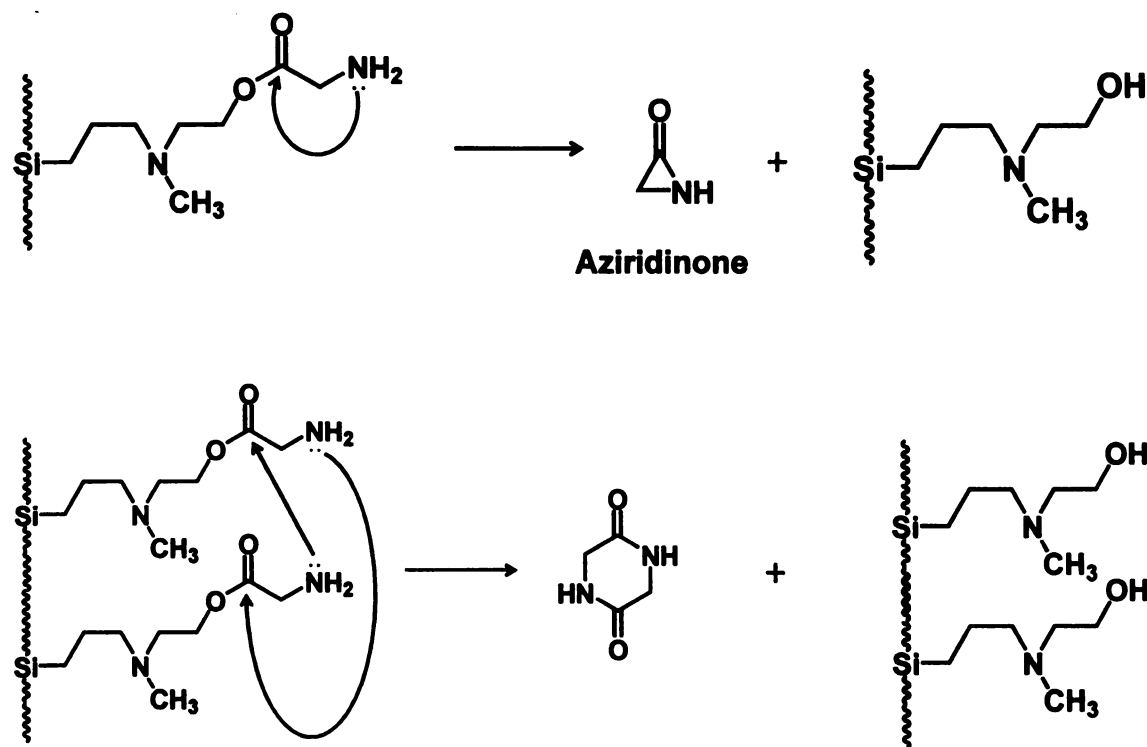
Scheme 4.1. Elimination of Glycidyl group by cyclization reaction



A similar type of cyclization reaction, called the mustard gas reaction³, has been observed at a sulfur center. Owing to this type of side reaction, we might lose more glycidyl groups than we expected.

A second possible complicating reaction that may occur on the mesostructure surface involves an internal nucleophilic cyclization to form an aziridinone species.⁴ Also, due to the strain of the three membered aziridinone ring, a more likely reaction is the formation of a dimer by cross reaction between two functional groups. The possible reactions are represented in the following schemes.

Scheme 4.2. Possible elimination mechanism of glycidyl group by nucleophilic cyclization



In order to circumvent the potential problems associated with the above reactions, two other organosilanes have been selected for the preparation of

diazo-functionalized mesoporous silica materials, namely (3-glycidoxypropyl) trimethoxysilane, and p-aminophenyltrimethoxysilane.

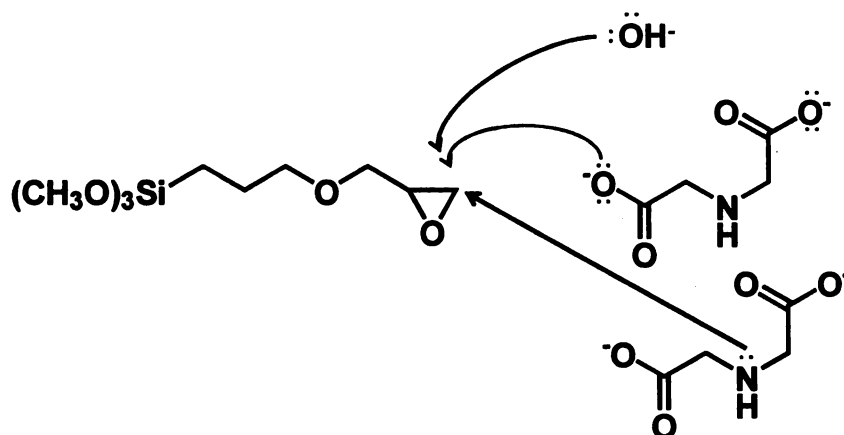
The (3-glycidoxypropyl) trimethoxysilane molecule has an epoxide ring at its terminal position, which should make it less likely to embed itself in the walls of a silica mesostructure in comparison to NHNMPTS. However, to serve as a precursor for diazotization the epoxy ring needs to be opened to generate a nucleophilic OH center.

With a p-aminophenyltrimethoxysilane, the phenyl group is hydrophobic and less likely to become embedded in the hydroxylated walls of the mesostructure. Thus more of the NH₂ groups may be accessible for diazotization. Also, the amine groups can directly react with nitrous acid to easily form a diazo functionality.

So far we have considered new diazo functionalized silica for the potential use in phosphorylated peptides separation. However, IMAC is still one of the most powerful tools for phosphorylated peptide enrichment at the present time. Recently, Zou *et al.*⁵ reported the enrichment of phosphopeptide by a MCM-41 silica that mimicks an IMAC column. He functionalized the MCM-41 silica by grafting reaction of a (3-glycidoxypropyl) trimethoxysilane that had been coupled to a metal chelating agent, namely iminodiacetic acid. However, the coupling of the iminodiacetic acid to the (3-glycidoxypropyl) trimethoxysilane looked very difficult. For the preparation of the organosilane, the solid iminodiacetic acid was dissolved in water, followed by an adjustment of the pH to 11 with sodium hydroxide. Then, this solution is mixed with (3-glycidoxypropyl) trimethoxysilane

very slowly at low temperature to limit hydrolysis of the alkoxide groups on silicon and the polymerization of the organosilane. The hydroxide anion, the carboxylate oxygen from iminodiacetic acid, and the nitrogen from iminodiacetic acid can compete for reaction with the epoxide group, whereas only the nitrogen from iminodiacetic acid is the desired nucleophile. Possible nucleophilic attack of (3-glycidoxypropyl) trimethoxysilane by the three competing centers is illustrated below. The two competing reaction by OH^- and the carboxylate oxygen centers at low iminodiacetic acid concentration is likely to lead to low yields of the desired iminodiacetic acid functionality.

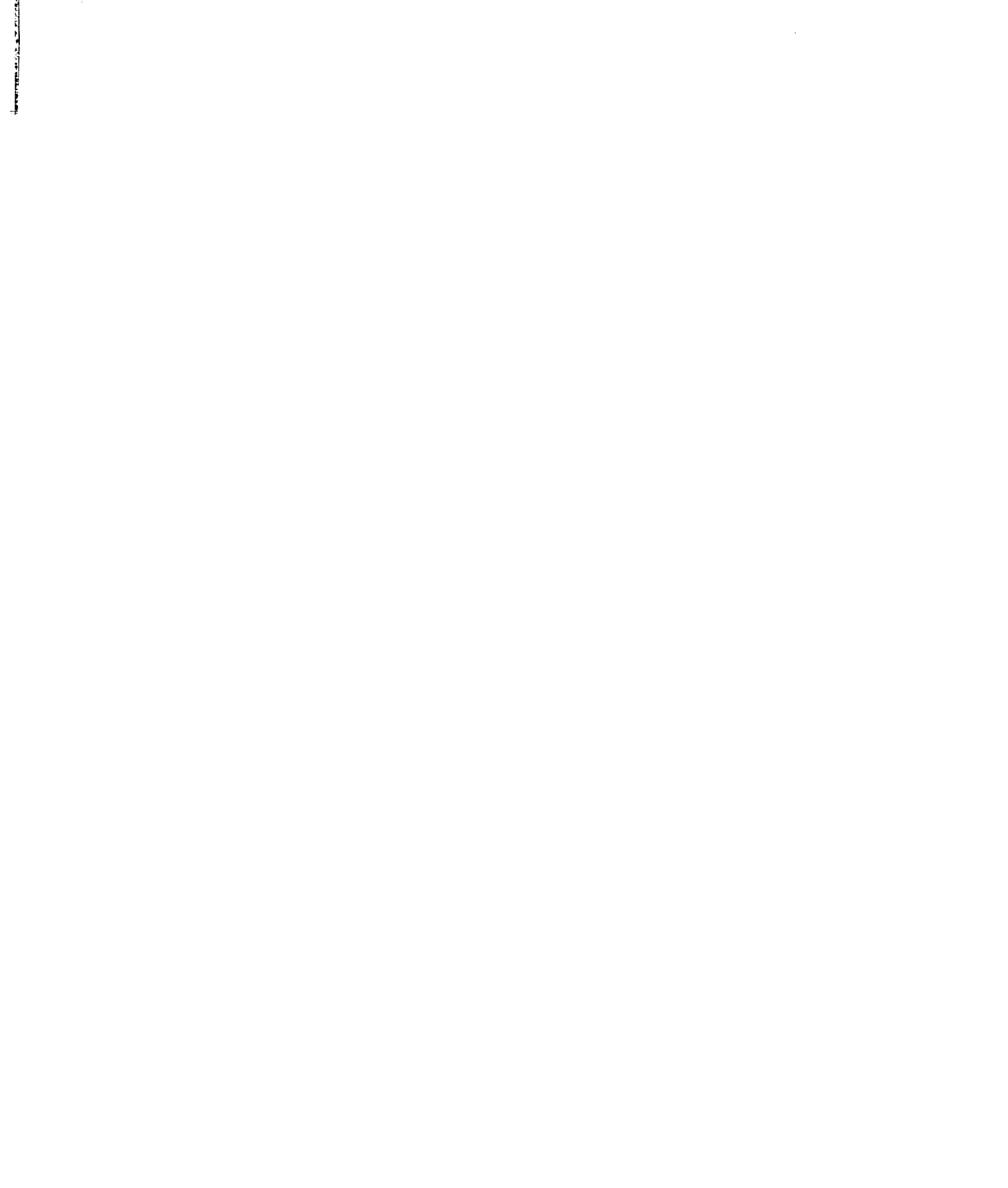
Scheme 4.3. Nucleophiles which possibly react with terminal epoxide group



This chapter examines a new pathway for the preparation of an IMAC type large pore mesoporous silica material for potential use for phosphorylated peptide enrichment.

4.2 Experimental

4.2.1 Reagents



The structure directing agent, Pluonic 123 ((EO)₂₀(PO)₇₀(EO)₂₀) was obtained from BASF for the preparation of large pore MSU-F mesoporous silica. As organosilane sources, (3-glycidoxypropyl)trimethoxysilane (GPTS), p-aminophenyltrimethoxysilane (APTS), and 3-(triethoxysilyl)propylsuccinic anhydride (SATS,95%) were purchased from Gelest Inc.. The silicate source, sodium silicate solution (14% NaOH, 27% SiO₂ by weight), was obtained from Aldrich. Lithium aluminum hydride (LiAlH₄) in tetrahydrofuran (1.0 M), dichloromethane, and tetrahydrofuran (THF) were also purchased from Aldrich. The dichloromethane and tetrahydrofuran were dried by use of a Solvtek drying kit. Glacial acetic acid, hydrochloric acid, perchloric acid, dried methanol and dried formamide were purchased from Spectrum. Dimethyl sulfoxide (DMSO) was purchased from EMD chemicals Inc. For an experiment of binding organophosphate, mono-methylphosphate bis(cyclohexyl ammonium) salt was purchased from Aldrich. Absolute ethanol was obtained in-house. Water used in the synthesis was from a double-exchanged Millipore filter apparatus. For the diazotization reaction, all the chemicals used in the synthesis were the same chemicals described in Chapter 3. All of reagents were used without further purification except for dichloromethane and tetrahydrofuran (THF).

4.2.2. GPTS-, APTS-, and SATS-functionalized MSU-F mesocellular silica foam by direct assembly

The GPTS-, APTS-, and SATS-functionalized MSU-F mesocellular silica foam was prepared by a direct assembly pathway using the organosilane

reagents (3-glycidoxypropyl)trimethoxysilane (GPTS), p-aminophenyltrimethoxysilane (APTS), and 3-(triethoxysilyl)propylsuccinic anhydride (SATS). Firstly, Pluronic 123 (0.80 g, 0.13 mmol) was dissolved in formamide (11.34 g, 252 mmol) mixed with glacial acetic acid (0.6 g, 10 mmol). In order to make the micro-emulsion template 0.6 g (5.0 mmol) of TMB (1, 3, 5 – trimethyl-benzene) was mixed with the surfactant solution for 30 minutes. After the preparation of the surfactant solution, GPTS (0.860 g, 3.639 mmole), APTS (0.766 g, 3.639 mmole), or SATS (0.389 g, 1.213 mmole) followed by the addition of sodium silicate solution. The mixture was stirred at 25°C for 20 hours, followed by static aging in an oven at 100°C for one day. Then the surfactant was removed by soxhlet extraction with ethanol for one day. The overall reaction stoichiometries used for the preparation of the MSU-F mesoporous silicas are given in Table 4.1.

Table 4. 1. Reaction stoichiometries used for the syntheses of GPTS-, APTS- and SATS-functionalized MSU-F foam silica.

Materials ^a	Silica source (mmole)	Organosilane (mmole)	P123 (mmole)	TMB (mmole)	HOAc (mmole)	Water (mole)	Formamide (mole)
30% GPTS MSU-F (D) ^b	8.49	3.64	0.14	5	10	1.6	0.25
30% APTS MSU-F (D) ^b	8.49	3.64	0.14	5	10	1.6	0.25
10% SATS MSU-F (D) ^b	11.1	1.21	0.14	5	10	2.3	0.25
30% SATS MSU-F (G) ^b	12.1	3.64	0.21	8.3	10	2.8	-

^a The percentage given in the materials designation indicated the targeted level of organofunctionalization

^b The designation "G" and "D" refer to the silane grafting and the direct assembly methods, respectively. In the case of the grafting method, the amount of organosilane is based on the amount of silicon source given in the table. The Grafting reaction was actually carried out on 0.5 g of MSU-F. The silica source was sodium silicate (Na₂SiO₃).

4.2.3. 30% SATS functionalized MSU-F silica by grafting method⁶

A 30% SATS-functionalized MSU-F silica was synthesized by grafting SATS organosilane on to pre-assembled MSU-F foam silica. For the preparation of pure MSU-F foam silica, Pluronic 123 (1.2 g, 0.206 mmol) was stirred in 1.0 M acetic acid (10 mL, 10 mmol) and water (10 ml) until it dissolved. To prepare the micro-emulsion template, TMB (1, 3, 5 – trimethyl-benzene) (1.0 g, 8.3 mmol) was mixed with the surfactant solution for 30min. Then, sodium silicate solution 2.43 g (12.1 mmol, sodium silicate) and 30 g H₂O (1.7 mole) were added to the micro-emulsion template. The final reaction mixture was stirred for one day at 25°C and kept under static conditions in an oven for one day at 100 °C. The product was filtered, dried and calcined at 500 °C for 4 hours. The calcined MSU-F silica was then functionalized by reaction with a SATS/DMF solution under reflux conditions for 4 hours. The detailed procedure for SATS functionalization was the same as that described for SBA-15 in section 3.2.2.

4.2.4. Diazotization reaction of 30% GPTS-functionalized MSU-F silica

The epoxide ring of 30% GPTS-functionalized MSU-F silica was opened using a base (LiAlH₄)⁷ or an acid catalyst (HClO₄)⁸. In the ring opening reaction with LiAlH₄⁷, 0.5 g of 30% GPTS functionalized MSU-F (1.6 mmole of organic moiety) was dispersed in the dried THF solvent (10 mL). Then, 10 mL of 1M LiAlH₄ in THF was added dropwise to a mixture of 30 % GPTS-functionalized MSU-F and THF in an ice bath. After the addition of 1M LiAlH₄, the reaction was allowed to equilibrate at ambient temperature for 2 hours. This reaction mixture

was cooled in an ice bath and the mixture was quenched with H₂O until the evolution of H₂ gas ended. This solid was filtered and mixed with 300 ml of 3.0 M HCl solution for 30 minutes to dissolve the aluminum side product. The resulting solid product was filtered, washed and air-dried.

For the acid catalyzed ring opening reaction⁸, 0.5 g of 30% GPTS functionalized MSU-F (1.6 mmole of epoxide) was mixed with 0.1 mL of HClO₄ in 50 mL of DMSO/H₂O (33 mL/17 mL). Then, this mixture was stirred at 80°C for 3 hours. The final product was filtered, washed with ethanol and air-dried.

After the epoxide ring-opening processes, diazotization reaction was performed using the three-step route which was described in Section 3.2.5.⁹ First, the hydroxyl groups of the ring-opened GPTS-silica was allowed to react with fmoc-glycine activated by 2,6-dichlorobenzoylchloride. In order to improve the reactivity of 2,6-dichlorobenzoylchloride, the ring opened GPTS-silica was air-dried overnight prior to use. After the fmoc-glycine ester bond was formed, deprotection of the fmoc group was achieved using 20% piperidine/DMF solution (2:8 by volume) at a ratio of 0.2 mmole of GPTS functional group to 10 ml of piperidine/DMF solution. As the last step, the amine group formed in the deprotecting fmoc reaction, was diazotized by reaction with the nitrosating agent. (acidified NaNO₂) A sodium nitrite solution (4.5 g, 55 mmol/ 10 ml water) and the mesostructured organosilica (100 mg) suspended in dichloromethane (10 ml) were placed in two separate flasks. By use of a canula, the flask containing the sodium nitrite solution was connected to flask containing the mesostructured organosilica flask. Then, the sodium nitrite solution was purged with nitrogen gas

overnight. To the sodium nitrite solution 5 ml of 10 % sulfuric acid solution was added to produce nitrous acid gas. These gases were allowed to mix with the amine functionalized mesostructure for 20-30 minutes. The final diazotized silica was filtered, washed with dichloromethane and air dried.

4.2.5. Diazotization reaction of 30% APTS functionalized MSU-F silica¹⁰

A 10 mg quantity of 30% aminophenyl functionalized MSU-F silica was mixed with 5 mL of water and 3 mL of concentrated hydrochloric acid, and the resulting mixture was heated in a hot water bath (70 °C). After 15 minutes, another 5 mL of concentrated hydrochloric acid was added. Then the mixture was stored in an ice bath. A second solution was prepared by dissolving 2.3 g of sodium nitrite in 6.7 mL of water and cooling the solution in an ice bath. After 30 minutes, the cold sodium nitrite solution was transferred to the protonated aminophenyl functionalized MSU-F silica mixture one pipetteful at a time. In order to keep the temperature low (0 °C ~ 5 °C) during transfer, additional pieces of ice were added to the diazotization flask, as needed. After another 30 minutes, the final solid product was filtered.

4.2.6. Absorption of organophosphate¹¹

A 20 mL quantity of 100 mM methyl phosphate bis(cyclohexyl ammonium) salt (2 mmole) in dried methanol was mixed with the diazotized APTS-functionalized MSU-F silica, and the mixture was heated to reflux temperature overnight. The product was then filtered and dried at room temperature. Finally,

in order to remove the ionically bonding species, the phosphate-bound MSU-F silica was mixed with 20 mL of 1.0 M HCl for 15 minutes. The final product was filtered with water, followed by wash with ethanol, and dried at room temperature.

4.2.7. Preparation of Fe³⁺ Immobilized on diacetate-functionalized MSU-F¹²

Fe³⁺-immobilized MSU-F was prepared from SATS-functionalized MSU-F foam silica. First, succinic anhydride functionalized MSU-F (1.6 mmole of the organic group) was suspended in 0.48 ml of concentrated acetic acid. The mixture was heated at 45 ~ 50 °C for 1~2 hours, followed by the addition of 2.42 mL of water. The white milky suspension was stirred at 60 °C for 3 hours. Afterward 0.024 mL of conc. HCl was added, and the mixture was stirred at ambient temperature overnight. The diacetate-product was filtered and dried. Finally, the diacetate functionalized MSU-F silica was mixed with an excess amount of 100 mM FeCl₃ solution for 30 minutes, rinsed with ethanol, and air-dried.

4.3. Physical characterization

GPTS-, APTS-, and SATS-functionalized MSU-F silica and their derivatives were characterized by reflectance-infrared spectroscopy, ²⁹Si, ³¹P solid state magic angle spinning nuclear magnetic resonance (MAS NMR) spectroscopy, and nitrogen adsorption-desorption analysis.

Infrared spectroscopy was performed using a Nicolet Protégé 400 Magna reflectance infrared spectrophotometer equipped with a Barnes analytical

/spectra-tech diffuse reflectance accessory. Infrared spectra (32 scans per spectrum) were collected in the range of 700 to 4000 cm^{-1} with a resolution of 1.928 cm^{-1} .

The degree of functionalization achieved for an each mesostructured organo-silica was determined by quantitative ^{29}Si MAS solid state NMR. ^{29}Si MAS NMR spectra were collected at 79 MHz on a Varian VXR-400S solid state NMR spectrometer. The sample spinning rate was 4 kHz, and the pulse delay was 400 seconds. Talc was used as a chemical shift reference (-98.1 ppm). ^{31}P MAS NMR was used to verify the incorporation of organo phosphate onto the mesostructure. The spectra were collected at 162 MHz on a Varian VXR-400S solid state NMR spectrometer operating in single pulse mode. The spinning frequency was 4 kHz and a pulse delay was 1 second. H_3PO_4 was used as the chemical shift reference. (0ppm)

N_2 adsorption-desorption isotherms were collected on a Micrometrics Tristar 3000 sorptometer. Before analysis, the samples were degassed at 90°C and 10^{-6} torr for about 12 hours. BET surface areas were calculated from the linear part of a BET plot. BJH pore size distributions were derived from the adsorption branch of the isotherm.

TEM images and EDX data were obtained on a JEOL 200FS transmission electron microscope which was operated at 200kV. The sample was prepared by sonification of the materials in ethanol for 30 minutes. This suspension then was dried on a carbon-coated holey film supported on a Cu grid.

4.4. Results and Discussion

4.4.1 30% GPTS functionalized MSU-F and its diazotization

The graphs in Figure 4.1 provide the nitrogen adsorption-desorption isotherms of 30% GPTS functionalized MSU-F silica and the pore (cell) and window size distributions obtained from the adsorption and desorption branches of the isotherms, respectively. The adsorption-desorption isotherms show typical type IV behavior, having a hysteresis loop between 0.7 and 0.95 relative pressure associated with the capillary condensation of nitrogen taking place in a large pore material. As shown on Figure 4.1, 30 % GPTS functionalized MSU-F silica shows bimodal 53 nm and 16 nm cell sizes and a 7nm window size. The BET surface area for these GPTS functionalized foam silica is 460 m²/g, and the pore volume is 1.85 cm³/g.

²⁹Si solid state MAS NMR was used to determine the degree of functionalization. As shown in Figure 4.2, the ²⁹Si solid state MAS NMR resonance lines of 30% GPTS functionalized MSU-F silica appear at -70, -104, and -112 ppm, which are assigned to RSi(OSi)₃ (T³), (OH)Si(OSi)₃ (Q³), and Si(OSi)₄ (Q⁴) sites, respectively. The ratio of organo silicon to total silicon, which is defined the degree of functionalization ($T^3/(T^3+Q^3+Q^4)$), is 29%. (c.f. Table 4.2) This degree of functionalization is higher than reported earlier for NHNMPTS- or BHAPS- functionalized MSU-F foam silica (see chapter 3). Presumably, the less hydrophilic the terminal functional group of organic moiety (ex. the hydrophilic hydroxyl group) is, the less it partitions in the surfactant during synthesis, which

leads to a high degree of framework functionalization. As it was mentioned in Chapter 2, a hydrophilic organo functional group, such as the hydroxyl group, can interact with hydrophilic groups of surfactants through H-bonding and have a better chance of being removed when surfactant is removed by solvent extraction, which might be the reason of the less functionalization of the product than what we attempt.

In the stepwise conversion of 30% GPTS-MSU-F to a diazotized analog, each reaction step was confirmed by IR spectra. The IR spectra in Figure 4.3 for the aminoacid ester formed by deprotection of the fmoc group shows a much stronger carbonyl stretching vibration than the derivative made from NHNMPTS MSU-F (see Chapter 3, Figure 3.8). The incorporation of the initial epoxide by direct synthesis places more of the organosilane at the pore wall surfaces for subsequent functionalization. In addition, the ^{29}Si solid state NMR spectrum (Figure 4.2) verified the incorporation of more GPTS groups in the framework walls of MSU-F in comparison to NHNMPTS groups. However, the last reaction step leading to diazotization occurs in low yield. The diazo stretching vibration at 2420 cm^{-1} is very weak and shifted from the expected frequency of 2110 cm^{-1} . The reason for the shift might arise from a dominant triple bond character instead of the stabilized resonance double bond character for unknown reasons. Also, the electron withdrawing effect of the vicinal hydroxyl group to the diazo functional group may make the diazo bond somewhat stronger and result in the higher frequency adsorption for diazo functional group in the IR spectrum.

The new peak at 1400 cm^{-1} can be assigned to a NO vibration band. In the diazotization reaction, this NO species reacts with amine group of the aminoacid ester and generates the diazo functional group. In an effort to decrease the NO band intensity and increase the diazo band intensity, the reaction was carried out with longer reaction time (1hr, 1hrs 30minutes, and 2hrs). However, this did not increase the diazo band intensity, nor did it decrease the intensity of the 1400 cm^{-1} band. Thus, the 1400 cm^{-1} band is unlikely to be associated with the formation of a diazo intermediate and may simply be NO adsorbed in the pores of the silica.

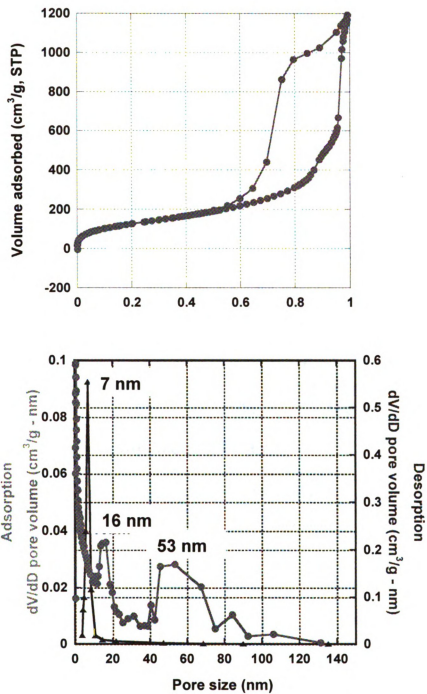


Figure 4.1. N₂ adsorption-desorption isotherm of 30% GPTS functionalized MSU-F prepared by direct assembly method (upper panel) and the cell size and window size distributions (lower panel) obtained by fitting the adsorption desorption data, respectively, to the BJH model.

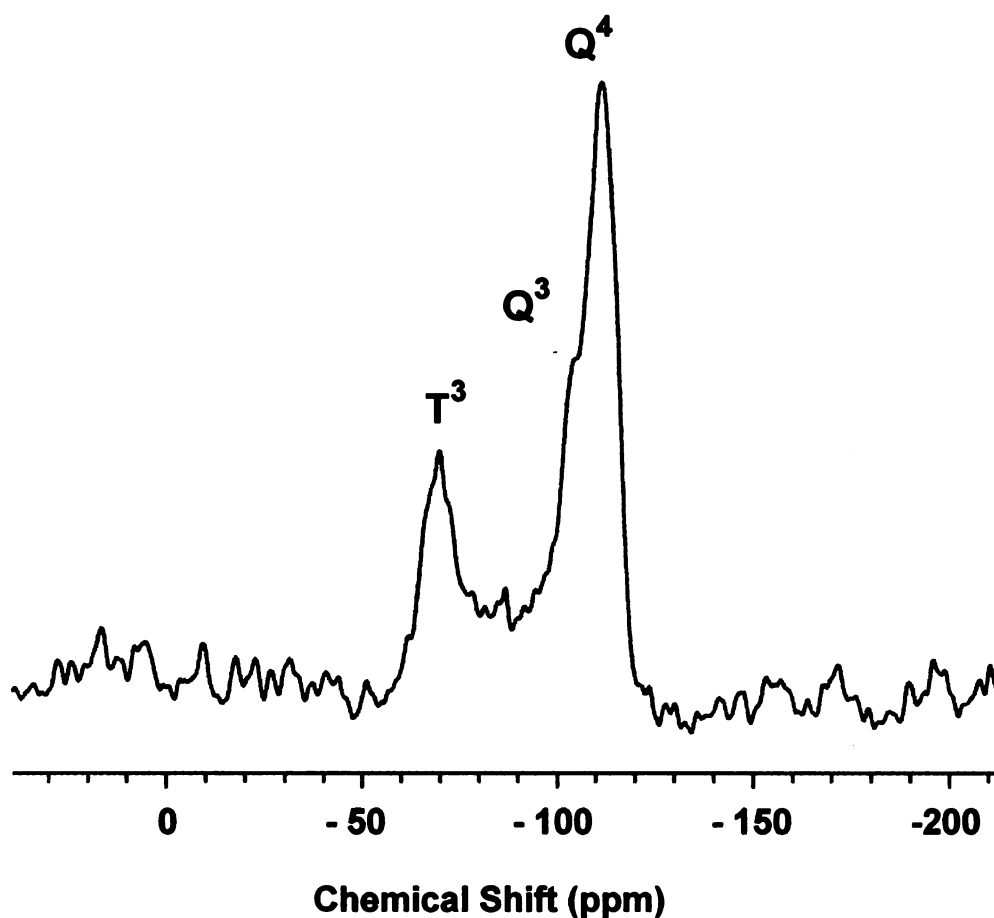


Figure 4. 2. ^{29}Si solid state MAS NMR spectrum of 30% GPTS functionalized MSU-F foam silica.

Table 4.2. ^{29}Si solid state MAS NMR data for 30% GPTS functionalized MSU-F foam silica. The degree of functionalization is determined by the ratio between the integral of the T^3 resonance intensity to the total integral intensity ($\text{T}^3/(\text{Q}^4 + \text{Q}^3 + \text{T}^3)$).

	Integrated peak areas			Degree of functionalization
	T^3	Q^3	Q^4	
30% GPTS MSU-F	65.2	79.0	82.7	29%

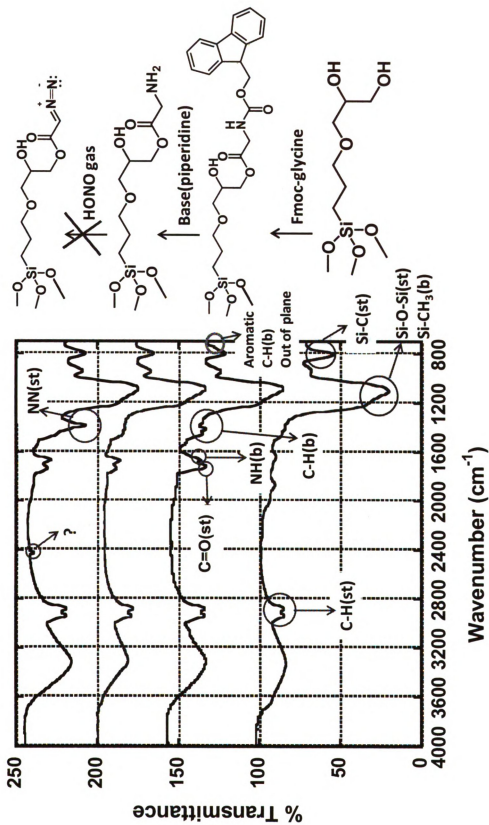


Figure 4.3. IR spectra for the step-wise conversion of 30% GPTS functionalized MSU-F foam (made by direct synthesis) to diazo functionalized MSU-F

4.4.2. Diazotization of Aminophenyl functionalized MSU-F silica

Up to this point, several approaches to the diazotization of MSU-F foam silica have been investigated starting from organosilane groups integrated into the pore walls. However, due to the complexities of the reaction steps, the yields of diazo functional groups were low. The largest degree of diazotization was achieved starting with 30% NHNMPTS MSU-F. (0.53mmole/g, Table 3.6 in Chapter 3, In the latter case, the functional group density was 4.53 mmol per gram.) A simpler pathway to diazotization is needed. Accordingly, a new organosilane, namely, p-aminophenyltrimethoxysilane (APTS) group was used as a reaction precursor to 30% APTS-functionalized MSU-F. The diazotization of p-aminophenyl group is a well-known simple one-pot synthesis. Also, the delocalized pi electrons of the diazo group and benzene might help to stabilize the diazo functionality.

For the characterization of 30% APTS functionalized MSU-F, the presence of mesopores was verified by N₂ adsorption-desorption isotherms. The surface organic groups involved in each reaction step were characterized by IR spectroscopy.

Figure 4.4 displays the nitrogen adsorption-desorption isotherms for 30% p-aminophenyl MSU-F foam silica. The isotherms for the soxhlet-extracted material shows an abrupt uptake of N₂ adsorption at the relative pressure 0.9 ~1.0 due to capillary condensation within the mesopores of the silica framework. This sharp adsorption step at partial pressures (P/P₀) greater than 0.9 is also indicative of presence of large pores, greater than 20nm in diameter. The lower

panel of Figure 4.4 illustrates the cell size distribution obtained by fitting the adsorption isotherm to the BJH model. Most of the cells are 20 – 60 nm in diameter. Additionally, this material has a relatively small window size (8.4 nm, obtained from the desorption isotherm) in comparison to the cell size, which can be classified as a “closed cell” structure. The BET surface area is 349 m²/g, and pore volume is 0.88 cm³/g.

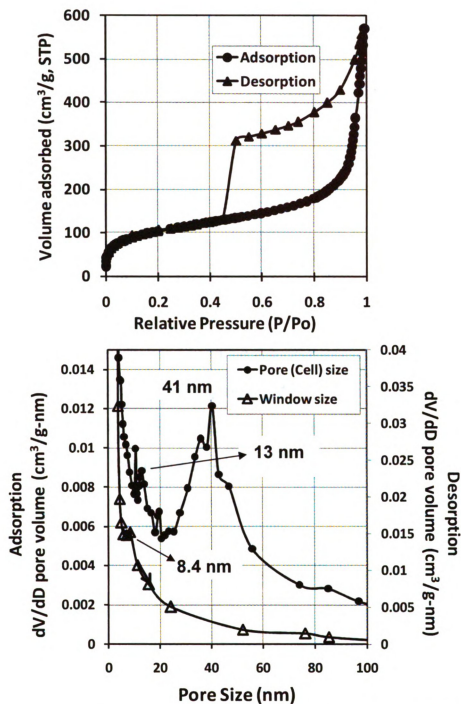


Figure 4.4 N₂ adsorption-desorption isotherms for 30% aminophenyl functionalized MSU-F silica prepared by direct assembly (upper panel) and the cell and window size distributions obtained from the adsorption and desorption branches of the isotherms, respectively (lower panel).

Figure 4.5 compares the infrared spectra of 30% aminophenyl functionalized MSU-F foam silica and its diazotized reaction product. An intense diazo stretching vibration is observed at 2273 cm^{-1} . This band is much stronger than previously observed diazo stretching vibrations. The position of the band at 2273 cm^{-1} is consistent with the presence of a positive net charge on the diazo group with the triple bond character.

The diazo-functionalized MSU-F silica was allowed to react with a simple organo phosphate (methyl phosphate ammonium salt) in order to verify the accessibility of the diazo group. The reaction between organo phosphate and diazo functionalized MSU-F silica is based on Sandmeyer-Gatterman aromatic substitution reaction.^{13,14} As shown on Figure 4.6, the ^{31}P solid state MAS NMR confirms the presence of covalently bonded methyl phosphate. The strong peak at -7ppm is assigned to the bonded phosphate and the two other peaks separated by 4 kHz are spinning side bands. In solid state NMR, in order to reduce the effect of anisotropy, the rate of sample spinning should be faster than the anisotropy interaction. However, when the anisotropy is large, as with covalent binding, the sample spinning rate may not be sufficient to remove the spinning side bands.¹¹ Therefore, we can assume the anisotropy of the phosphate group is large due to the covalent binding of methyl phosphate to the mesostructure, which results in the spinning side bands at -32 ppm and 18 ppm, in agreement with the spinning rate of 4 kHz. The low signal to noise ratio is result from the low concentration of phosphate group in the material. The assignment of the -7 ppm resonance to covalently bonded organophosphate is

further confirmed by the chemical shift in comparison to ionically bonded organophosphate. As shown by the spectrum in Figure 4.7 and 4.8, the shifts for $[\text{PO}_3(\text{OCH}_3)]^{2-}$ ions character on APTS-MSU-F silica and pure MSU-F silica occur at 1.5 ppm and 1.7 ppm, respectively. These values are consistent with the shift (2.2 ppm) reported previously for organophosphate dianion.¹⁶ In this electrostatic interaction between phosphate and amine group, methyl phosphate mostly bound to ammonium species instead of aniline on APTS because of the low pKa value of anilinium ion species compared to alkylammonium. (pKa of anilinium ion: 4.6, pKa of alkylammonium: 10.6) This is the reason why only one chemical shift of phosphorous was shown in Figure 4.7. The weak NMR resonances for the covalently formed organophosphate in Figure 4.6 are a consequence of hydrolysis that occurs when the reaction product is worked with dilute HCl in order to remove ionically bound organophosphate. If the reaction product is not washed with dilute HCl, then a much more intense NMR spectrum is obtained, as shown in Figure 4.9. The spectrum contains intense resonance lines for both covalently bound and ionically bound organophosphate, along with a third resonance at about 23 ppm, which is unassigned. The dramatic difference in intensity between the spectra in Figure 4.6 and Figure 4.9 indicates that both ionically bound and covalently bound organophosphate are removed by the acid wash.

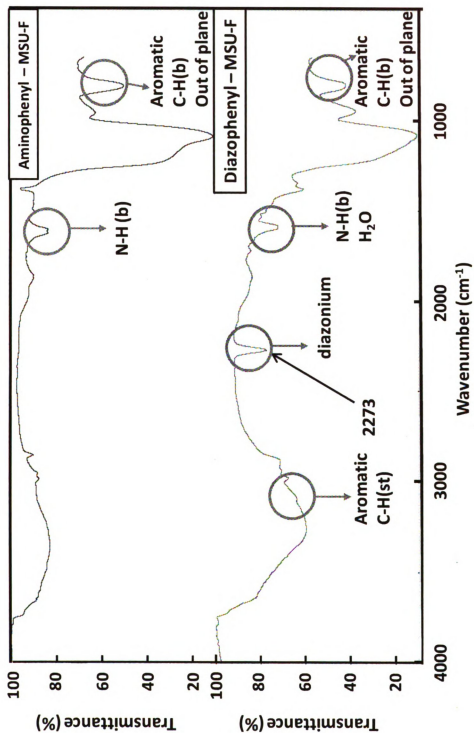


Figure 4.5. Infrared spectra for aminophenyl functionalized MSU-F silica and the corresponding diazotized derivative made by reaction with sodium nitrite

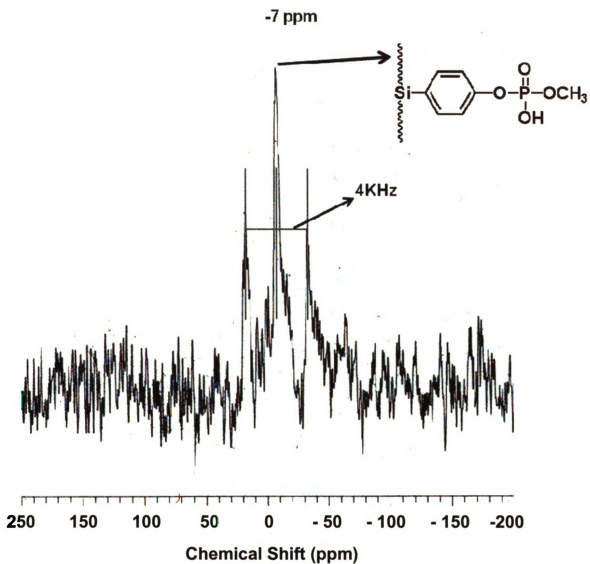


Figure 4.6. ^{31}P Solid state NMR spectrum of methyl phosphate covalently bonded to MSU-F foam silica wall by Sandmeyer-Gattermann aromatic substitution reaction after hydrochloric acid washing. The two peaks separated by 4kHz from the line at -7ppm are spinning side bands.

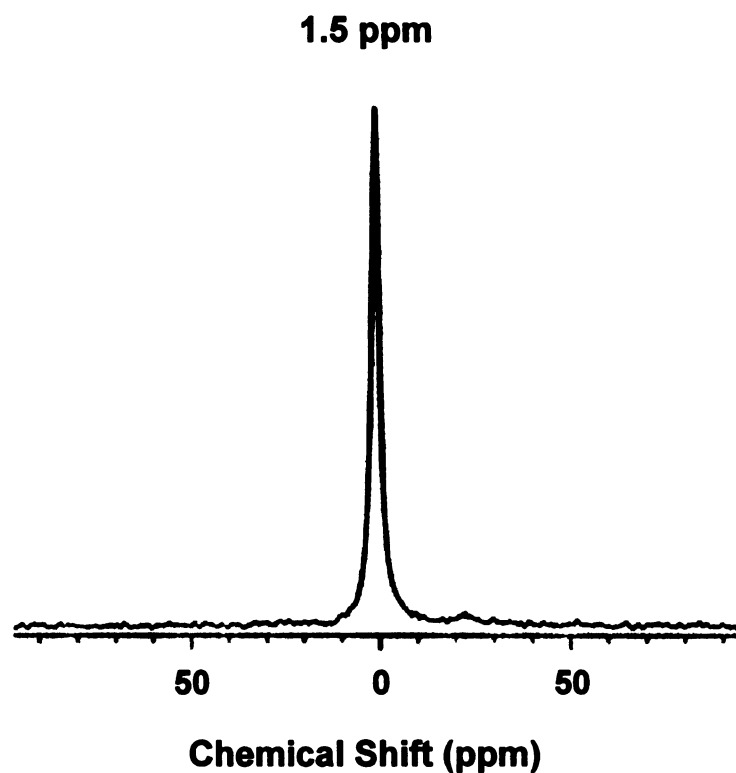


Figure 4. 7. ^{31}P Solid state NMR spectrum of methyl phosphate on 30% aminopheyl functionalized MSU-F. The organophosphate anion was introduced into aminophenyl-functionalized MSU-F silica with the cyclohexyl ammonium salt of $[\text{PO}_3(\text{OCH}_3)]^{2-}$ in methanol solution.

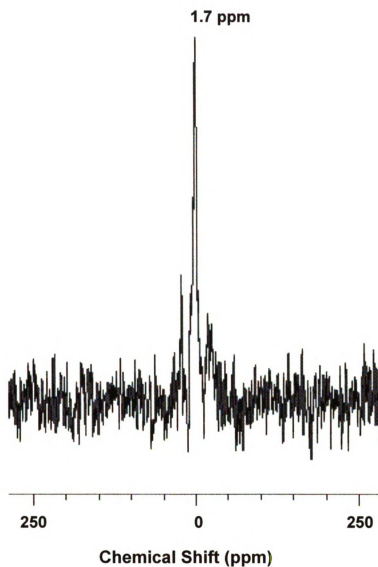


Figure 4. 8. ^{31}P Solid state NMR spectrum of methyl phosphate electrostatically bonded to cyclohexyl ammonium on pure MSU-F. The organophosphate anion was introduced into MSU-F silica with the cyclohexyl ammonium salt of $[\text{PO}_3(\text{OCH}_3)]^{2-}$ in methanol solution.

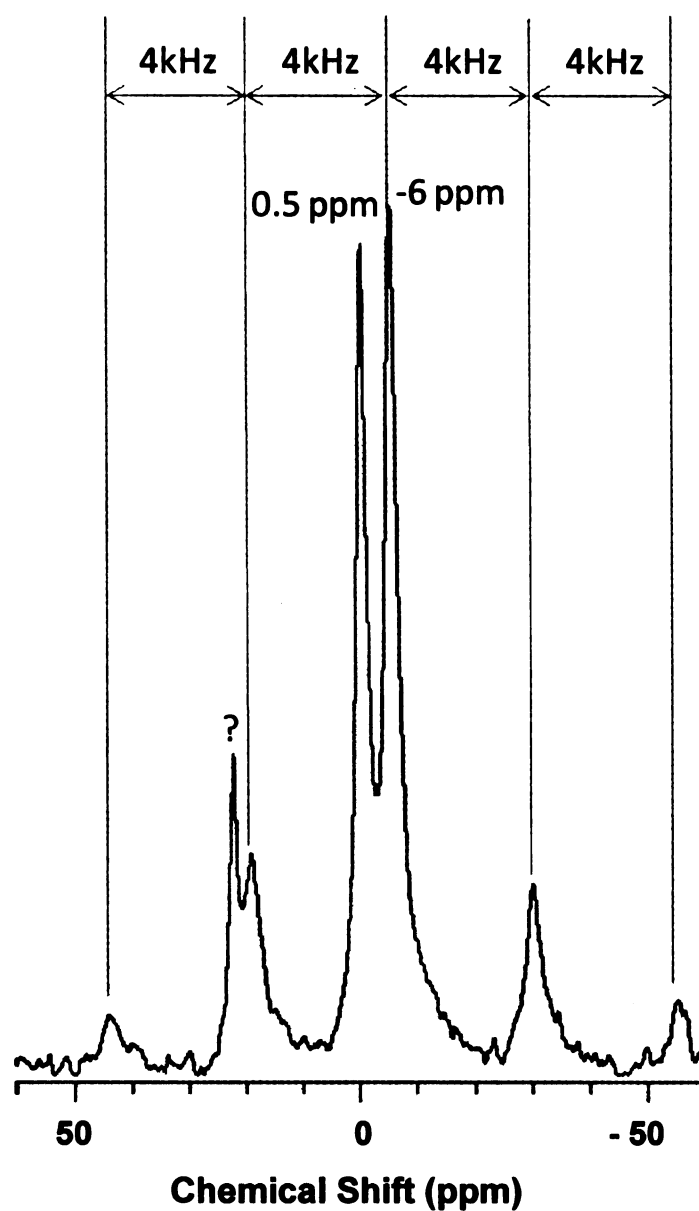


Figure 4.9. ^{31}P Solid state NMR spectrum of methyl phosphate covalent bonded to MSU-F foam silica wall by Sandmeyer-Gattermann aromatic substitution reaction. The four peaks separated by 4kHz as shown above is the spinning side bands of covalently bonded methyl phosphate species at -7 ppm.

4.4.3. Immobilization of Fe³⁺ on a succinate-functionalized MSU-F silica foam

Two succinic anhydride functionalized foams of MSU-F silica were synthesized by grafting (30% functionalization) and direct assembly (10% functionalization) methods, using 3-(triethoxysilyl)propylsuccinic anhydride (SATS) as the organosilane. The physical properties of those foams were characterized by N₂ adsorption-desorption isotherms. Further organic modification of the grafted derivative, such as the ring opening reaction of succinic anhydride, were characterized by IR, TEM and EDX.

Figure 4.10 provides the N₂ adsorption-desorption isotherms for 10% SATS functionalized MSU-F silica made by direct assembly. As shown in Figure 4.10, the isotherm exhibits a Type IV isotherm with capillary condensation occurring between 0.9 and 1.0 relative partial pressure (P/P₀), which reflects the very large and broad cell size (37nm) as illustrated in the lower panel of Figure 4.10. Also, this material shows a small adsorption step around P/P₀ ~0.9, which corresponds to secondary cell size having a diameter of 16 nm. The window size obtained from the desorption isotherm is 6 nm, which is the characteristic ratio for a “closed cell” type of mesocellular foam. The BET surface area is 423 m²/g, and pore volume is 1.47 cm³/g. The textural properties of pure MSU-F silica also were determined by N₂ adsorption-desorption methods. As shown on Figure 4.11, this silica has very narrow window and cell sized distributions, and very large pore volume. The window and cell size were 11.4nm and 21nm, respectively. The BET surface area is 517 m²/g, and pore volume is 2.23 cm³/g.

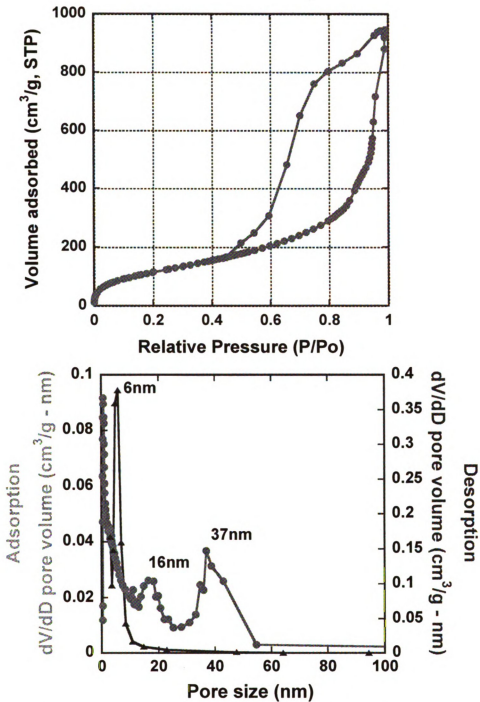


Figure 4.10. N₂ adsorption-desorption isotherms for 10% succinic anhydride (SATS) functionalized MSU-F silica prepared by direct assembly method (upper panel) and the cell and window size distributions obtained from the adsorption and desorption isotherm (down panel), respectively.

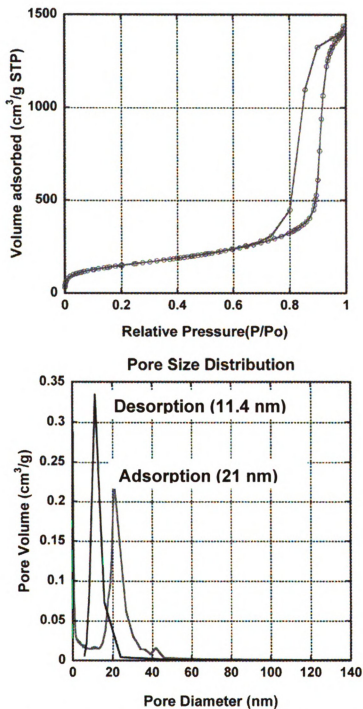


Figure 4.11. N_2 adsorption-desorption isotherms for pure MSU-F silica (upper panel) and the cell and window size distributions obtained from the adsorption and desorption isotherms, respectively. This silica was used to prepare a 30% succinic anhydride functionalized derivative by the grafting method.

Each reaction step in the modification of the surface was monitored by FT-IR spectroscopy. The FT-IR spectra in Figure 4.12 confirm the presence of the acidic carbonyl group formed by the ring opening of succinic anhydride. The immobilized Fe³⁺ species in the MSU-F silica foam. The spectrum of succinic acid-MSU-F (upper panel in Figure 4.12) shows a sharp and intense absorption peak of the acid carbonyl group at 1722 cm⁻¹. When this material was mixed with aqueous ferric chloride, the obtained solid exhibited a new carbonyl stretching band at 1590cm⁻¹, which is due to the coordination of Fe (III) to the carboxylate linkages.

In order to verify the stability of the mesostructure during the grafting process and the presence of Fe(III), the transmission electron microscopy (TEM) image and the energy dispersive X-ray spectrum (EDX) shown in figure 4.13 were obtained. The upper panel in Figure 4.13 shows the bright field TEM images of the mesoporous foam silica. The image shows a very uniform cell size (20nm), in accord with size obtained by N₂ adsorption. From this image region, EDX analysis was performed. The bottom panel in Figure 4.13 shows the characterized peaks of Fe, which verifies immobilization of Fe (III) on the succinic acid functionalized MSU-F silica.

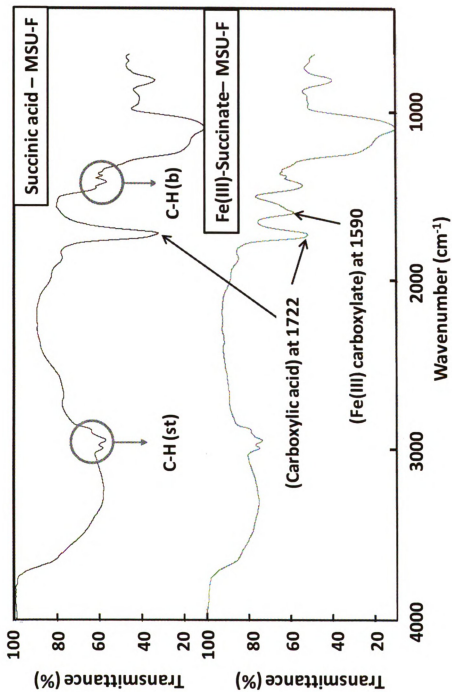


Figure 4.12. IR spectra for succinate-functionalized MSU-F silica prepared by grafting reaction of SATS and for the corresponding derivative containing complexed Fe(III) cation.

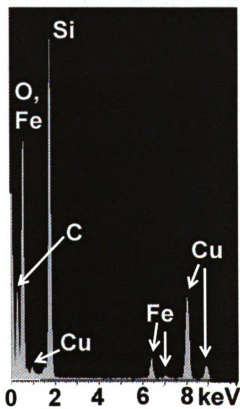
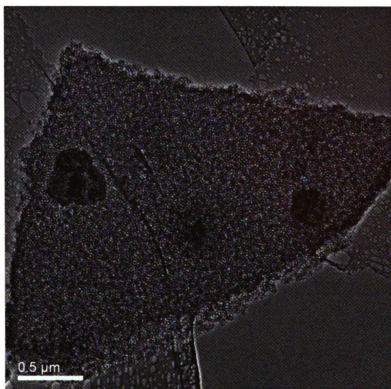


Figure 4.13. TEM image (upper panel) and EDX spectrum (lower panel) for Fe(III) succinate functionalized MSU-F silica prepared by grafting method.

4.4.4. Conclusion.

In this chapter, three different mesoporous organosilica syntheses have been carried out for potential proteomic separations in the future. Unexpectedly, the first GPTS functionalized mesostructure showed a low concentration of immobilized diazo species as judged by the IR spectra in Figure 4.3. This result reflects low yield involved in the multi-step reaction sequence. However, the simple one-pot synthesis of immobilized diazo-phenyl groups and Fe³⁺ carboxylated groups were successfully performed. The one pot synthesis of diazophenyl group showed a very intense diazo vibration at 2273cm⁻¹. In addition, the resulting derivative provided good covalent coupling to methyl phosphate. Lastly, the Fe³⁺ foam silica, containing immobilized Fe (III) carboxylate groups may be suitable for phosphoprotein enrichment by the most popular method IMAC. Both materials may prove to be good candidates for future studies of phosphorylated peptide enrichment.

4.5. Reference

- (1) Novabiochem Catalog and Peptide synthesis Handbook, **1997/1998**, method 16.
- (2) MilliGen Techniccal Note 3.10.
- (3) Veterans at Risk: The Health Effects of Mustard Gas and Lewisite, Institute of Medicine **2005**, 72
- (4) Tanabe Seiyaku Company Limited, *GB1336460* **1973**
- (5) Pan, C., Ye, M, Liu, Y., Feng, S., Jiang, X., Han, G., Zhu, J. and Zou, H. *Journal of Proteome Research* **2006**, 5, 11, 3114-3124
- (6) Mier-Vinue, J., Montana, A. M., Moreno, V., and Prieto, M Z. *Anorg. Allg. Chem.* **2005**, 631, 2054-2061
- (7) McCarthy, J. R., mcCowan, J., Zimmerman, M. B., Wenger, M. A., Emmert, L. *W. J. Med. Chem.* **1986**, 29, 1586-1590
- (8) Hoffmann, H. M. R., Brandes, A. *Tetrahedron*, **1995**, 51, 1, 155-164
- (9) Lansdell, T. A., Tepe, J. J. *Tetrahedron Lett.* **2004**, 45, 91-93
- (10) Lehman, J. W. *Operational Organic Chemistry* **1999**
- (11) Hodgson, H. H., Clifford, K. *Journal of the Chemical Society* **1942**, 581-583
- (12) Dunn, J. D., Watson, J. T., Bruening, M. L. *Anal. Chem.* **2006**, 78, 1574-1580
- (13) Sandmeyer T., *Ber.*, **1884**, 17, 1633; **1890**, 23, 1880.
- (14) Gatterman L., *Ber.*, **1890**, 23, 1218.
- (15) Duer, M. J. Introduction to Solid-State NMR spectroscopy **2004**, 62-66
- (16) Benoit-Marquie, F., de Montety, C., Gilard, V., Martino, R., Maurette, M. T., Marlet-Martino, M. *Environ. Chem. Lett.* **2004**, 2, 93-97

Chapter 5

Phosphorylated protein enrichment based on diazo functionalized mesoporous silica film

5.1. Introduction

Protein phosphorylation is one of key mechanisms in biological regulatory process, such as cell proliferation, differentiation, and apoptosis in a signaling process.¹⁻³ In order to identify phosphorylated peptides and their sequences, mass spectrometry has emerged as a powerful analytical technique.⁴ However, due to the low abundance of phosphorylated proteins and variations of phosphorylation sites, the analysis of phosphorylated proteins is quite challenging. Therefore, to improve the analysis of phosphorylated proteins, a numbers of recent studies have been focused on separation and enrichment methods of phosphorylated proteins combined to mass spectrometry analysis. So far the most common technique in the enrichment of phosphorylated proteins is IMAC (Immobilized Metal Affinity Chromatography).^{5,6,7,8} However, its lack of selectivity for peptides containing acidic amino acid residue, namely Glu and Asp, and lots of variables of experimental conditions result in impurity with non-phosphorylated proteins.

For more effective method for the enrichment, recently, covalent bonding enrichment strategies have been addressed. In this early study, the β -eliminations of phosphate groups followed by the conjugation of thiol groups can lead to covalent bindings on solid phase bead.^{9,10} However, there are few

limitations. First of all, unprotected cysteine and methionine residue can be involved in unwanted side reaction. O-linked sugar moiety can undergo the β -elimination reaction and lead to complication of enrichment result. In addition, this method excludes the enrichment of phosphotyrosine species. Therefore, alternative method and strategies were still needed.

In order to overcome this limitation, Tepe *et al.*¹¹ in 2004 established a new type of solid support that contains α -diazo functional group on the Wang resin surface. In this method, α -diazo groups can be easily replaced by phosphate group in phosphorylated protein enrichment process.

In 2006, Pflum *et al.*¹² also published new covalent binding enrichment method. By using glycine conjugate Wang resin, she bound phosphate groups in phosphorylated peptide to amine on Wang resin, which leads to phosphoramidates on Wang resin.

Above two cases, they have advantages in the direct and simple enrichment of phosphorylated protein without any phosphate group modification. However, due to the swelling characteristic of polymer resin, surface functional group can be only accessible in a certain solvent.

In the study of new enrichment strategies to enhance the selectivity of phosphorylated enrichment, we applied new α -diazo functionalized high surface area silica films which contain nanometer size pores. This α -diazo functionalized mesoporous silica films have some advantages in this application. First of all, due to the considerably large surface area, it generates high binding capacity. These materials also have open framework structures, which lead to free access

of phosphorylated protein on the surface of α -diazo functional group without any solvent limitation. In addition, because this method is a direct on-plate enrichment method, the enrichment process can be facilitated with minimizing the sample loss during process. In this chapter, I will describe how to prepare new types of materials and show the very efficient, selective enrichment method of phosphorylated proteins, which can have strong potential in phosphorylated protein analysis.

5.2 Experimental

5.2.1 Reagents

The amine surfactant, dodecylamine, was purchased from Aldrich for the synthesis of mesoporous film. As silicate source, tetraethylorthosilicate (TEOS) and triethoxysilylpropionitrile were also obtained from Aldrich. For the tryptic digestion, trypsin was obtained from Promega. Bovine β -casein and chicken egg ovalbumin were purchased from Sigma. Other reagents used in the tryptic digestion, like Tris-HCl, urea, 1, 4-dithio-DL-threitol, iodoacetamide and ammonium bicarbonate, were purchased from Invitrogen, J.T. Baker, BioChemika, Sigma, and Columbus Chemical Industries, respectively. HPLC grade acetonitrile, anhydrous methanol, trifluoroacetic acid, acetyl chloride, 2,5-dihydroxybenzoic acid, hydrochloric acid, and 1% aqueous phosphoric acid were obtained from Aldrich. Acetic acid, ammonium hydroxide, hydrogen peroxide and sulfuric acid were obtained Spectrum. All the above reagents were used

without further purification. Absolute ethanol was purchased in-house, and water was purified by a double-exchanged Millipore filter apparatus.

5.2.2 Synthesis of diazo functionalized mesoporous film

The diazo functionalized mesoporous silicate film was prepared by direct assembly method from triethoxysilylpropionitrile. Dodecylamine (1.2 g) was dissolved in the mixture of ethanol (13.3 g) and water (11.2 g). Then, the mixture of 4.0 g tetraorthosilicate and 1.065 g triethoxysilylpropionitrile were added to the surfactant solution at an ambient temperature. After 1 minute, additional 111 g of ethanol were added to the previous prepared solution.

Before functionalized mesoporous silica film synthesis, silicon substrates (1.5 cm x 1.5 cm) were cleaned with 100 mL of 75 % sulfuric acid with hydrogen peroxide for 2 hours at 98 °C. These cleaned silicon wafers were spin-coated by the previous prepared silicate solution. These films on the wafers were aged for 3 days at room temperature.

For the further modification from nitrile to carboxylic acid, nitrile functionalized mesoporous silicate wafer was added to 36 g of 55% of sulfuric acid solution and heated 92~95 °C for 1.5 hours. These wafers were washed with copious amount of water and dried with nitrogen. For the diazo functionalization, 0.085 mL of anhydrous N,N-dimethyl formamide in 30 mL of dried dichloromethane was added on the previous prepared vacuum dried carboxylic acid functionalized mesoporous film, which was followed by addition of 1.42 mL of oxalyl chloride. This reaction mixture were stirred at 0 °C for 30

minutes and then stirred at 25 °C for 1 hour. After this reaction, the mesoporous film on silicon substrate was transferred to another container under the nitrogen condition. On this film, 6 mL of tetrahydrofuran was added, which was followed by 3 mL of trimethylsilyldiazomethane at 0 °C. After 2 hours, the diazo functionalized mesoporous film on silicon wafer was dried under nitrogen.

5.2.3 Protein digestion

100 µg of proteins were dissolved in 20 µL urea (6M)/Tris-HCl (50mM). 5 µL of 10mM 1,4-dithio-DL-threitol was added on the protein solution and heated at 65 °C for 1 hour. After cooling, 160 µL of 50mM ammonium bicarbonate was added to the protein solution, which was followed by addition of 10 µL of 100 mM iodoacetamide. The result solution was kept for 1 hour in the dark. Subsequently, 10 µL of 0.5 µg/µL trypsin was added to the protein solution, and the protein solution was incubated for 16 hours at 37 °C. The digestion solution was quenched by the addition of 11 µL of acetic acid, which was stored in a -70 °C freezer until use.

5.2.4 Methyl esterification of protein

Tryptic digested protein was dried by using Speedvac. 200 µL of methanolic HCl (320 µL of acetyl chloride in 2 mL of anhydrous methanol) was added to the protein digested. The final solution was placed for 2 hours at room temperature, and dried by Speedvac.

5.2.5 Phosphorylated protein enrichment

For the enrichment of phosphorylated protein, the dried methyl esterified and non-methyl esterified phosphorylated peptides were diluted with the mixture of 5% acetic acid and H₂O (v:v, 1:1) to make 10 μM of tryptic digested protein solution. The 1 μL of prepared digested protein solution was applied in 2 mm circular trench on diazo functionalized mesoporous film. For 1 hour, water was kept adding to prevent from drying of protein solution. After 1 hour, resulting silicon wafer was rinsed with 20 mL of acetic acid, acetonitrile, and H₂O mixture solution.(v:v:v, 3:30:67) For the dissociation of phosphate bond from diazo functionalized silicon wafer, 2 μL of NH₄OH (pH11) was dropped on the film in the process of methyl esterified phosphorylated peptide enrichment. 0.7 μL of matrix solution (2mg of 2,5-dihydroxybenzoic acid, 100 μL of 1% phosphoric acid, and 100 μL of acetonitrile) was applied on the 2mm circular trench. The final wafer was attached onto the modified MALDI plate by double side tape.

5.3 Physical Characterization

The organo-functionalized mesoporous silica films were characterized by powder x-ray diffraction analysis, reflectance-infrared spectroscopy, and transmission electron microscopy. In addition, the enrichment of phosphorylated protein is confirmed by the matrix assist laser desorption ionization. (MALDI)

Powder XRD data were collected on a Regaku Rotaflex Diffractometer with CuK α radiation ($\lambda = 1.542\text{\AA}$) which is generated at 45kV and 100mA. The diffraction data were collected from 1.5 degree to 10 degree of 2θ with an

increment of 0.02 degree. To confirm the chemical transformations in each step from nitrile to diazo groups on mesoporous film surface, Nicolet Protg 400 Magna reflectance infrared spectrometer equipped with a Barnes analytical/spectra-tech diffuse reflectance accessory was used. Each spectrum was collected in the 700 to 400 cm^{-1} spectral region. The number of scan was 16 and data spacing was 1.928 cm^{-1} .

To verify the pore morphology on organo-functionalized mesoporous silica film, TEM images were obtained on a JOEL 2200FS instrument with an accelerating voltage of 200kV. TEM samples were prepared dipping the copper grid in the solution used in the film synthesis.

For the identification of enriched phosphorylated peptides, MALDI linear ion trap mass spectrometer (Thermo vMALDI LTQ XL) has been used.

5.4 Result and discussion

5.4.1. X-ray diffraction analysis

Figure 5.1 shows the low angle XRD reflections of nitrile functionalized mesoporous silica film on silicon wafer. The presence of a low angle diffraction, which is 3.8 nm in d spacing, indicates the average pore-pore distance for a wormhole structure.

5.4.2. Reflectance infrared spectroscopy

Figure 5.2 illustrates the IR spectra between 4000 and 700 cm^{-1} of nitrile, carboxylic acid, and diazo functionalized mesoporous silica films. In all spectra,

the peaks around between 1000 and 1200 cm^{-1} represent the stretching vibration of the Si-O-Si bonds. The broad bands at 3400 cm^{-1} show the hydrogen bonding interaction of silanol groups in mesoporous silica films. The stretching vibrations of the C-H centers on organic moieties of each functional group are shown at 2800~2900 cm^{-1} . In addition, the each reaction step was confirmed by the presence of specific IR adsorption vibration, namely, nitrile group at 2275 cm^{-1} , carboxylic acid group at 1720 cm^{-1} , diazo group at 2107 cm^{-1} .

5.4.3. Transmission electron microscopy

The wormhole framework structure is confirmed by TEM shown on Figure 5.3. The pore to pore distances for wormhole structure from TEM correspond to the value obtained from the d spacing value from the XRD analysis. In the image of Figure 5.3, the dark and light regions well represents the walls and pores of the typical wormhole mesoporous materials, respectively.

5.4.4. Matrix assist laser desorption ionization mass spectrometry analysis

In order to examine the selective binding of phosphorylated peptides onto diazo functionalized mesoporous silica thin films, three different protein samples has been studied to verify the enrichment, such as tryptic digested ovalbumin, methyl esterified tryptic digested ovalbumin, methyl esterified tryptic digested β -casein. Because of their well know phosphorylation sites of three samples, we were able to confirm them easy on MALDI mass spectra.

Tryptic digested ovalbumin

Tryptic digested ovalbumin has three well known phosphorylated peptides fragments, namely, m/z 2089 (EVVGpSAEAGVDAASVSEEFR), 2512 (LPGFGDpSIEAQCGTSVNVHSSLR), and 2903 (FDKLPFGDpSIEAQCGTSVNVHSSLR).

As shown on Figure 5.4a, the tryptic digested ovalbumin without enrichment showed three monophosphorylated peptides fragments at m/z 2089, 2512, and 2903 among complex peptide fragments. After the enrichment by diazo functionalized mesoporous silica thin films, phosphorylated peptide fragments of ovalbumin are successfully enriched down to 10 pmole level. In Figure 5.4b, it showed the strongest peak at m/z 2089, which represents selective enrichment of phosphorylated peptide. However, due to the low concentration of binding or difficulty in dissociation of covalent binding after enrichment, the signal to noise ratio is quite high. Moreover, the peaks at m/z 2512 and m/z 2903 were too small to detect it. The reason of the enrichment difficulty of these fragments might be low ionization efficiency in detection and unfavorable hydrophobic character of high weight peptide fragments.

Methyl esterified tryptic digested ovalbumin

To eliminate the possible binding with carboxylic acid moiety, tryptic digested ovalbumin was methyl esterified. As shown on figure 5.5a, the methyl esterified tryptic digested ovalbumin without enrichment represents three monophosphorylated peptides fragments at m/z 2173 (EVVGpSAEAGV-

DAASVSEEFR), 2554 (LPGFGDpSIEAQCG--TSVNVHSSLR), and 2960 (FDKLPGFGDpSIEAQCGTSVNVHSSLR). In Figure 5.5b, the spectra showed better selective enrichment compared to non-methylated sample. However, it is still difficult to find high mass fragments, such as m/z 2554 and m/z 2960.

Methyl esterified tryptic digested β -casein

In order to generalize the covalent enrichment method, methyl esterified tryptic digested β -casein were also tested. In Figure 5.6a, it didn't show clearly three possible phosphorylated peptides fragments, namely, m/z 2160 (FQpSEEQQTEDELQDK), m/z 3078 (ELEELNVPGEIVEpSLpSpSpSEESITR), m/z 3235 (RELEELNVPGEIVEpSLpSpSpSEESITR). As shown on Figure 5.6b, however, three possible fragments are shown distinctly by comparing to non enrichment methyl esterified tryptic digested β -casein spectra. This result represents the successful enrichment of methyl esterified tryptic digested β -casein on diazo functionalized mesoporous silica thin film.

5.5 Conclusion

we firstly and successfully applied high surface area mesoporous silica thin films with selective covalent binding of phosphorylated proteins as a new phosphorylated peptides enrichment method. This covalent enrichment method by high surface area thin film showed selective and facile enrichment by comparing to other enrichment process. The results in this study show the strong potential in the enrichment and analysis of phosphorylated proteins.

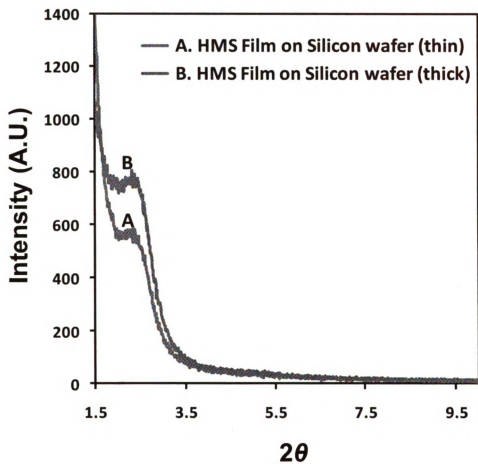


Figure 5.1. Powder X-ray diffraction pattern for HMS film on silicon wafer. (Structure directing agent was removed by Soxhlet ethanol extraction.)

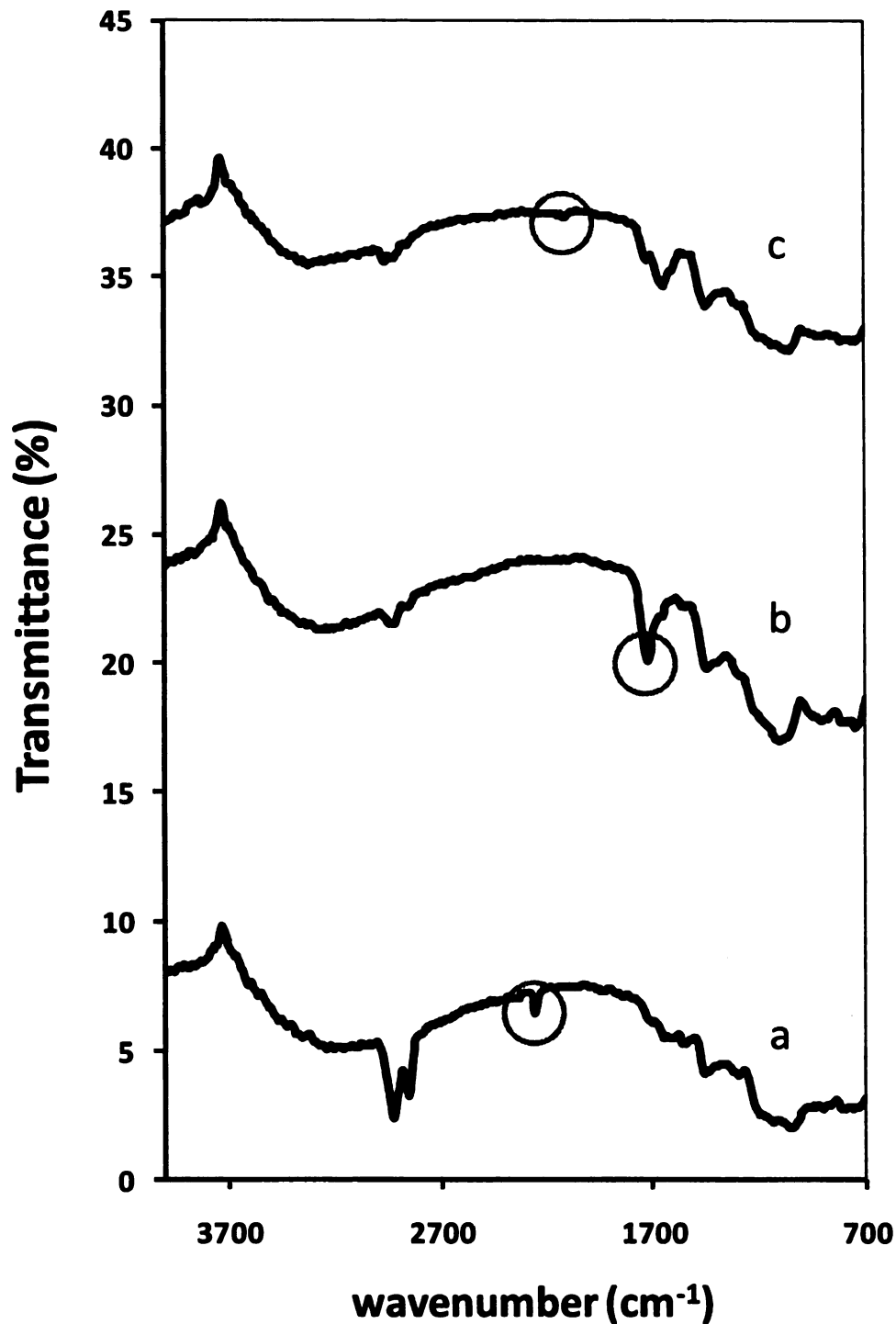


Figure 5.2. IR spectra obtained in each reaction step for the diazo functionalized mesoporous silica film synthesis. a) nitrile functionalized mesoporous silica film, b) carboxylic acid functionalized mesoporous silica film, c) diazo functionalized mesoporous silica film. Circles indicate the characteristic vibration of functional group. Each spectrum is offset by 15.

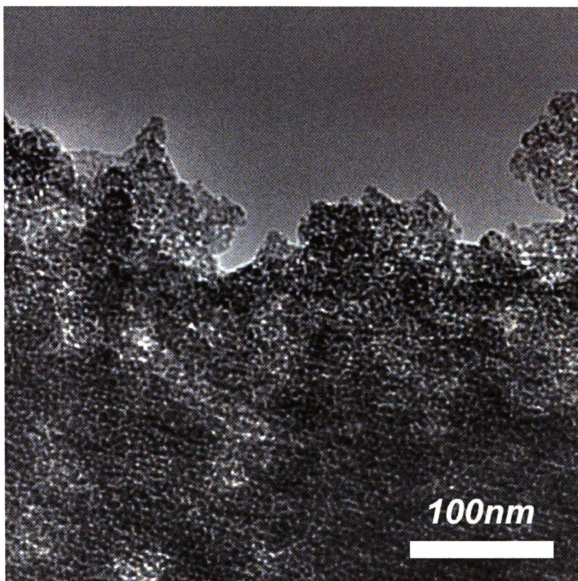


Figure 5.3. TEM image for organo-functionalized (COOH) mesoporous silica film

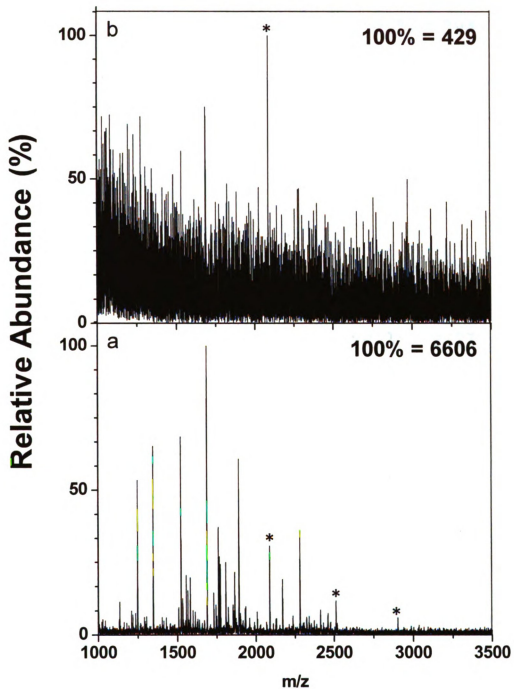


Figure 5.4. MALDI mass spectra of 10 pmole of tryptic digested ovalbumin. a) conventional MALDI spectra of ovalbumin (no enrichment), b) ovalbumin enrichment on diazo mesoporous silica film. (The asterisks indicate the phosphorylated peptide fragments.)

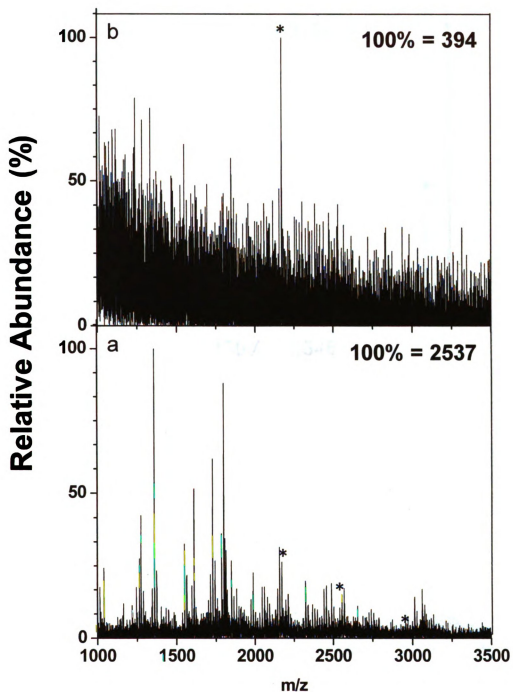


Figure 5.5. MALDI mass spectra of 10 pmole of tryptic digested methyl-esterified ovalbumin. a) conventional MALDI spectra of methyl esterified ovalbumin (no enrichment), b) methyl esterified ovalbumin enrichment on diazo mesoporous silica film. (The asterisks indicate the phosphorylated peptide fragments.)

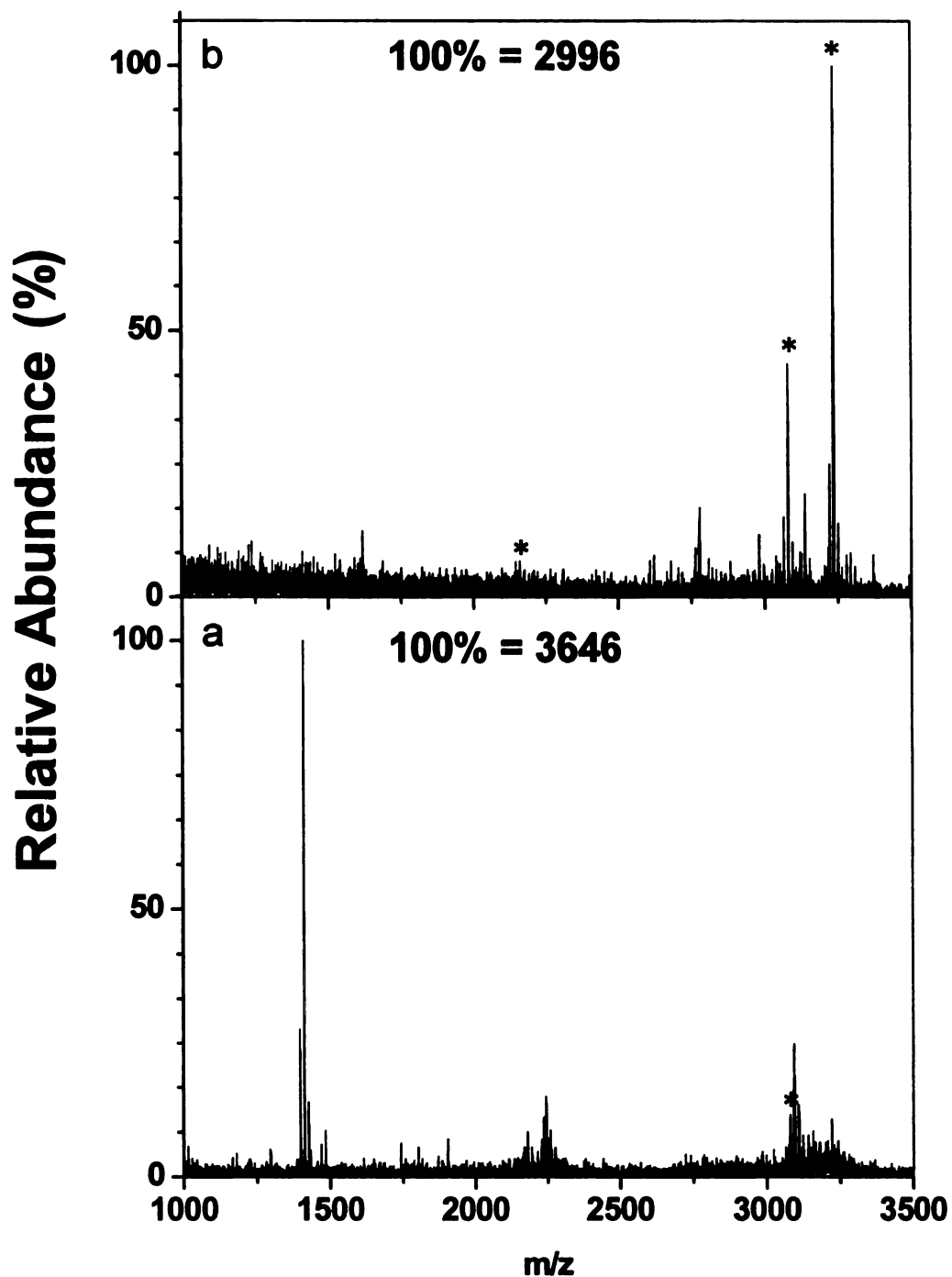


Figure 5.6. MALDI mass spectra of 10 pmole of tryptic digested methyl esterified β -casein. a) conventional MALDI spectra of β -casein (no enrichment), b) methyl esterified β -casein enrichment on diazo mesoporous silica film. (The asterisks indicate the phosphorylated peptide fragments.)

5.6 Reference

- (1) Koch, C. A., Anderson, D., Moran, M. F., Ellis, C., Pawson, T. *Science*, **1991**, 252, 668.
- (2) Pawson, T., Scott, J. D. *Science*, **1997**, 278, 2075.
- (3) Hunter, T. *Cell*, **2000**, 100, 113.
- (4) McLachlin, D. T., Chait, B. T. *Curr. Opin. Chem. Biol.*, **2001**, 5, 591.
- (5) Porath, J., Carlsson, J., Olsson, I., Belfrage, G. *Nature*, **1975**, 258, 598.
- (6) Andersson, L. Porath, J. *Anal. Biochem.*, **1986**, 154, 250.
- (7) Cao, P. Stults, J. T. *J. Chromatogr. A*, **1999**, 853 225.
- (8) Zhou, W., Merrick, B. A., Khaledi, M. G., Tomer, K. B. *J. Am. Soc. Mass Spectrom.*, **2000**, 11, 273.
- (9) Oda, Y., Nagasu, T., Chait, B. T. *Nat. Biotechnol.* **2001**, 19, 379-382
- (10) Meyer, H. E., Eisermann, B., Heber, M., Hoffmann-Posorske, E., Korte, H., Weigt, C., Wegner, A., Hutton, T., Donella-Deana, A., Perich, J. W. *Faseb. J.* **1993**, 7, 776-782
- (11) Lansdell, T. A., and Tepe, J. J. *Tetrahedron Lett.* **2004**, 45, 91-93.
- (12) Warthaka, M., Karwowska-Desaulniers, P., Pflum, M. *ACS Chemical Biology*, **2006**, 1, 11, 697-701

MICHIGAN STATE UNIVERSITY LIBRARIES



3 1293 03062 9442